bcn324612

ORE DEPOSITIONAL PROCESSES IN THE FORMATION OF THE NAVAN ZINC/LEAD DEPOSIT, CO. MEATH, IRELAND.

IAIN KERR ANDERSON

A THESIS SUBMITTED FOR THE DEGREE OF
DOCTOR OF PHILOSOPHY

STRATHCLYDE UNIVERSITY, GLASGOW
DEPT. OF APPLIED GEOLOGY
1990

VOLUME II TABLES AND FIGURES

LIST OF TABLES

Table 1.1 Grades and tonnages of different types of Zn/Pb deposits throughout the world.

Deposit	Tonnage (Mt)	% Zn	% Pb	% Cu	Ag (g/t)
SEDEX					
Howards Pass District, Canada	>500[1]	5.4	2.1	-	-
McArthur River, Australia	227	9.2	4.1	0.2	41
Broken Hill, Australia	180	9.8	11.3	0.2	170
Mt. Isa (Zn/Pb), Australia	88.6	6.1	7.1	0.06	160
Sullivan, Canada	155	5.7	6.6	-	68
Red Dog, Alaska	>85	17.1	5.0	-	75
Meggen, Germany	60	10.0	1.3	0.2	3
Rammelsberg, Germany	30	19.0	9.0	1.0	103
Silvermines, Ireland	18.4	7.4	2.8	-	21
Tynagh, Ireland	12.3	4.5	4.9	0.4	58
MVT					
Viburnam Trend, USA	≈800	1.0	6.0	-	-
Tri-State District, USA	≈500	2.3	0.6	-	-
Pine Point, Canada	84	6.6	2.9	-	-
VMS					
Kidd Creek, Canada	>100	6.0	0.2	2.46	70
Neves Corvo, Portugal	≈66	3.5	0.7	4.1	-
Matsumine, Japan	30	2.4	1.0	3.6	-

[1] Total of indicated plus inferred ore reserves.

Table 1.2 Characteristic features of Irish, carbonate hosted Zn-Pb deposits.

Deposit	(Mt)	%Zn	%Pb	Age of host rocks	Host rocks	Styles of mineralization	Structural control	Specific features
Navan	69.9	10.27	2.6	Courceyan	Pale Beds micrites and a variety of calcarenites (Navan Group)	Dominantly stratiform Zn/Pb ± Fe ore lenses with sub-seafloor relacement, open space infill and lesser veining. Pyrite-rich sulphides occur in the overlying sedimentary-early diagenetic CGO, which also contains clasts of the underlying mineralized Pale Beds.[1]	Located near the SW flank of a complex faulted Lower Palaeozoic inlier. None of the faults observed (ENE-trending) are mineralized, however there is evidence for an early ENE structural control on the mineralization, which acted as precursors to the presently observed faults.[1]	Mineralization extends through 120m of the stratigraphic section in places; clasts of mineralized Pale Beds in the pre-Arundian, submarine Boulder Conglomerate places constraints on the timing of mineralization in the Pale Beds; ore horizons in the Pale Beds occur at the contact between a calcarenite or micrite and an overlying dolomite.
Silvermines	17.7	6.4	2.5	Courceyan	Waulsortian mudbank, mudbank and dolomite breccias, dolomites, and Old Red Sandstones. (Navan and ABC Groups)	Dominantly stratiform Fe/Ba ± Zn/Pb ore lenses. Veining and replacement are common in lower ore zones (ORS and dolomite-hosted) and exhalative mineralization in the upper ore zones (Waulsortian reef/breccia-hosted) is coeval with a bedded barite deposit at Magcobar.	Situated on the northern flank of a Lower Palaeozoic inlier, adjacent to the ENE-trending Silvermines Fault, but with WNW-trending faults and sulphides on the down-dip side. ENE-trending faulting is thought to have controlled rapid subsidence associated with the growth of Waulsortian mudbanks and the onset of mineralization.	Hydrothermal chimneys in the pyritic upper orebody; strong eH control on the sulphide/sulphate/carbonate depositional facies; debris flow deposition of some sulphide and the hanging wall dolomite interpreted as tectonic instability during and after the mineralization.[2]
Tynagh	9.4	3.2	3.0	Courceyan	Waulsortian mudbank (ABC Group)	Lenticular orebodies with sulphides deposited within a dilatant fracture system associated with the forceful injection of the ore fluids into the Waulsortian mudbank adjacent to the Tynagh Fault. A banded iron formation occurs at the stratigraphically equivalent horizon to those which host the base metal mineralization.[3,4]	Located on the NE side of a Lower Palaeozoic inlier. The orebody occurs at the point of maximum throw on the hanging wall side of the E-W trending Tynagh Fault.	The iron formation occurs more distally north from the Tynagh Fault and possibly represents seafloor deposition; pyrite chimneys within the sulphide support evidence for some sea floor deposition of the base metals; manganese enrichment occurs within the Waulsortian mudbank around the deposit; late-stage copper/dolomite association.[3,4,5]
Keel/(Garrycam)	5.0	(7.0)		Courceyan	Basal clastics through to Shaley Pales in the Navan Group (base metals) and Waulsortian mudbank in the ABC Group (barite).	Sulphides occur in sub-vertical features as fracture-fill, breccia-matrix and disseminations. Bedded barite at Garrycam occurs stratigraphically above the Zn/Pb sulphides within the Waulsortian mudbank.	Located on the southern flank of a Lower Palaeozoic inlier, on an ENE trending fault system. The barite occurs on the hanging wall side of a major ENE-trending fault.	Faults are mineralized; high cadmium content (greater than 1% wt) in the sphalerite.
Ballinalack	3.5	(7.0)		Courceyan	Waulsortian mudbank (ABC Group)	Pods of sulphide formed by replacement of Waulsortian mudbank, similar to Tynagh, and infill of stromatactid cavities.	Located on the NW flank of a an upstanding block of Lower Palaeozoics and on the hanging wall of the NE-trending Ballinalack Fault.	Mineralization in the stromatactid cavities is regarded as occurring prior to the final stage, diagenetic calcite cements.

Table 1.2 Characteristic features of Irish, carbonate hosted Zn-Pb deposits.

Deposit	(Mt)	%Zn	%Pb	Age of host rocks	Host rocks	Styles of mineralization	Structural control	Specific features
Tatestown/ Scallanstown	3.1	(5.4)		Courceyan	Pale Beds micrites and calcarenites [1] (Navan Group)	Stratabound, syndiagenetic mineralization as void fills, fracture-fill and local replacement.	Mineralization is preferentially developed in the immediate hanging wall of an ENE-trending, northerly-dipping, normal fault.	Main ore horizons are concentrated below dolomites in the Pale Beds micrites.
Oldcastle	3.0	(4.9)		Courceyan	Pale Beds micrites (Navan Group)	Stratiform mineralization with syndiagenetic to epigenetic, cross-cutting fractures and veins.	Located on the southern flank of the Longford Down inlier. The mineralization occurs on both sides of the Drumlerry Fault.	Mineralization occurs below a dolomicrite, with evaporites recorded in micrites in the footwall below.
Abbeytown	1.1	3.8	1.5	Chadian to Arundian	Dolomitized crinoidal calcarenites, micrites and calcareous sandstones (ABC Group)	Statabound, epigenetic replacement, veins and open space infill.	Mineralization occurs in two NNE-trending fault/fracture systems. These fracture systems possibly formed in a pull-apart structure between the termination zones of the Ballysodare and Ox Mountains Faults.	Intensive dolomitization pre-dates the mineralization.
Harberton Bridge	0.5	(7.0)		Courceyan to Arundian	Waulsortian mudbank and overlying pelsparrites (ABC and MLG Groups)	Epigenetic sulphide breccias, breccia-matrix infills and fracture-fill mineralization.	Located on the northern side of Lower Palaeozoic inlier. No major faults are associated with the mineralization, however an early structural control during sulphide emplacement has been suggested.	
Galmoy	6.9	12.5	1.1	Courceyan	Dolomitized Waulsortian mudbank (ABC Group)	Stratiform lenses formed by replacement of host rock.[6]	No data at present ?	

Brackets around ore grade figures indicate combined Zn+Pb.

Tonnage and grade figures are the totals of all orebodies/lenses for each deposit, eg Navan/Silvermines are composed of many discrete orebodies.

Data and information on the deposits is taken from various papers in the "Geology and Genesis of Mineral Deposits in Ireland" (Andrew et al., 1986, eds). Additional information is from:

[1] Andrew and Ashton, 1985
[2] Boyce et al., 1983
[3] Russell, 1975
[4] Boast et al., 1981
[5] Banks, 1986
[6] Various recent press releases on the Galmoy deposit.

Table 5.1 A list of underground headings, levels and ore Lenses referred to in the text.

Lens	Level	Underground heading(s)
2-1	1435	226-229N
2-1	1345	204-206W
2-1	1315	222W
2-2	1285	W20S-W40S
2-3	1435	224N
2-3	1375	240N
2-3	1315	252S and 253S
2-4	1315	252S and 253S
2-5	1330	242S
2-5	1315	242S
2-5	1190	Haulage
1-5	1330	Block 2, 181-183N
1-5	1315	Block 2, 173N
1-5	1315	Block 6, FW contour drifts
1-5	1315	Block 7, panel 7
1-5	1230	Block 14, 131-133W
CGO	1420	2 Zone Upper
CGO	1405	3 Zone access
CGO	1390	3 Zone access

Table 6.1 A summary of the $\delta^{34}S$ values in sulphides from the Navaṅ deposit analyzed by Boast (1978).

Lens	Mineral	$\delta^{34}S$ (‰)
2-5	sphalerite	+2.9
2-5	galena	-2.3
2-5	sphalerite	-9.0
2-5	barite	+22.6
2-5	sphalerite	-14.3
2-5	sphalerite	-12.1
2-5	sphalerite	-14.5
2-4	sphalerite	-1.8
2-4	barite	+19.6
2-3	sphalerite	-23.8
2-1	sphalerite	-8.0
2-1	sphalerite	-3.9

Table 6.2a Tabulated summary of the sulphur isotopic composition of sphalerite formed by the bedding-parallel replacement of semi-lithified calcarenites, pyrite/marcasite in bedding-parallel cavities associated with the sphalerite replacement, and pyrite in the CGO.

Table 6.2b Tabulated summary of the sulphur isotopic composition of different styles of mineralization within the coarse galena/sphalerite massive sulphides formed by bedding-parallel veining, cross-cutting fracturing, and replacement.

Texture	Code	No. of samples	Range of $\delta^{34}S$ values (‰)	Mean (‰)
allochem replacement by sphalerite	ALL	17	-23.0 to -14.5	-19.7
colloform pyrite and marcasite in bedding-parallel cavities in 2-1 Lens	COL	7	-37.3 to -28.2	-31.7
framboidal pyrite in the CGO	FRA	3	-32.0 to -30.2	-31.0

Texture	Code	No. of samples	Range of $\delta^{34}S$ values (‰)	Mean (‰)
coarse bladed galena from massive sulphides	BVN	55	-1.1 to +14.1	+7.1
coarse, poorly zoned sphalerite	ZON	11	+3.7 to +12.3	+8.6
zoned sphalerite replacement	MAS	4	-0.1 to +7.2	+3.6
rhythmically banded sphalerite including small, coeval geopetals	RHY	12	-15.6 to +11.3	-2.3
massive sphalerite in 2-5 Lens west	MSA	1	-15.6	-15.6
layered and cubic galena in 2-5 Lens west	CBU	2	-20.3 to -19.5	-20.1
colloform pyrite on galena in 1-5 Lens	CLO	1	-26.6	-26.6
late-stage bournonite crystals	BRN	3	-17.2 to -4.2	-12.1

Table 6.2c Tabulated summary of the sulphur isotopic composition of different styles of mineralization in the bedding-parallel sulphide horizons characterized by open space growths and similar styles within more cross-cutting sulphides confined to the micrites.

Table 6.2d Tabulated summary of the sulphur isotopic composition of different sulphide textures within cross-cutting veins. Codes VNB and YRH refer to the cockscomb-type veins whereas codes YHR, DCP and HBY refer to the large vein swarm in 2-5 Lens.

Texture	Code	No. of samples	Range of $\delta^{34}S$ values (‰)	Mean (‰)
layered, internal sphalerite sediment	LAM	32	-23.5 to -3.3	-13.9
layered galena within sphalerite layers	LAY	5	-24.8 to -15.6	-19.4
dendritic/skeletal and platelet galena growths	DPC	9	-20.8 to -6.1	-12.0
coarse cubic galena	CUB	6	-12.0 to +0.2	-7.5
stalactitic growths	STL	6	-32.6 to -12.9	-18.6
rhythmically banded or colloform sphalerite	RYH	2	-18.3 to -10.2	-14.3
honeyblende sphalerite	HYB	16	-18.2 to -3.6	-12.4

Texture	Code	No. of samples	Range of $\delta^{34}S$ values (‰)	Mean (‰)
coarse bladed galena and marcasite in veins	VNB	8	+0.2 to +14.9	+8.8
rhythmically banded sphalerite in veins	YRH	2	+9.0 to +9.3	+9.2
rhythmically banded sphalerite in the 2-5 Lens vein swarm	YHR	2	-17.0 to -14.6	-15.8
skeletal-cubic galena in the 2-5 Lens vein swarm	DCP	2	-10.3 to -6.8	-8.6
honeyblende in the 2-5 Lens vein swarm	HBY	1	-14.4	-14.4

Table 6.2e Tabulated summary of the sulphur isotopic composition of barite and gypsum in the deposit.

Table 6.2f Tabulated summary of the sulphur isotopic composition of diagenetic pyrite within Lower Paleozoic rocks below the deposit and minor sulphides within veinlets within the Lower Paleozoic rocks.

Texture	Code	No. of samples	Range of $\delta^{34}S$ values (‰)	Mean (‰)
barite laths and rosettes	LAT	27	+17.9 to +39.1	+22.8
gypsum crystals	GYP	3	+21.0 to +24.9	+22.8

Texture	Code	No. of samples	Range of $\delta^{34}S$ values (‰)	Mean (‰)
diagenetic pyrite clots and concretions	DGN	10	+6.0 to + 61.1	+24.3
sulphides within veinlets in the Lower Palaeozoics	VNT	4	+1.8 to +3.6	+3.3

LIST OF FIGURES

CHAPTER 2

CHAPTER 3

CHAPTER 4

CHAPTER 5

CHAPTER 6

CHAPTER 7

Figure 2.1 Simplified general geology of Ireland and location of the Navan deposit.

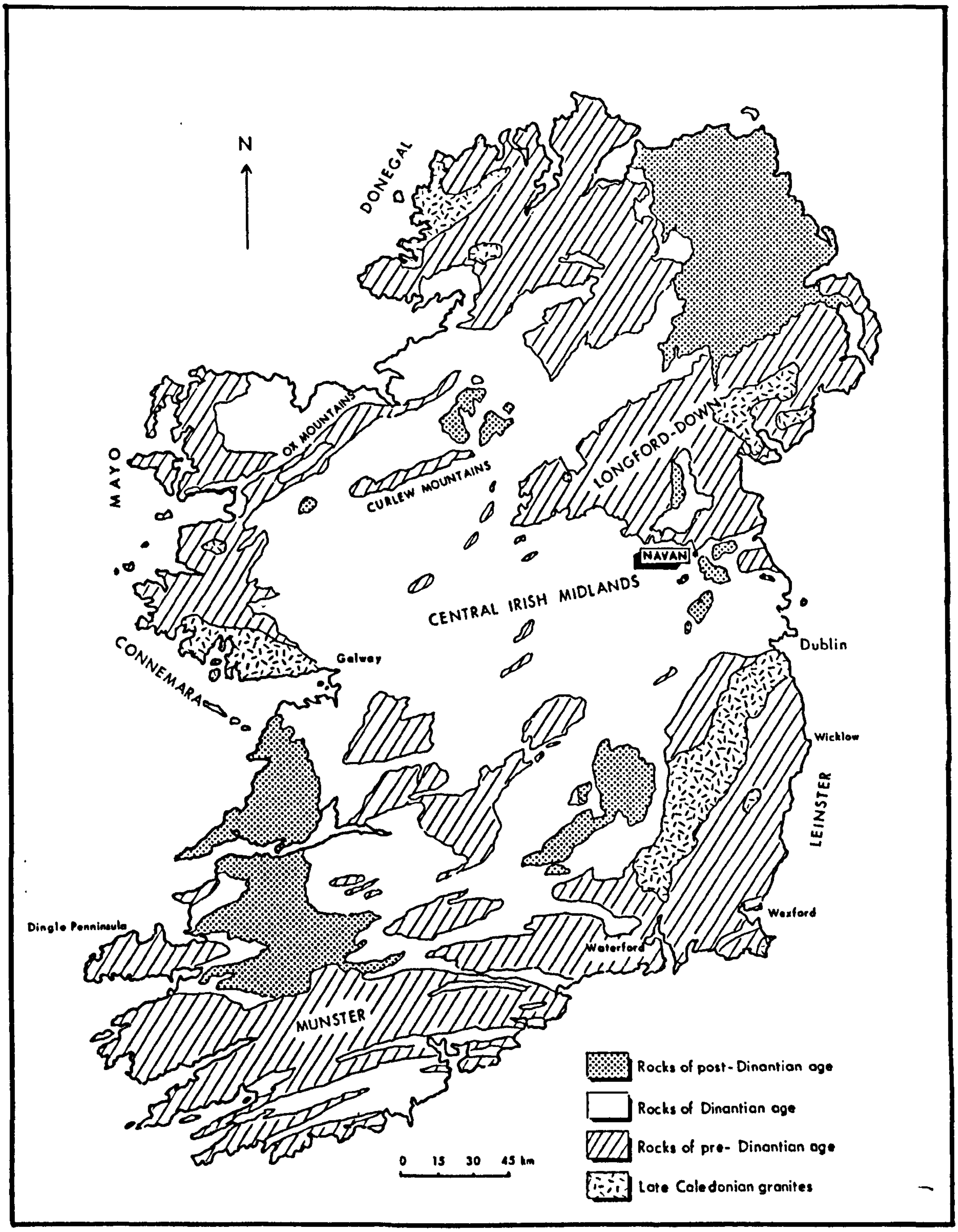
N
DONEGAL
MAYO
OX MOUNTAINS
CURLEW MOUNTAINS
LONGFORD-DOWN
NAVAN
CENTRAL IRISH MIDLANDS
CONNEMARA
Galway
Dublin
Wicklow
LEINSTER
Wexford
Waterford
Dingle Penninsula
MUNSTER
0 15 30 45 km
Rocks of post-Dinantian age
Rocks of Dinantian age
Rocks of pre- Dinantian age
Late Caledonian granites

Figure 2.2 Variation in Lower Carboniferous carbonate depositional facies prior to the onset of Zn/Pb mineralization in Ireland (compiled from Navan Resources company data).

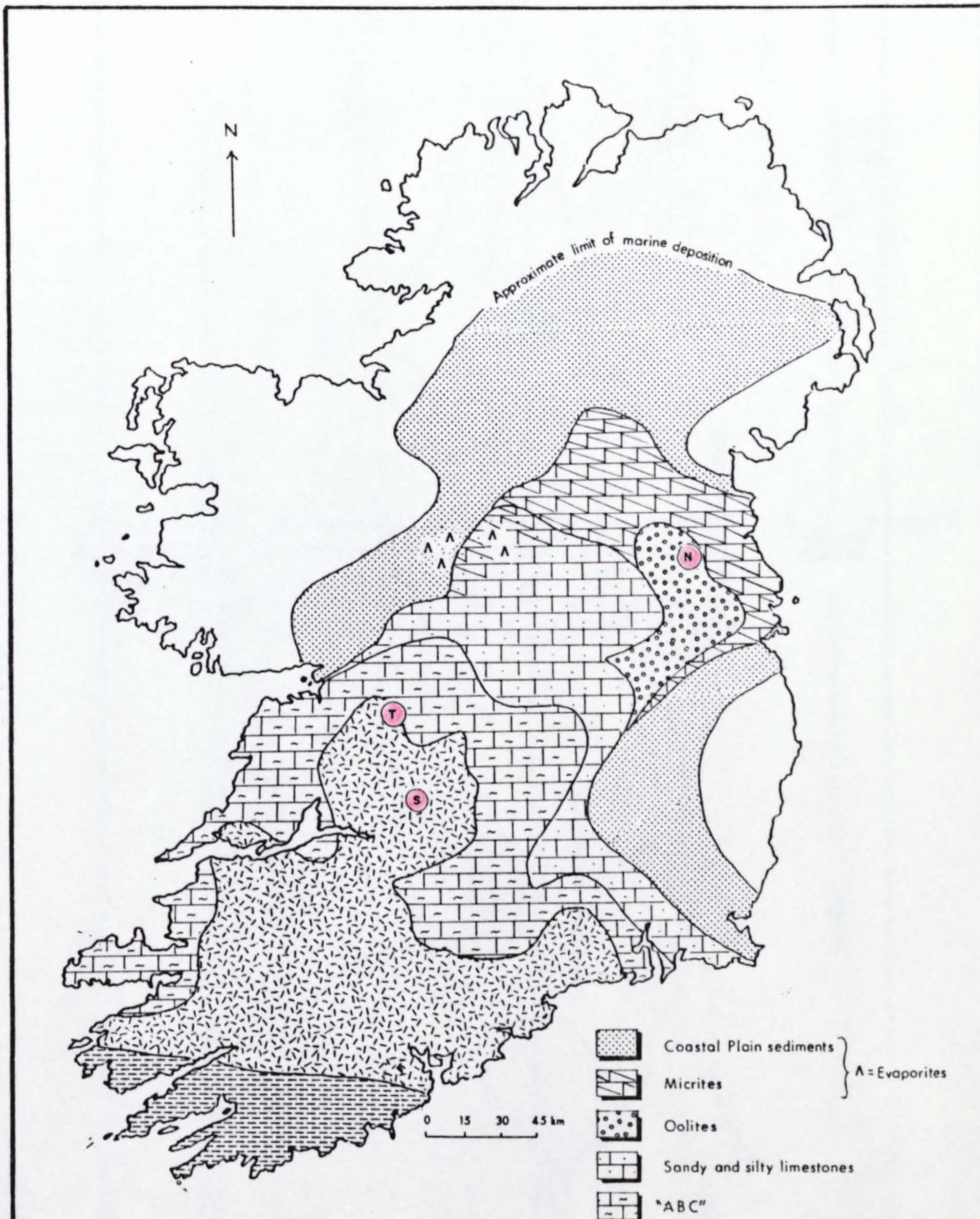

N
Approximate limit of marine deposition
N
T
S
0 15 30 45 km
Coastal Plain sediments
Micrites
Λ = Evaporites
Oolites
Sandy and silty limestones
"ABC"
Waulsortian mudbank
Basinal mudrock, in the South Munster Basin
N= Navan, S= Silvermines, T= Tynagh.

Figure 2.3 Schematic diagram illustrating the general diachronous nature of the major formations in the Courceyan stage and the stratigraphic position of the mineralization at Navan and Silvermines (modified from Andrew, 1986c).

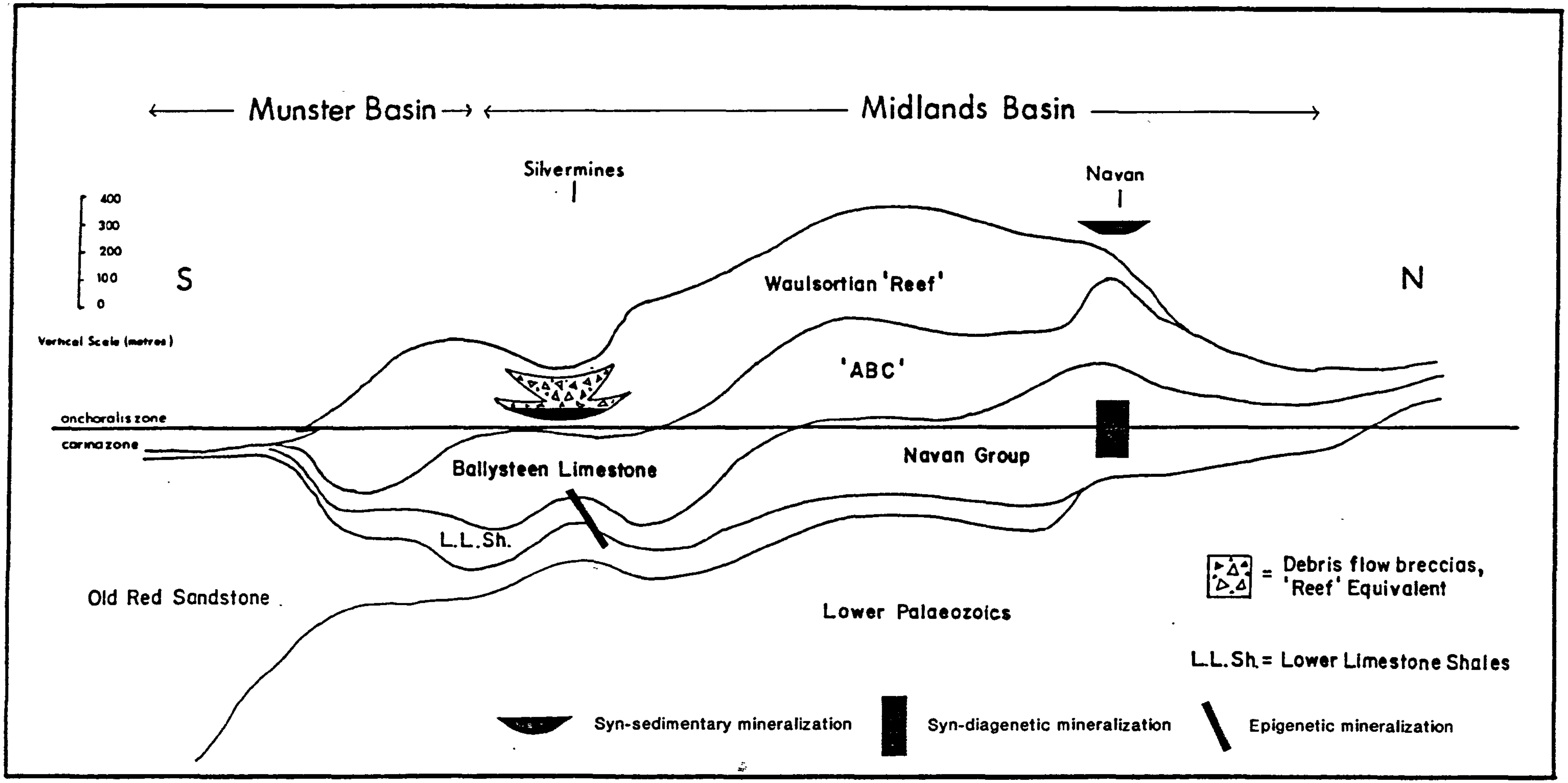

Munster Basin
Midlands Basin
Silvermines
Navan
400
300
200
100
0
Vertical Scale (metres)
S
N
Waulsortian 'Reef'
'ABC'
oncharalis zone
carina zone
Ballysteen Limestone
Navan Group
L.L.Sh.
Old Red Sandstone
Lower Palaeozoics
= Debris flow breccias, 'Reef' Equivalent
L.L.Sh. = Lower Limestone Shales
Syn-sedimentary mineralization
Syn-diagenetic mineralization
Epigenetic mineralization

Figure 2.4 Simplified structural geology of Ireland (adapted from Gill, 1962; Phillips and Sevastopulo, 1986).

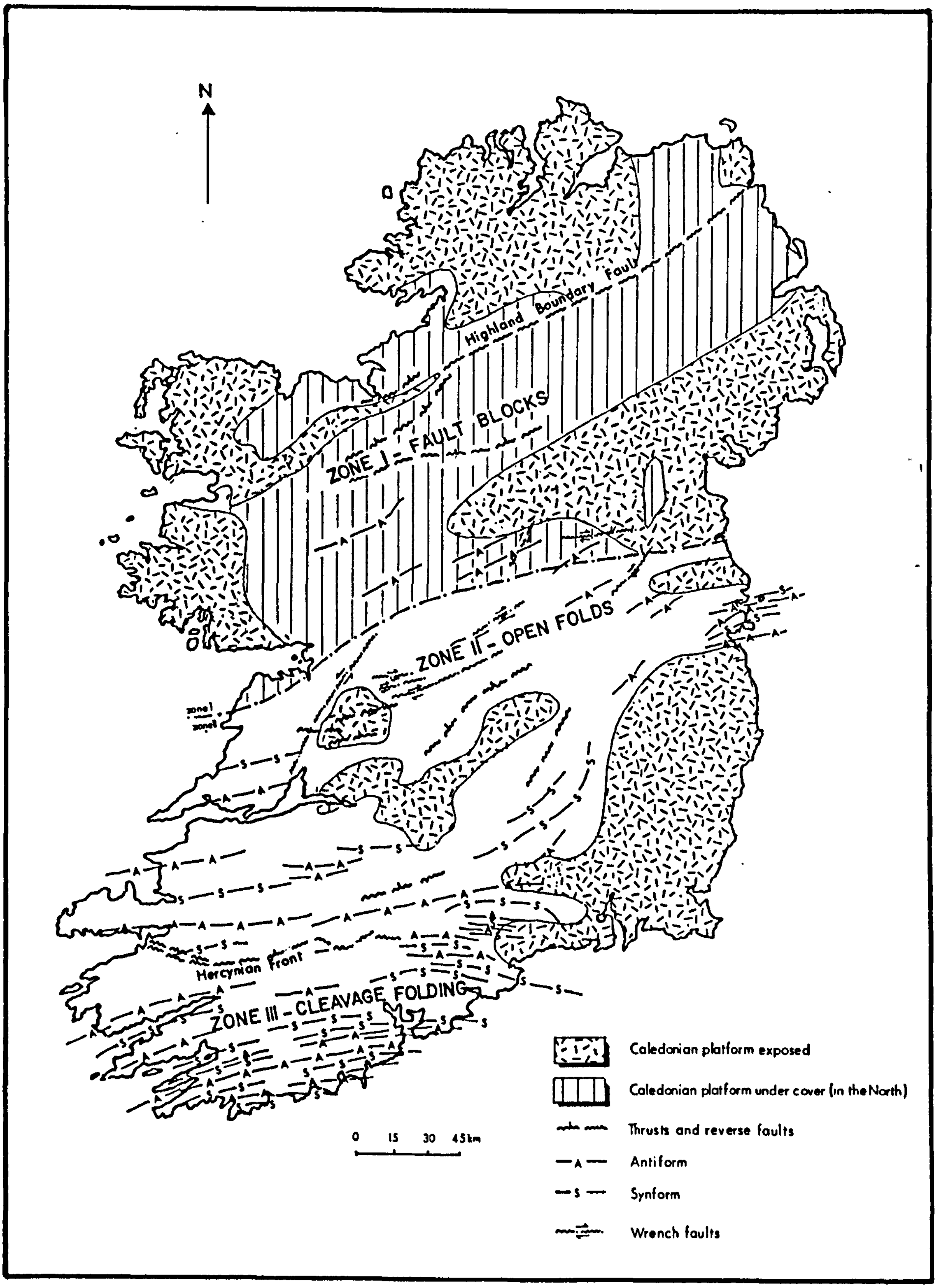
N
Highland Boundary Fault
ZONE I - FAULT BLOCKS
ZONE II - OPEN FOLDS
zone I
zone II
Hercynian Front
ZONE III - CLEAVAGE FOLDING
0 15 30 45km
Caledonian platform exposed
Caledonian platform under cover (in the North)
Thrusts and reverse faults
Antiform
Synform
Wrench faults

Figure 2.5 Surface geology of the Navan area and the location of the Navan orebody (from Ashton et al., 1986).

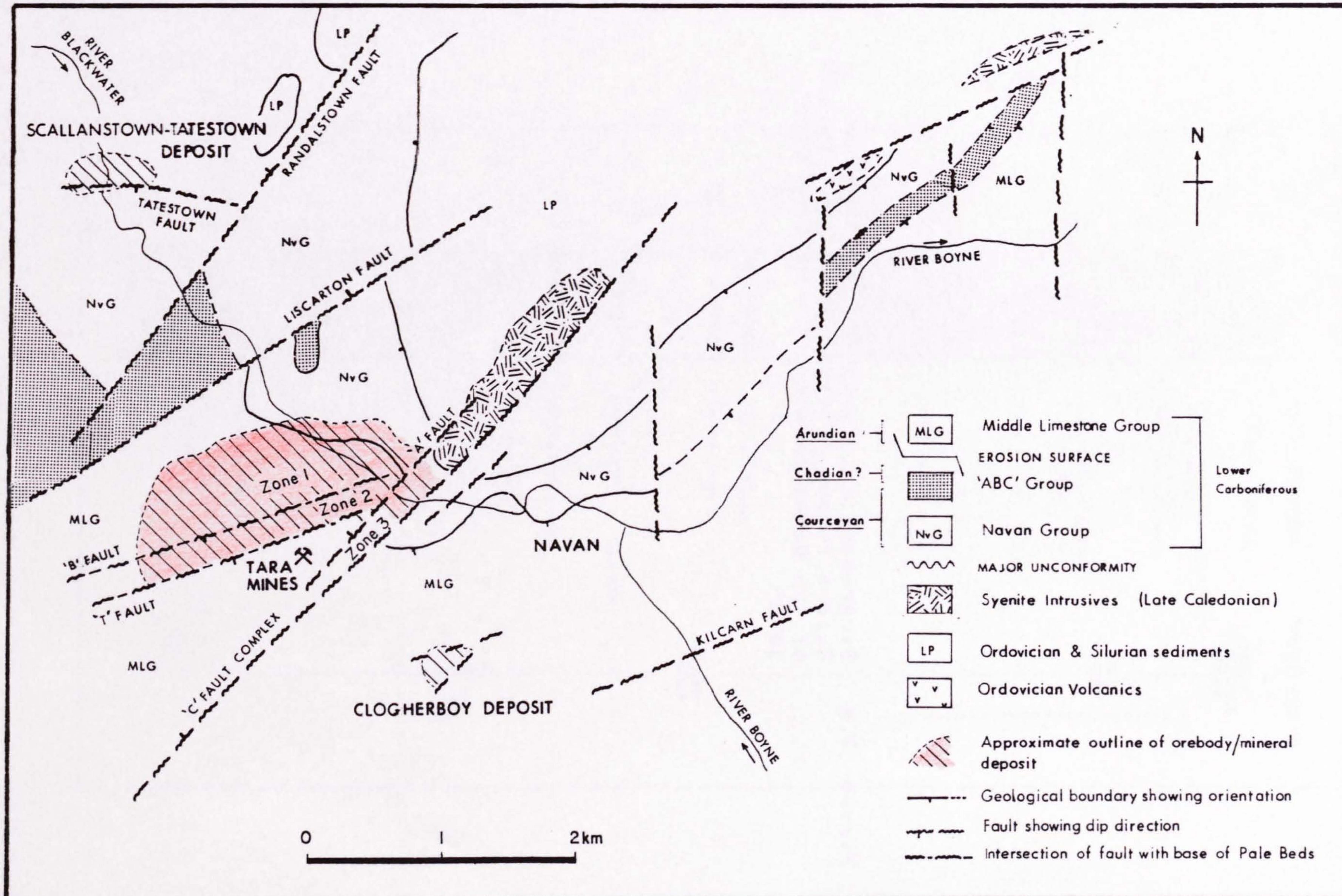
RIVER BLACKWATER
LP
LP
SCALLANSTOWN-TATESTOWN DEPOSIT
RANDALSTOWN FAULT
TATESTOWN FAULT
NvG
LP
LISCARTON FAULT
NvG
NvG
NvG
MLG
NvG
MLG
RIVER BOYNE
N
'A' FAULT
Zone 1
Zone 2
Zone 3
'B' FAULT
'T' FAULT
TARA MINES
NAVAN
Nv G
MLG
MLG
'C' FAULT COMPLEX
CLOGHERBOY DEPOSIT
KILCARN FAULT
RIVER BOYNE
0
1
2km
Arundian
Chadian?
Courceyan
MLG Middle Limestone Group
EROSION SURFACE
'ABC' Group
NvG Navan Group
Lower Carboniferous
MAJOR UNCONFORMITY
Syenite Intrusives (Late Caledonian)
LP Ordovician & Silurian sediments
Ordovician Volcanics
Approximate outline of orebody/mineral deposit
Geological boundary showing orientation
Fault showing dip direction
Intersection of fault with base of Pale Beds

Figure 2.6 Diagrammatic illustration of the Lower Carboniferous stratigraphy in the vicinity of the Navan orebody (from Ashton et al., 1986).

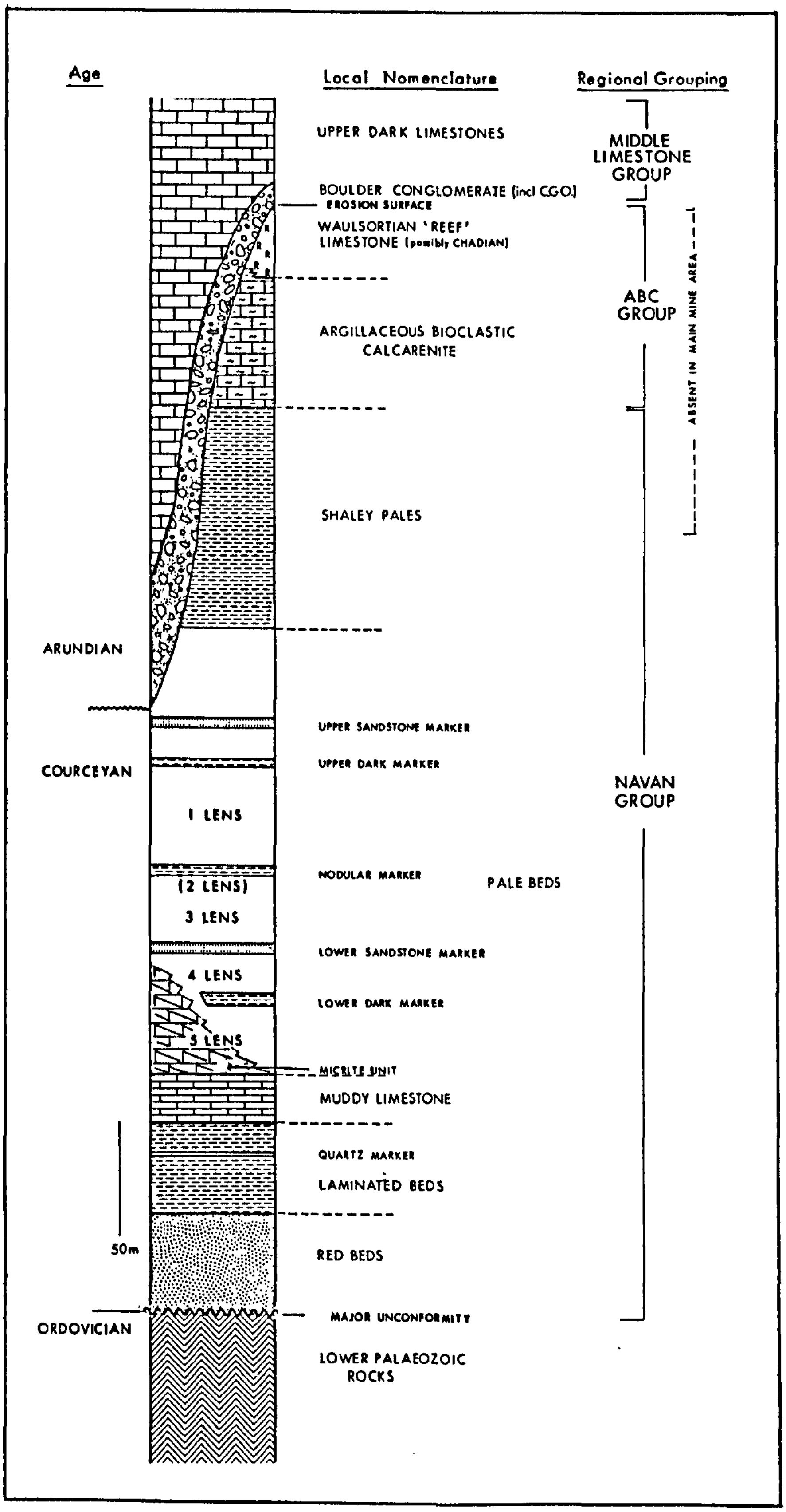
Age
Local Nomenclature
Regional Grouping
UPPER DARK LIMESTONES
MIDDLE LIMESTONE GROUP
BOULDER CONGLOMERATE (incl CGO)
EROSION SURFACE
WAULSORTIAN 'REEF' LIMESTONE (possibly CHADIAN)
ABC GROUP
ARGILLACEOUS BIOCLASTIC CALCARENITE
ABSENT IN MAIN MINE AREA
SHALEY PALES
ARUNDIAN
UPPER SANDSTONE MARKER
COURCEYAN
UPPER DARK MARKER
NAVAN GROUP
1 LENS
NODULAR MARKER
PALE BEDS
(2 LENS)
3 LENS
LOWER SANDSTONE MARKER
4 LENS
LOWER DARK MARKER
5 LENS
MICRITE UNIT
MUDDY LIMESTONE
QUARTZ MARKER
LAMINATED BEDS
50m
RED BEDS
MAJOR UNCONFORMITY
ORDOVICIAN
LOWER PALAEOZOIC ROCKS

Figure 2.7 Location of Lower Carboniferous, carbonate-hosted mineral deposits in Ireland and other localities referred to in the text.

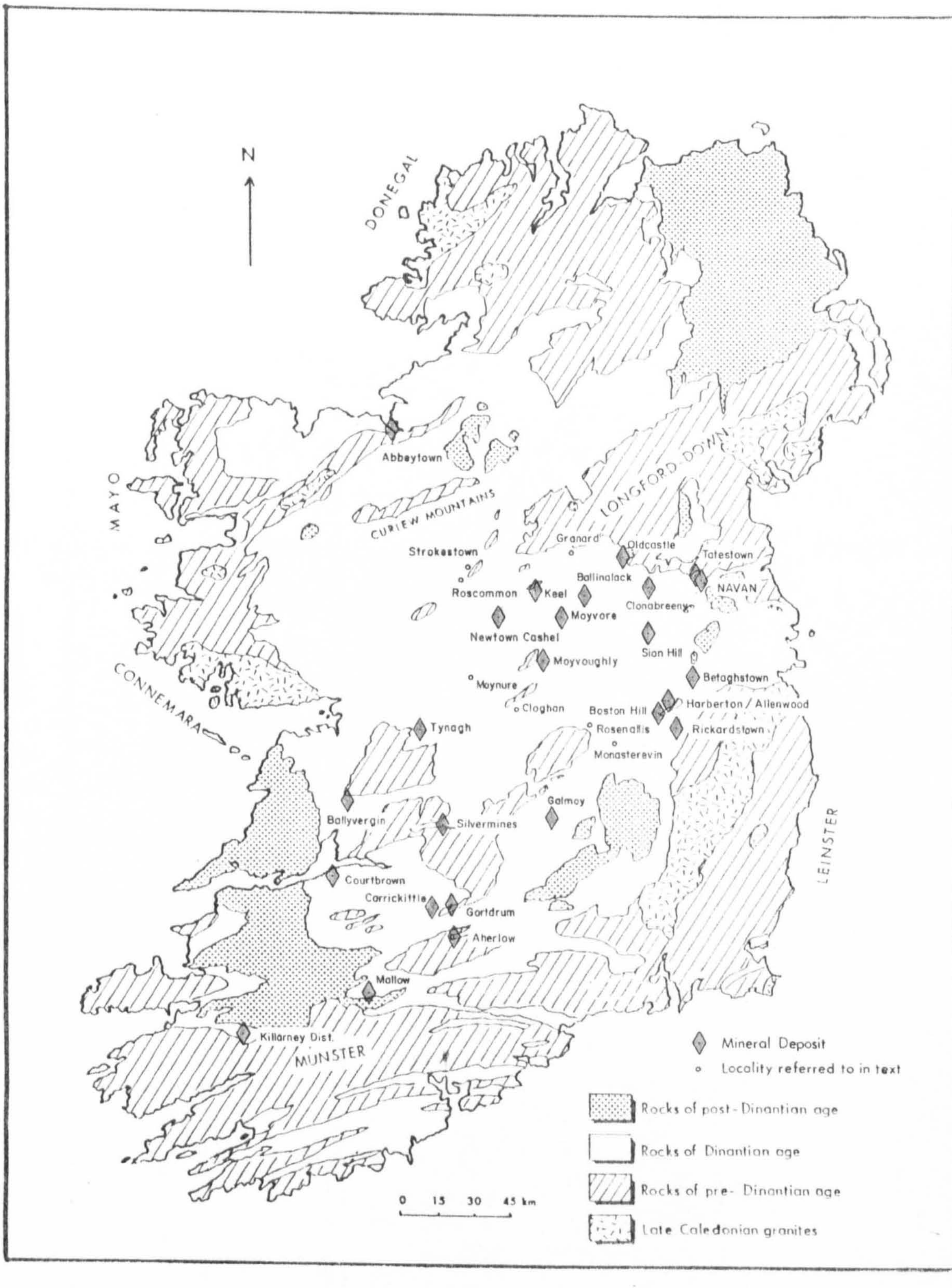
N
DONEGAL
MAYO
CONNEMARA
CURLEW MOUNTAINS
LONGFORD-DOWN
LEINSTER
MUNSTER
Abbeytown
Strokestown
Roscommon
Keel
Granard
Oldcastle
Ballinalack
Tatestown
NAVAN
Clonabreeny
Moyvore
Newtown Cashel
Sion Hill
Moyvoughly
Betaghstown
Moynure
Cloghan
Boston Hill
Harberton / Allenwood
Rosenallis
Rickardstown
Monasterevin
Tynagh
Galmoy
Ballyvergin
Silvermines
Courtbrown
Carrickittle
Gortdrum
Aherlow
Mallow
Killarney Dist.
Mineral Deposit
Locality referred to in text
Rocks of post-Dinantian age
Rocks of Dinantian age
Rocks of pre-Dinantian age
Late Caledonian granites
0 15 30 45 km

Figure 2.8 Schematic diagram illustrating the major facies variations in the Pale Beds across the Central Irish Midlands.

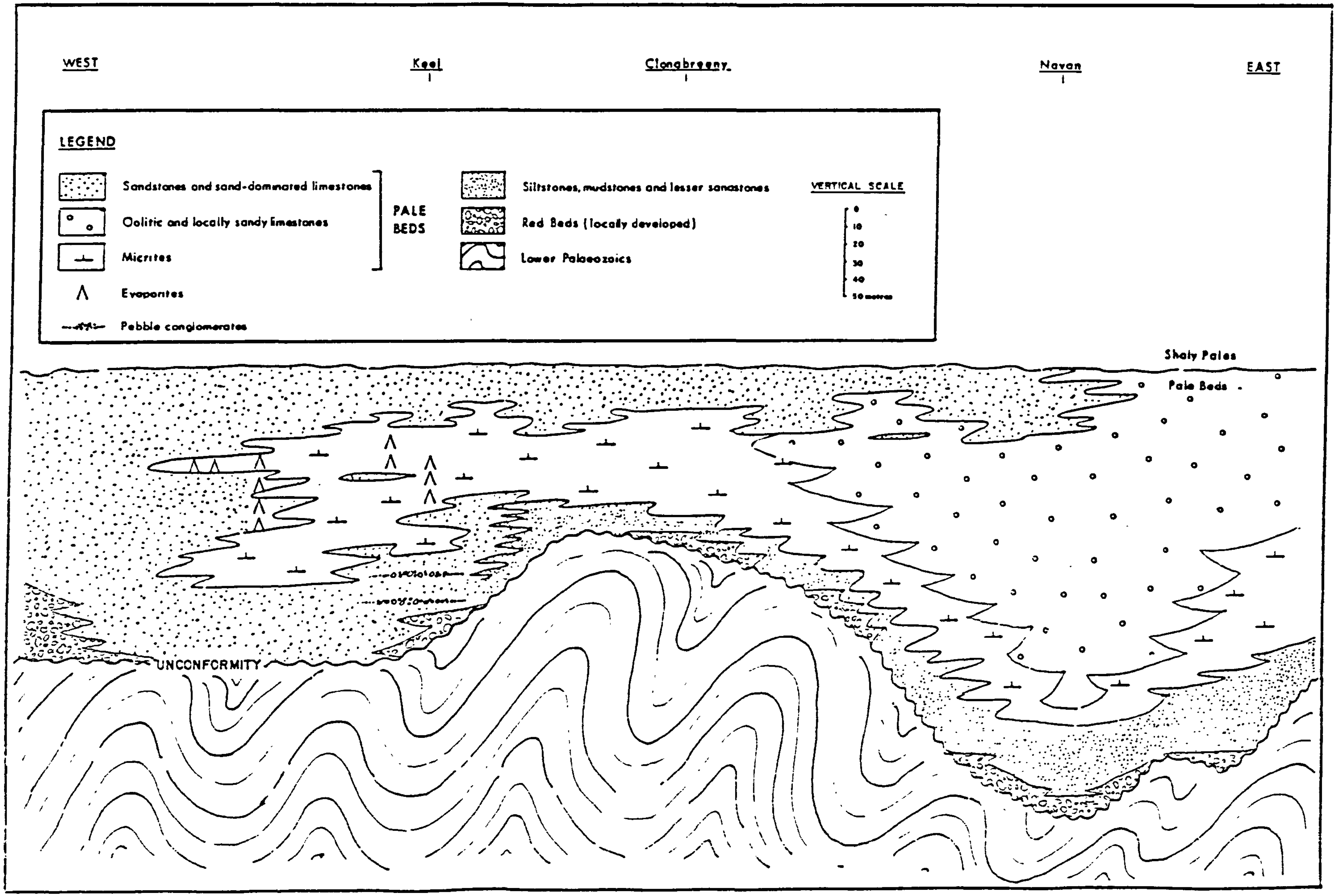
WEST
Keel
Clonabreeny
Navan
EAST
LEGEND
Sandstones and sand-dominated limestones
Oolitic and locally sandy limestones
Micrites
PALE BEDS
Evaporites
Pebble conglomerates
Siltstones, mudstones and lesser sandstones
Red Beds (locally developed)
Lower Palaeozoics
VERTICAL SCALE
0
10
20
30
40
50 metres
Shaly Pales
Pale Beds
UNCONFORMITY

Figure 2.9 Structural plan of the Navan orebody drawn at the base of the 5 Lens.

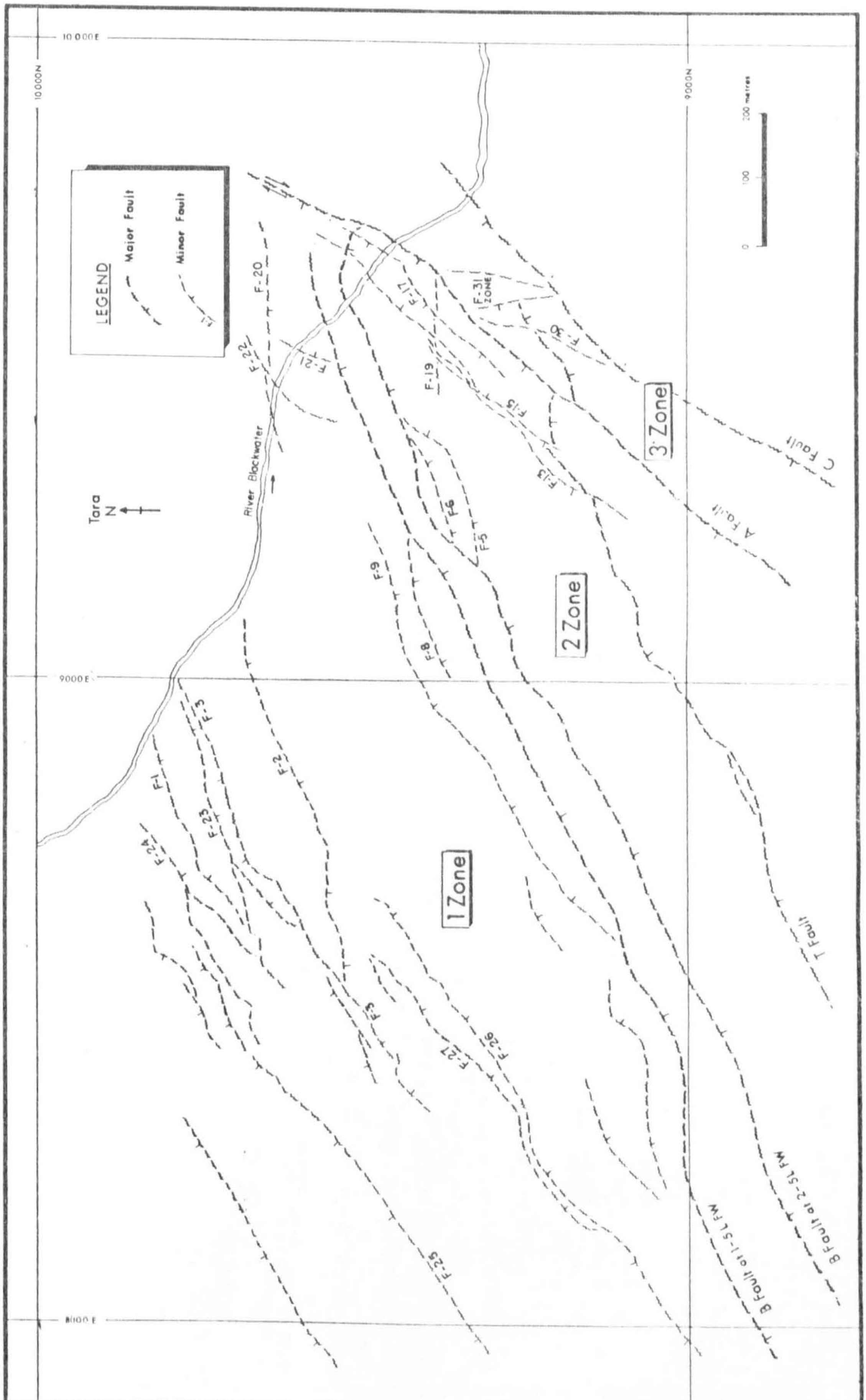

LEGEND
Major Fault
Minor Fault
Tara
N
River Blackwater
10 000 E
9000 E
8000 E
10 000N
9000N
0
100
200 metres
1 Zone
2 Zone
3 Zone
F-1
F-2
F-3
F-3
F-5
F-6
F-8
F-9
F-13
F-15
F-17
F-19
F-20
F-21
F-22
F-23
F-24
F-25
F-26
F-27
F-31 ZONE
A Fault
C Fault
T Fault
B Fault at 1-5L FW
B Fault at 2-5L FW

Figure 2.10 Strike section through the central part of the Navan orebody (from Ashton et al., 1986).

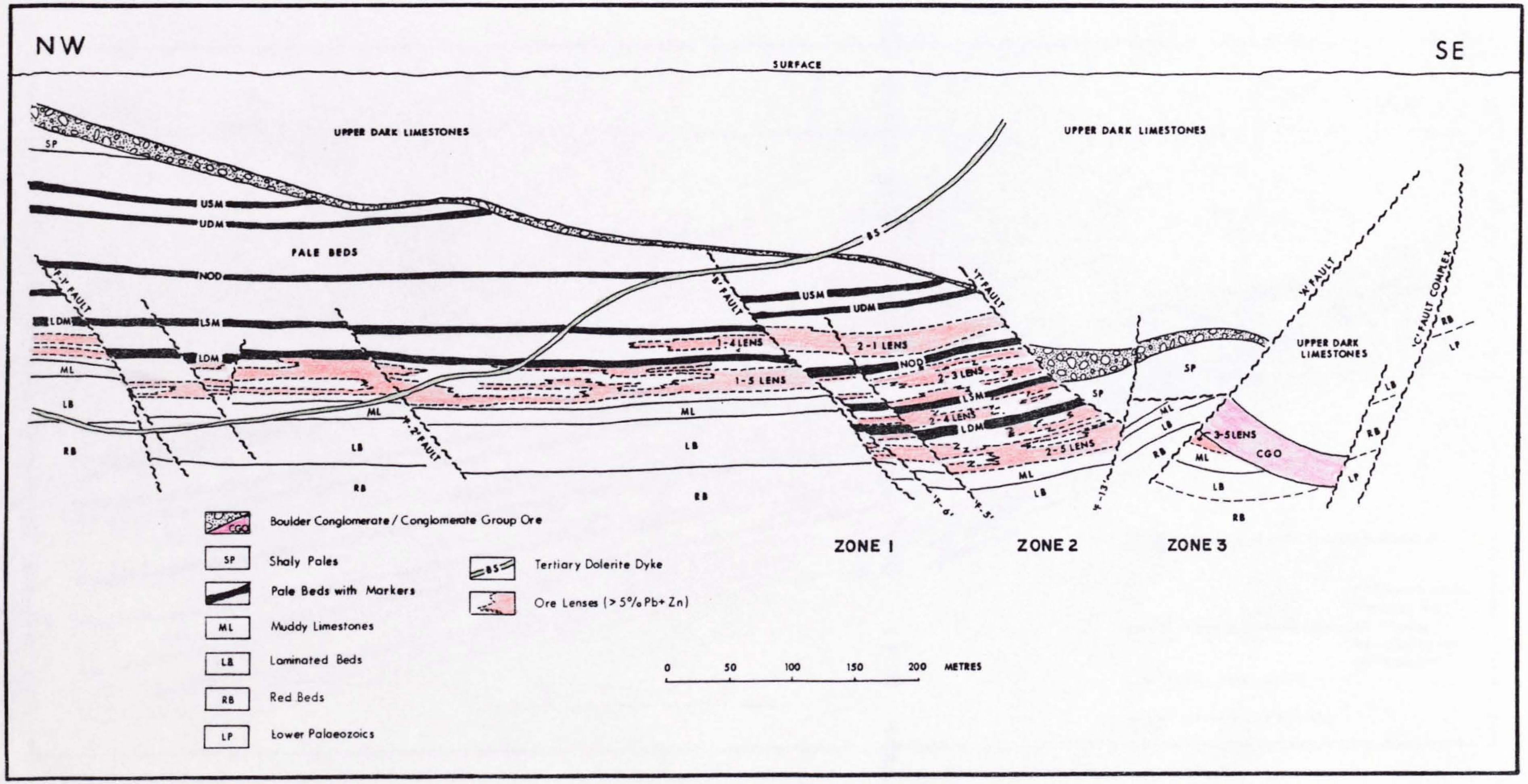

NW
SE
SURFACE
UPPER DARK LIMESTONES
UPPER DARK LIMESTONES
SP
USM
UDM
PALE BEDS
NOD
LDM
LSM
LDM
ML
LB
RB
ML
LB
RB
ML
LB
RB
BS
'P-H' FAULT
'P-2' FAULT
'B' FAULT
'T' FAULT
'W' FAULT
'C' FAULT COMPLEX
USM
UDM
1-4 LENS
1-5 LENS
2-1 LENS
NOD
2-3 LENS
LSM
2-4 LENS
LDM
2-5 LENS
SP
SP
3-5 LENS
CGO
UPPER DARK LIMESTONES
LP
ZONE I
ZONE 2
ZONE 3
Boulder Conglomerate / Conglomerate Group Ore
Shaly Pales
Pale Beds with Markers
Muddy Limestones
Laminated Beds
Red Beds
Lower Palaeozoics
Tertiary Dolerite Dyke
Ore Lenses (> 5% Pb+ Zn)
0 50 100 150 200 METRES

Figure 2.11 Dip section through 2 Zone (from Ashton et al., 1986).

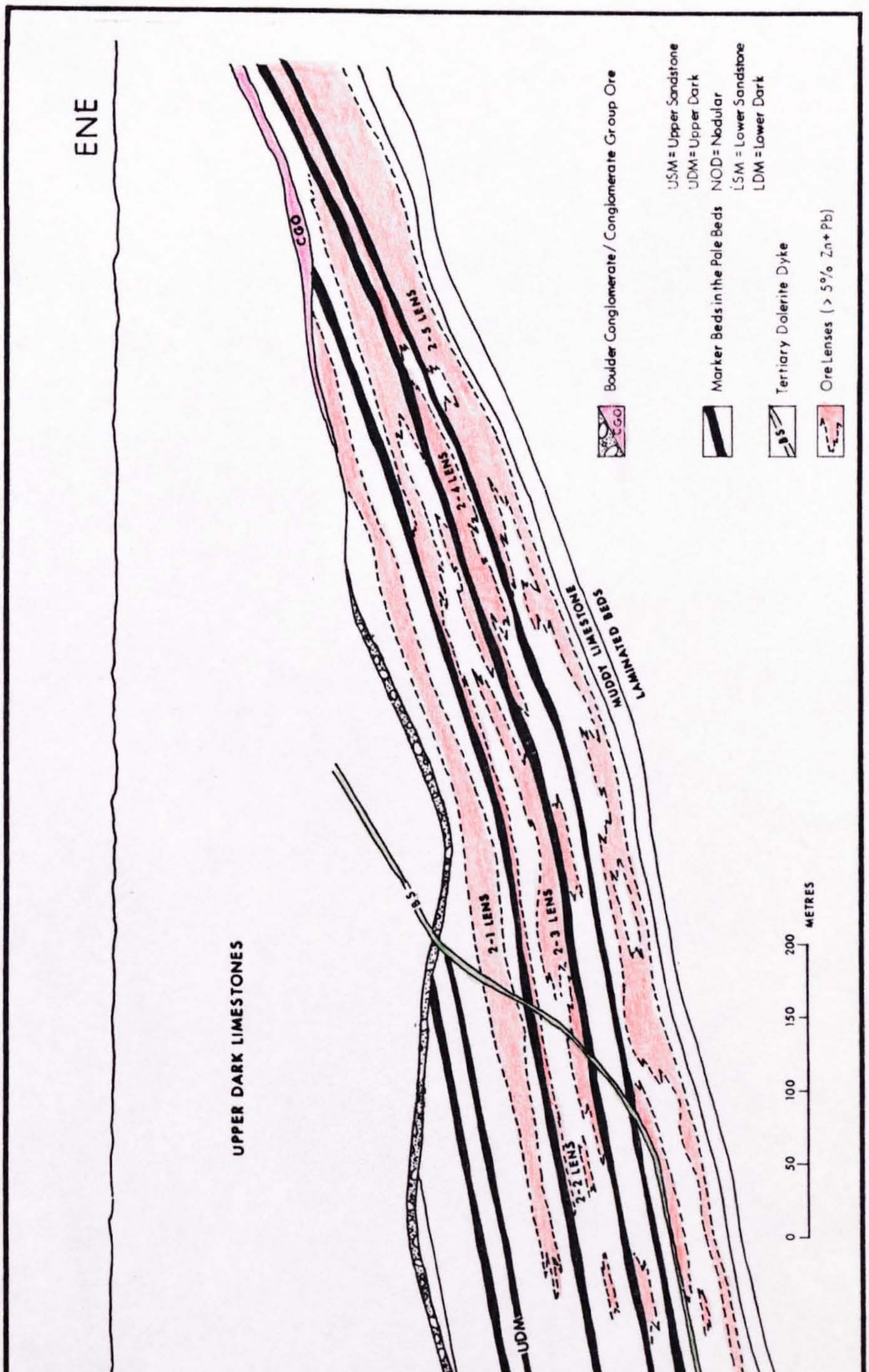
WSW
ENE
SURFACE
UPPER DARK LIMESTONES
PALE BEDS
SHALY PALES
USM
UDM
NOD
LSM
LDM
2-1 LENS
2-2 LENS
2-3 LENS
2-4 LENS
2-5 LENS
2-5 LENS
CGO
BS
MUDDY LIMESTONE
LAMINATED BEDS
0
50
100
150
200
METRES
Boulder Conglomerate / Conglomerate Group Ore
Marker Beds in the Pale Beds
USM = Upper Sandstone
UDM = Upper Dark
NOD = Nodular
LSM = Lower Sandstone
LDM = Lower Dark
Tertiary Dolerite Dyke
Ore Lenses (> 5% Zn + Pb)

Figure 3.1 A comparison of detailed graphic stratigraphic logs from the main mine area (N314) and the western mine (N910) area respectively.

GENERALIZED STRATIGRAPHIC SECTIONS THROUGH THE LOWER CARBONIFEROUS ROCKS AT NAVAN

GENERALIZED STRATIGRAPHIC SECTIONS THROUGH THE CENTRAL AND WESTERN MINE AREAS, BASED ON DRILL HOLES N314 AND N910 RESPECTIVELY, ILLUSTRATING THE MAIN STRATIGAPHIC UNITS, THICKNESS AND FACIES VARIATIONS ACROSS THE DEPOSIT.

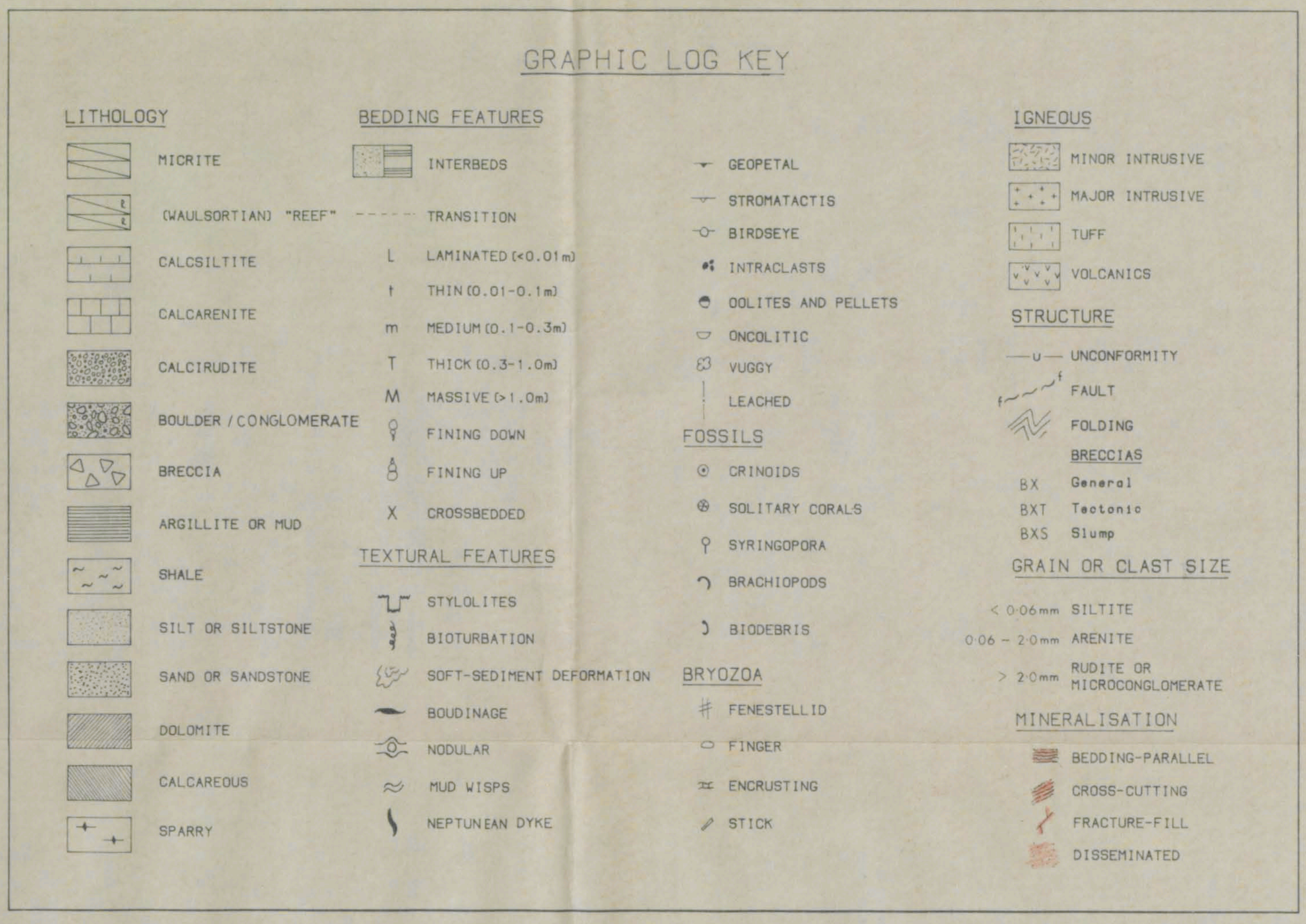

WESTERN MINE AREA

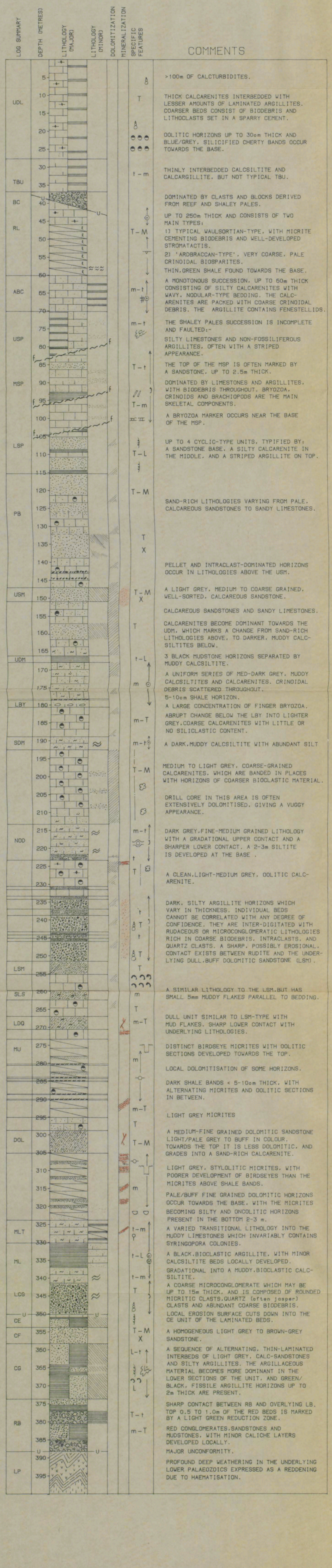

UDL = UPPER DARK LIMESTONES
TBU = THINLY BEDDED UNIT
BC = BOULDER CONGLOMERATE
REEF = REEF LIMESTONES
ABC = ARGILLACEOUS BIOCLASTIC CALCARENITE
USP = UPPER SHALEY PALES
MSP = MIDDLE SHALEY PALES
LSP = LOWER SHALEY PALES
PB = PALE BEDS
USM = UPPER SANDSTONE MARKER
UDM = UPPER DARK MARKER
LBY = LOWER BRYOZOAN MARKER
SDM = SUB DARK MARKER
NOD = NODULAR MARKER
LSM = LOWER SANDSTONE MARKER
SLS = SUB LOWER SANDSTONE
LDQ = LOWER DARK MARKER EQUIVALENT
LDM = LOWER DARK MARKER
MU = MICRITE UNIT
BDM = BOTTOM DARK MARKER
DOL = DOLOMITE
MLT = MUDDY LIMESTONE TRANSITION
ML = MUDDY LIMESTONES
LCG = LIMESTONE CONGLOMERATE

CB, CC, CD, CE, CF, CG: SUBDIVISIONS OF THE LAMINATED BEDS

RB = RED BEDS
LP = LOWER PALAEOZOICS

CENTRAL MINE AREA

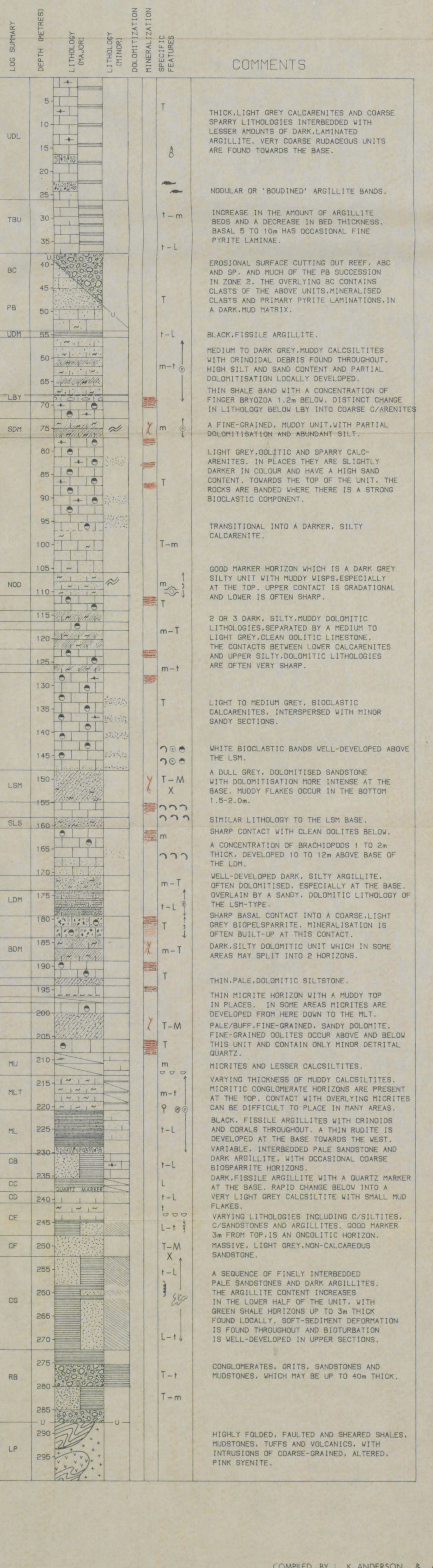

I. K. ANDERSON
PhD THESIS
1990
"ORE DEPOSITIONAL PROCESSES....."

COMPILED BY : K. ANDERSON & A. BLACK
DRAWN BY : K. ANDERSON & P. McDERMOTT

Figure 3.2 Diagram illustrating the correlation of dolomitized horizons in the 5 Lens interval in 1 Zone.

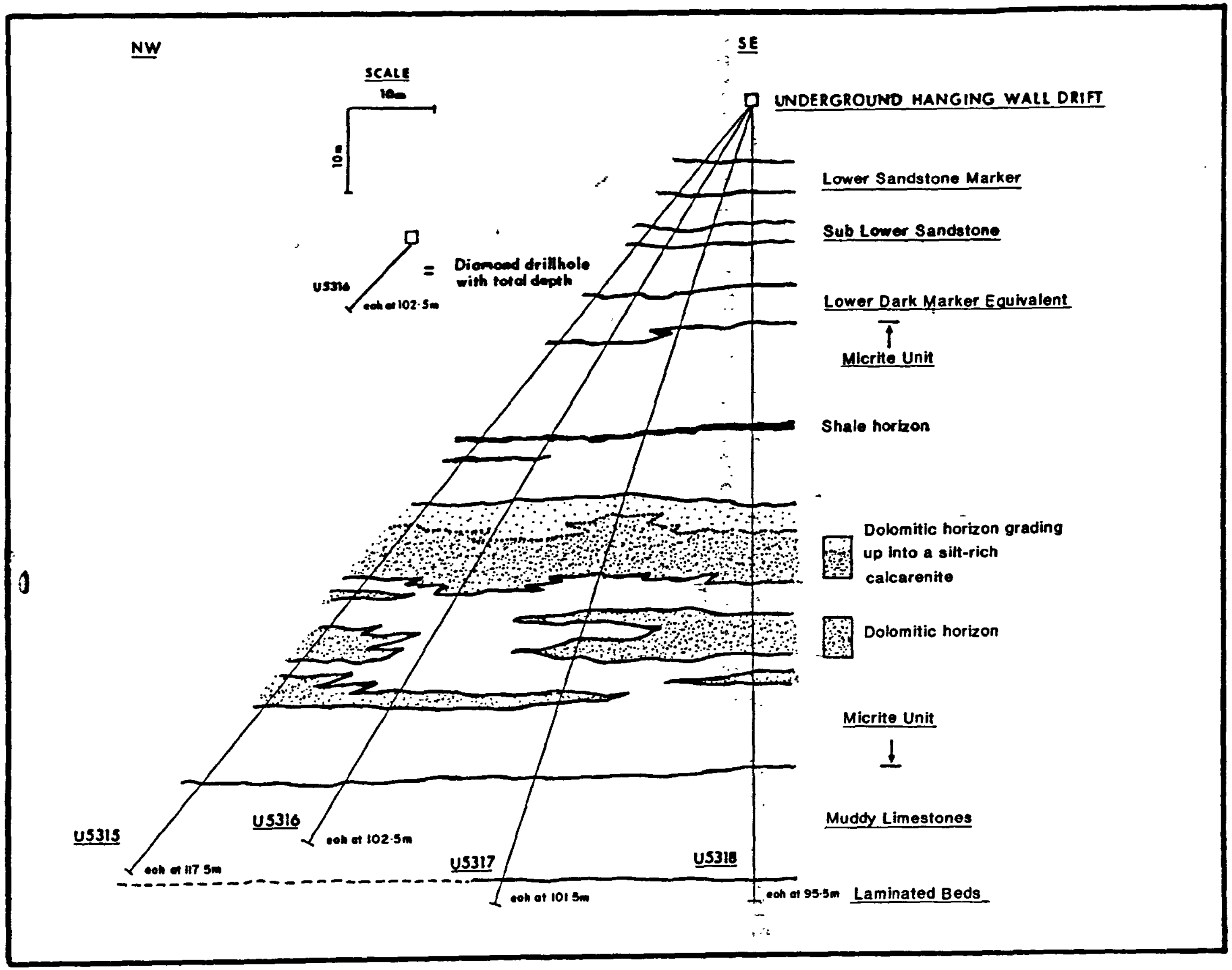
NW
SE
SCALE
10m
10m
U5316
eoh at 102·5m
= Diamond drillhole with total depth
UNDERGROUND HANGING WALL DRIFT
Lower Sandstone Marker
Sub Lower Sandstone
Lower Dark Marker Equivalent
Micrite Unit
Shale horizon
Dolomitic horizon grading up into a silt-rich calcarenite
Dolomitic horizon
Micrite Unit
Muddy Limestones
U5315
eoh at 117·5m
U5316
eoh at 102·5m
U5317
eoh at 101·5m
U5318
eoh at 95·5m
Laminated Beds

Figure 3.3 Detailed cross-section (NE-SW) through t Zone illustrating the major facies variations.

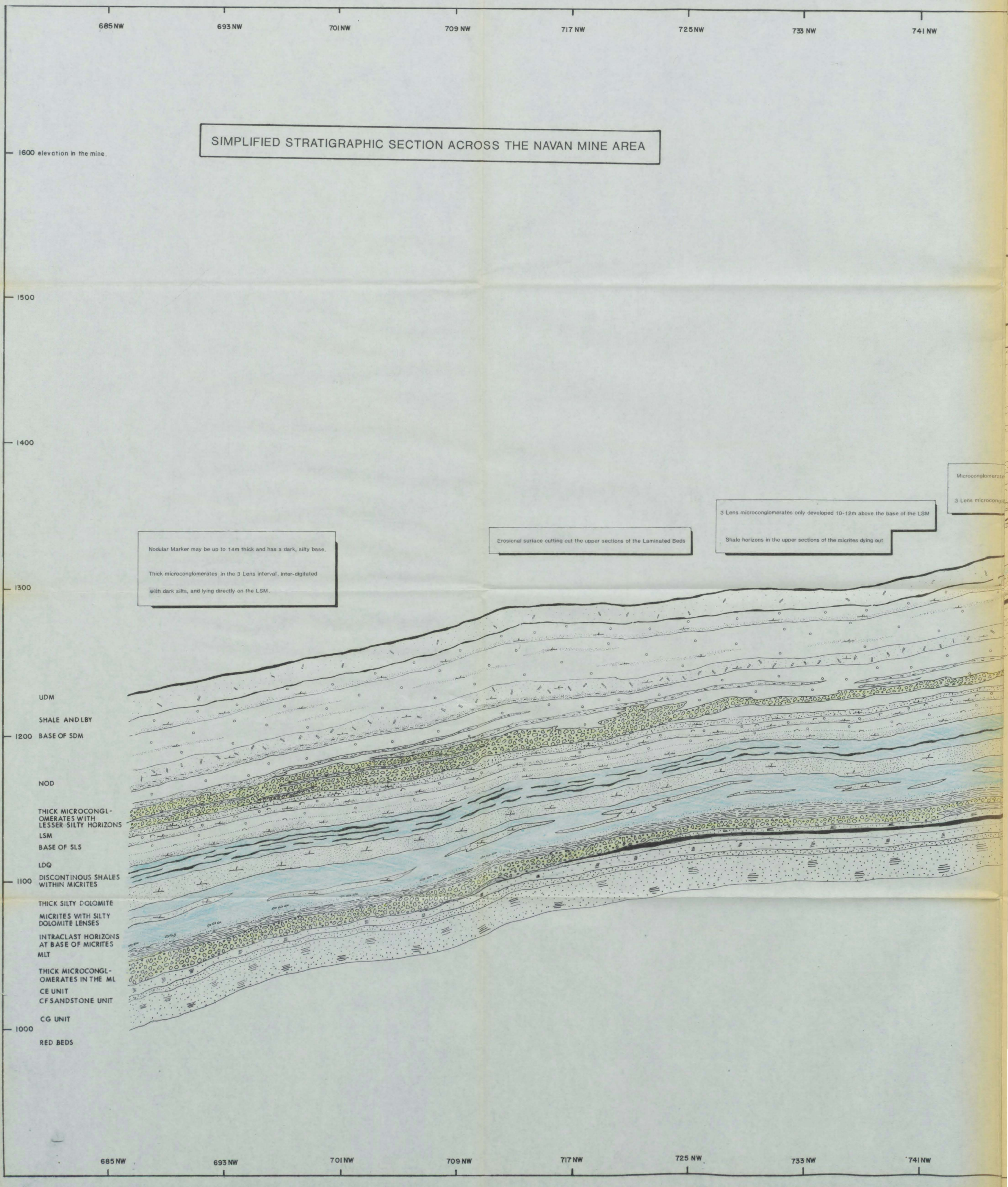
685 NW
693 NW
701 NW
709 NW
717 NW
725 NW
733 NW
741 NW
SIMPLIFIED STRATIGRAPHIC SECTION ACROSS THE NAVAN MINE AREA
1600 elevation in the mine.
1500
1400
1300
1200
1100
1000
Nodular Marker may be up to 14m thick and has a dark, silty base.
Thick microconglomerates in the 3 Lens interval, inter-digitated with dark silts, and lying directly on the LSM.
Erosional surface cutting out the upper sections of the Laminated Beds
3 Lens microconglomerates only developed 10-12m above the base of the LSM
Shale horizons in the upper sections of the micrites dying out
UDM
SHALE AND LBY
BASE OF SDM
NOD
THICK MICROCONGL-OMERATES WITH LESSER SILTY HORIZONS
LSM
BASE OF SLS
LDQ
DISCONTINOUS SHALES WITHIN MICRITES
THICK SILTY DOLOMITE
MICRITES WITH SILTY DOLOMITE LENSES
INTRACLAST HORIZONS AT BASE OF MICRITES
MLT
THICK MICROCONGL-OMERATES IN THE ML
CE UNIT
CF SANDSTONE UNIT
CG UNIT
RED BEDS

749 NW
757 NW
765 NW
773 NW
781 NW
789 NW
797 NW
805 NW
813 NW
821 NW
829 NW
837 NW
845 NW
1600
1500
1400
1300
1200
1100
1000
Variable thickness of pelletal/bioclastic/oolitic limestones directly below the LDM
LSM is up to 8m thick
Micrites thining down to 1-2m in places and 5 Lens dominated by oolitic and coarse bioclastic limestones
Erosion Surface
Shale developed locally on top of the micrites
Begining of the Lower Dark Marker
Distinct, coarse sparry limestone below the LDQ
Nodular Marker thinning to 5 or 6m in thickness
Thinning of upper sections of the micrites, which become inter-fingering with oolites and local dolomites
5 Lens dominated by micrites
glomerates in the Muddy Limestones thining out
croconglomerates dying out
UPPER DARK MARKER
SHALE AND BRYOZOA HORIZON
BASE OF SUB-DARK MARKER
SILTY HORIZONS THROUGHOUT OOLITIC LIMESTONES
NODULAR MARKER
SUB NODULAR SILTY, MUDDY MARKERS
SILTY HORIZONS THROUGHOUT OOLITIC LIMESTONES
LOWER SANDSTONE MARKER
SUB LOWER SANDSTONE MARKER
BRACHIOPOD HORIZON
LOWER DARK MARKER
COARSE PELLETAL, BIOCLASTIC, OOLITIC LIMESTONE
BOTTOM DARK MARKER
MIXED LITHOLOGIES WITH MICRITES ONLY 2m THICK IN PLACES
SILTY MUDDY LIMESTONE TRANSITION AT BASE OF MICRITES
DARK MUDDY LIMESTONES
CB UNIT
CC SHALE UNIT
CD UNIT
CE UNIT
CF SANDSTONE UNIT
CG UNIT
RED BEDS
LEGEND
HORIZONTAL SCALE = VERTICAL SCALE
0 10 20 30 40 50 m
Sand
Silt
Shales
Mud
Interbedded muds and sands
Micrites
Calcareous muds
"Microconglomerates"
Dolomitic
Oolitic
Bioclastic
Pelletal
Brachiopod horizons (⌒ becoming impersistant)
Intraclasts
I.K. ANDERSON
PhD THESIS
1990
"ORE DEPOSITIONAL PROCESSES...."

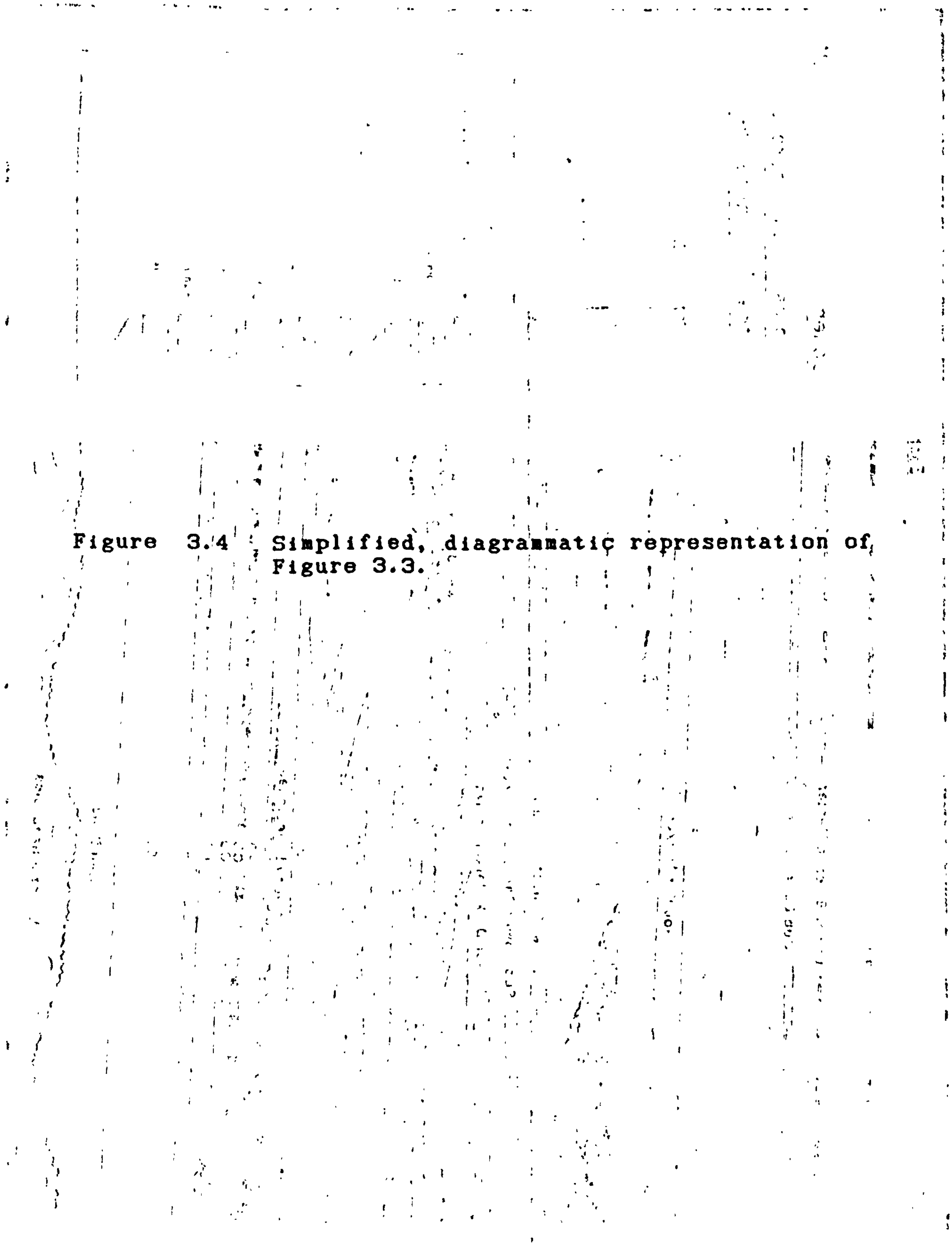

Figure 3.4 Simplified, diagrammatic representation of Figure 3.3.

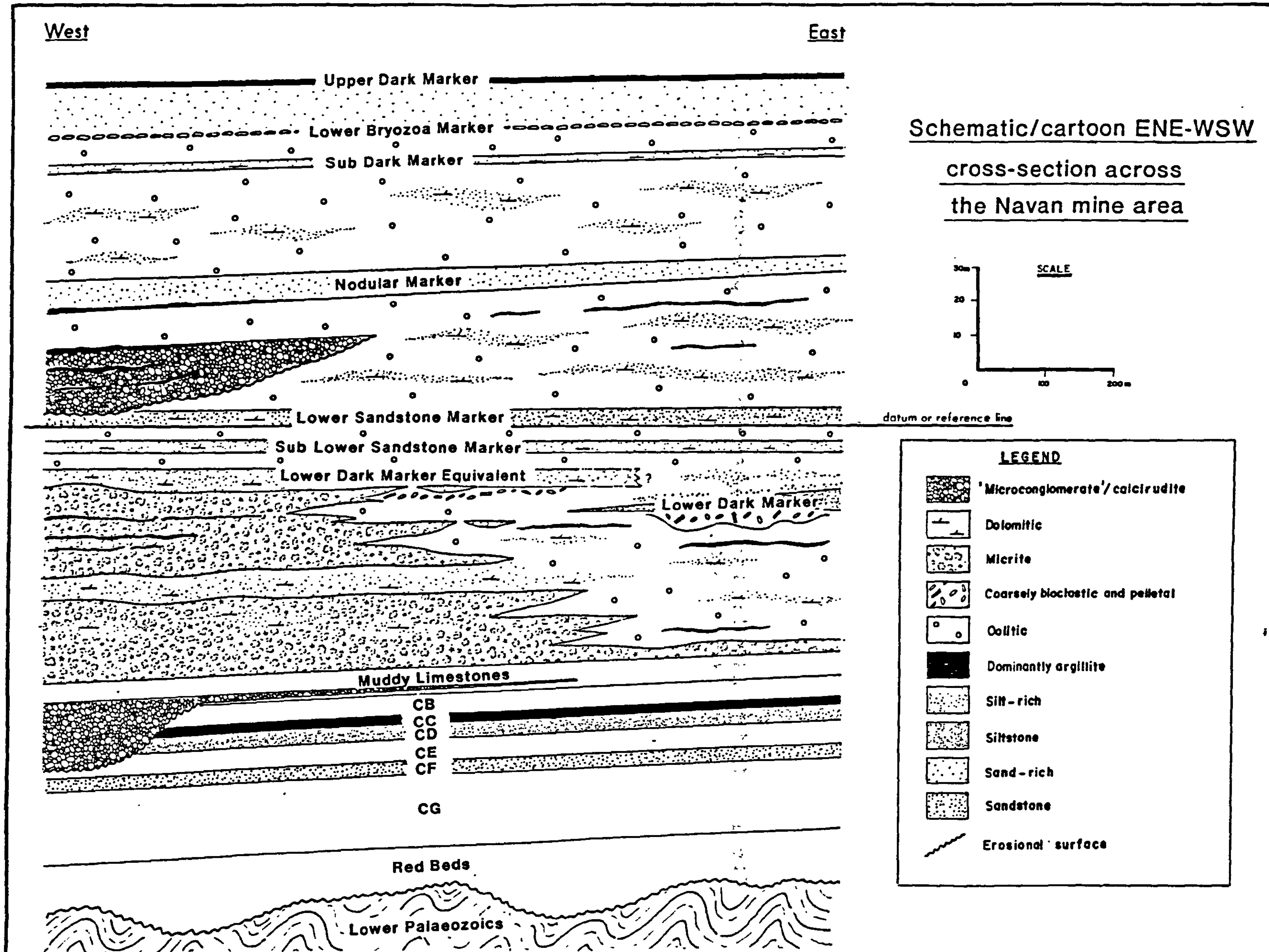
West
East
Upper Dark Marker
Lower Bryozoa Marker
Sub Dark Marker
Nodular Marker
Lower Sandstone Marker
Sub Lower Sandstone Marker
Lower Dark Marker Equivalent
Lower Dark Marker
Muddy Limestones
CB
CC
CD
CE
CF
CG
Red Beds
Lower Palaeozoics
Schematic/cartoon ENE-WSW
cross-section across
the Navan mine area
SCALE
datum or reference line
LEGEND
'Microconglomerate'/calcirudite
Dolomitic
Micrite
Coarsely bioclastic and pelletal
Oolitic
Dominantly argillite
Silt-rich
Siltstone
Sand-rich
Sandstone
Erosional surface

Figure 3.5 Plan view of the major facies variations and trends across the Navan mine area.

THE LOCATION AND TRENDS OF FACIES CHANGES
IN THE NAVAN MINE AREA
Tara N
National N
Muddy Limestone
CB
CC
CD
oncolite bed
CE
Thickest microconglomerates in the ML developed in this area
Muddy Limestones resting on the CE unit of the Lam. Beds
(below oncolite bed)
(above oncolite bed)
Muddy Limestones resting on the CD unit of the Laminated Beds
Muddy Limestones resting on the CC unit of the Laminated Beds
Muddy Limestones resting on the CB unit of the Laminated Beds
Approximate limit of 3 Lens "microconglomerates"
Limit of shale development in upper sections of the micrites
Substantial thickening of the micrites west of this "line"
Limit of development of the Lower Dark Marker
LDM siltstone is greater than 5m thick east of this line
RIVER BLACKWATER CENTRE LINE
1 Zone
2 Zone
3 Zone
?
?
B Fault at FW of 1-5 Lens
B Fault at FW of 2-5 Lens
T Fault at FW of 2-5 Lens
A Fault at FW of 2-5 Lens
LEGEND
Fault
Mining Limit
SCALE
0 20 40 60 80m
I.K. ANDERSON
Ph D THESIS
1990
"ORE DEPOSITIONAL
PROCESSES..."

Figure 3.6 Contoured plan of the thickness of micrites across the Navan mine area.

CONTOURING OF THE THICKNESS OF THE MICRITE UNIT
IN 1 ZONE (thicknesses include the MLT)
Tara N
National N
① THINING HERE IS DUE TO THE UPPER SECTIONS OF THE MICRITE UNIT RAPIDLY DYING OUT
② MICRITES THICKENING FROM THE BASE DOWNWARDS
Cartoon sketch illustrating features ① and ②
MICRITE UNIT
MICRITE UNIT IS LESS THAN 20m THICK, BUT EXTREMELY DIFFICULT TO CONTOUR
THINNED MICRITES PROBABLY DUE TO NE-SW FAULTING
THINNED MICRITES PROBABLY DUE TO NE-SW FAULTING
RIVER BLACKWATER CENTRE LINE
1 Zone
2 Zone
3 Zone
B Fault at FW of 1-5 Lens
B Fault at FW of 2-5 Lens
T Fault at FW of 2-5 Lens
LEGEND
50m Thickness contour for the micrites
50m Inferred contour
Fault
Mining limit
SCALE
0 20 40 60 80m
I.K. ANDERSON
PhD THESIS
1990
"ORE DEPOSITIONAL PROCESSES ...."

Figure 3.7 Diagram illustrating a tidal channel model to explain the thinning of the micrites in the central mine area.

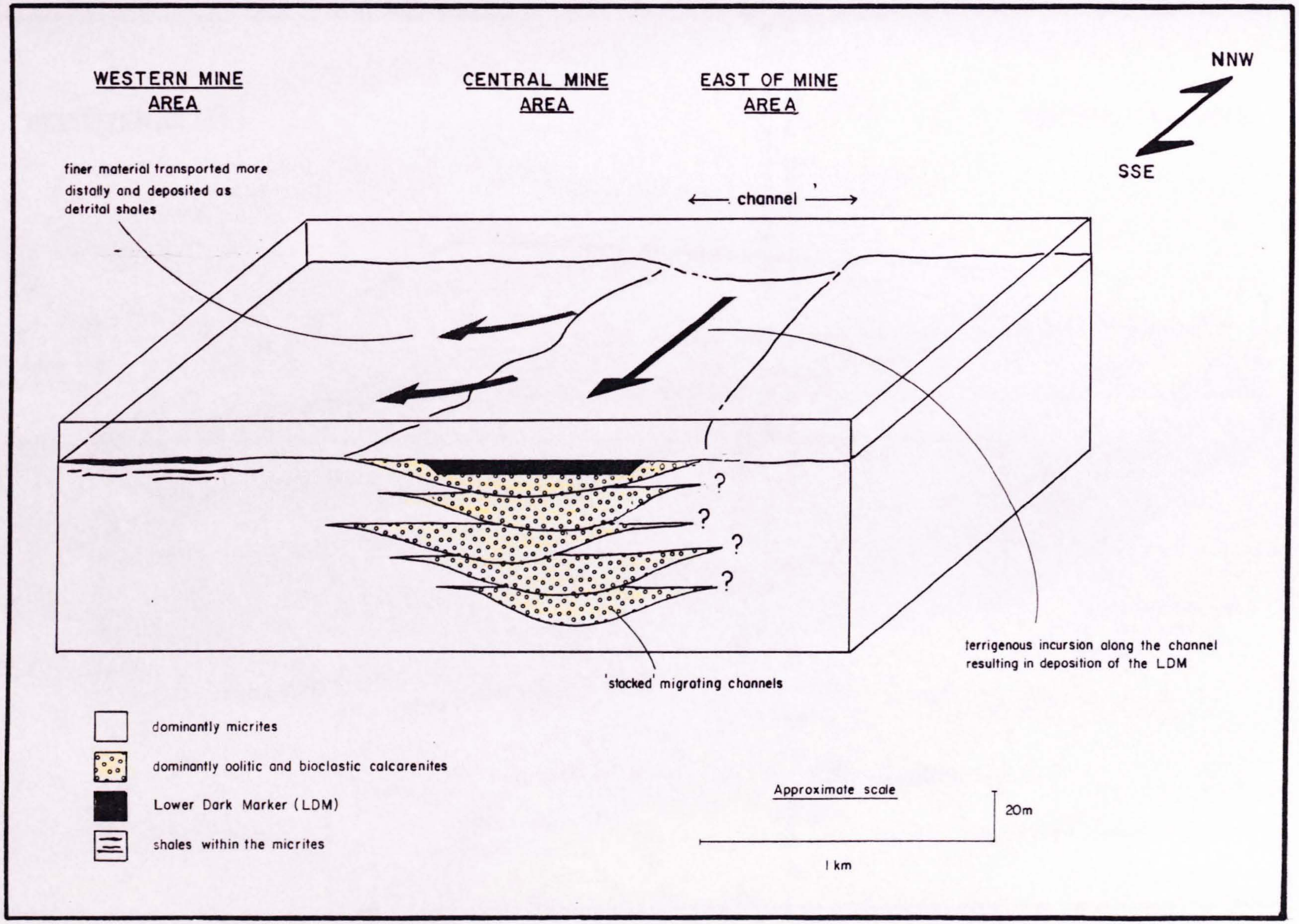

WESTERN MINE AREA
CENTRAL MINE AREA
EAST OF MINE AREA
NNW
SSE
finer material transported more distally and deposited as detrital shales
channel
?
?
?
?
terrigenous incursion along the channel resulting in deposition of the LDM
'stacked' migrating channels
dominantly micrites
dominantly oolitic and bioclastic calcarenites
Lower Dark Marker (LDM)
shales within the micrites
Approximate scale
20m
1 km

Figure 3.8 Diagram illustrating a palaeoslope model to explain the thinning of the micrites in the central mine area.

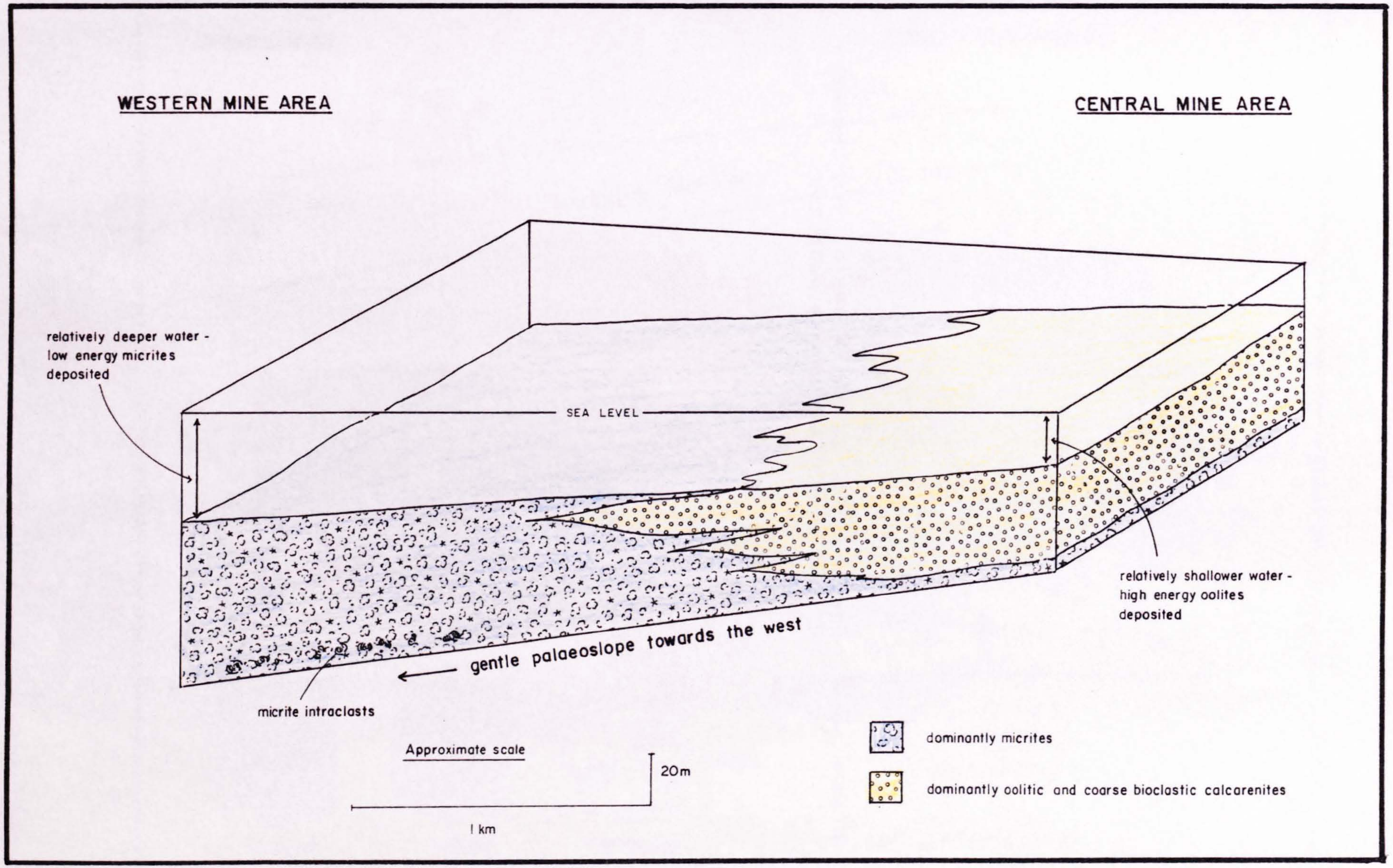
WESTERN MINE AREA
CENTRAL MINE AREA
relatively deeper water - low energy micrites deposited
SEA LEVEL
relatively shallower water - high energy oolites deposited
gentle palaeoslope towards the west
micrite intraclasts
Approximate scale
20m
1 km
dominantly micrites
dominantly oolitic and coarse bioclastic calcarenites

Figure 3.9 Diagrammatic illustration of the features of the 3 Lens microconglomerates.

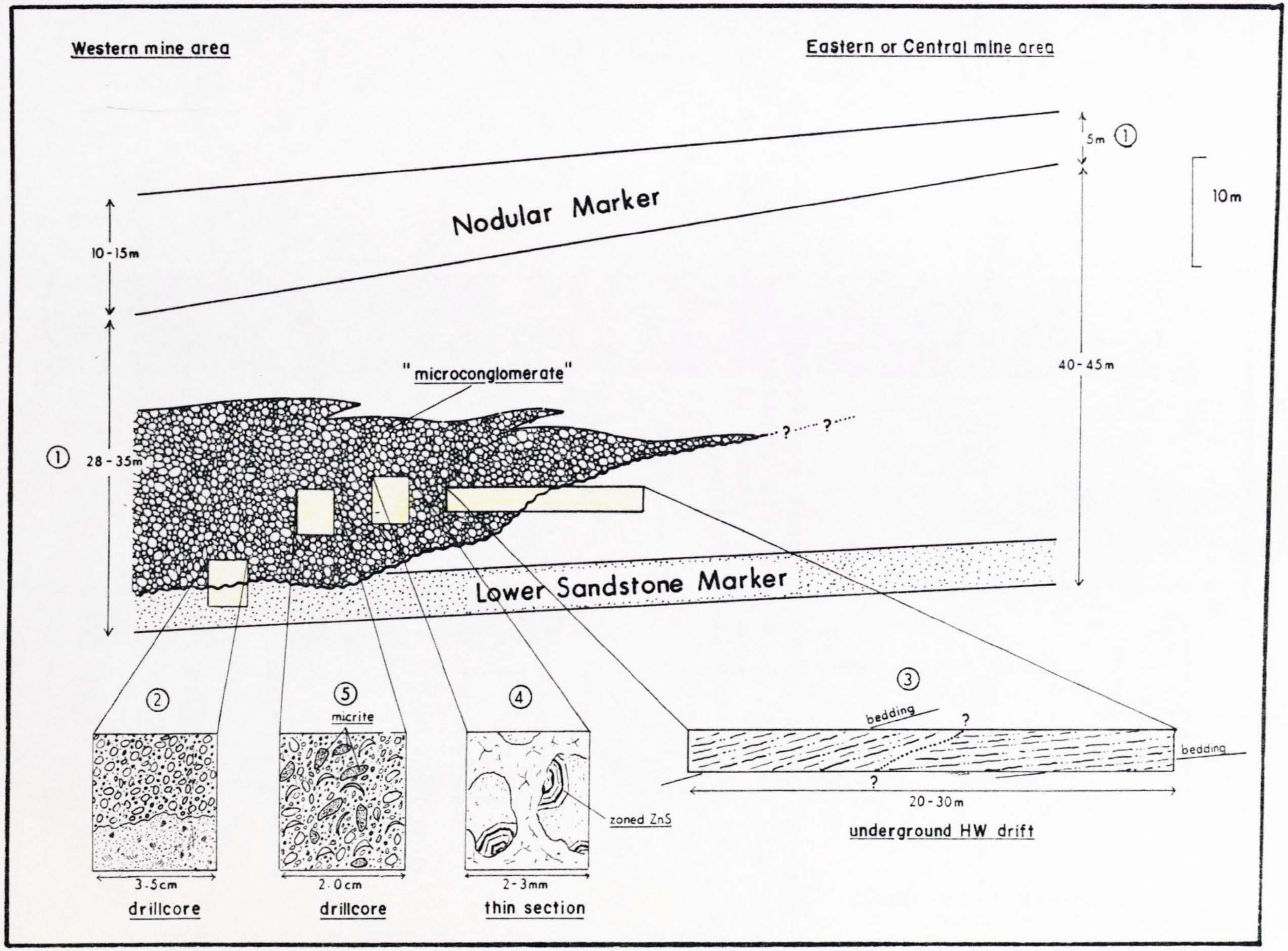
Western mine area
Eastern or Central mine area
5m ①
10m
Nodular Marker
10-15m
40-45m
"microconglomerate"
? ····· ? ·····
① 28-35m
Lower Sandstone Marker
②
⑤
④
③
micrite
bedding
?
bedding
?
zoned ZnS
3.5cm
drillcore
2.0cm
drillcore
2-3mm
thin section
20-30m
underground HW drift

Figure 3.10 Depositional environment for the Lower Carboniferous stratigraphy in the Navan mine area (inset is a comparison with the Bowland Basin).

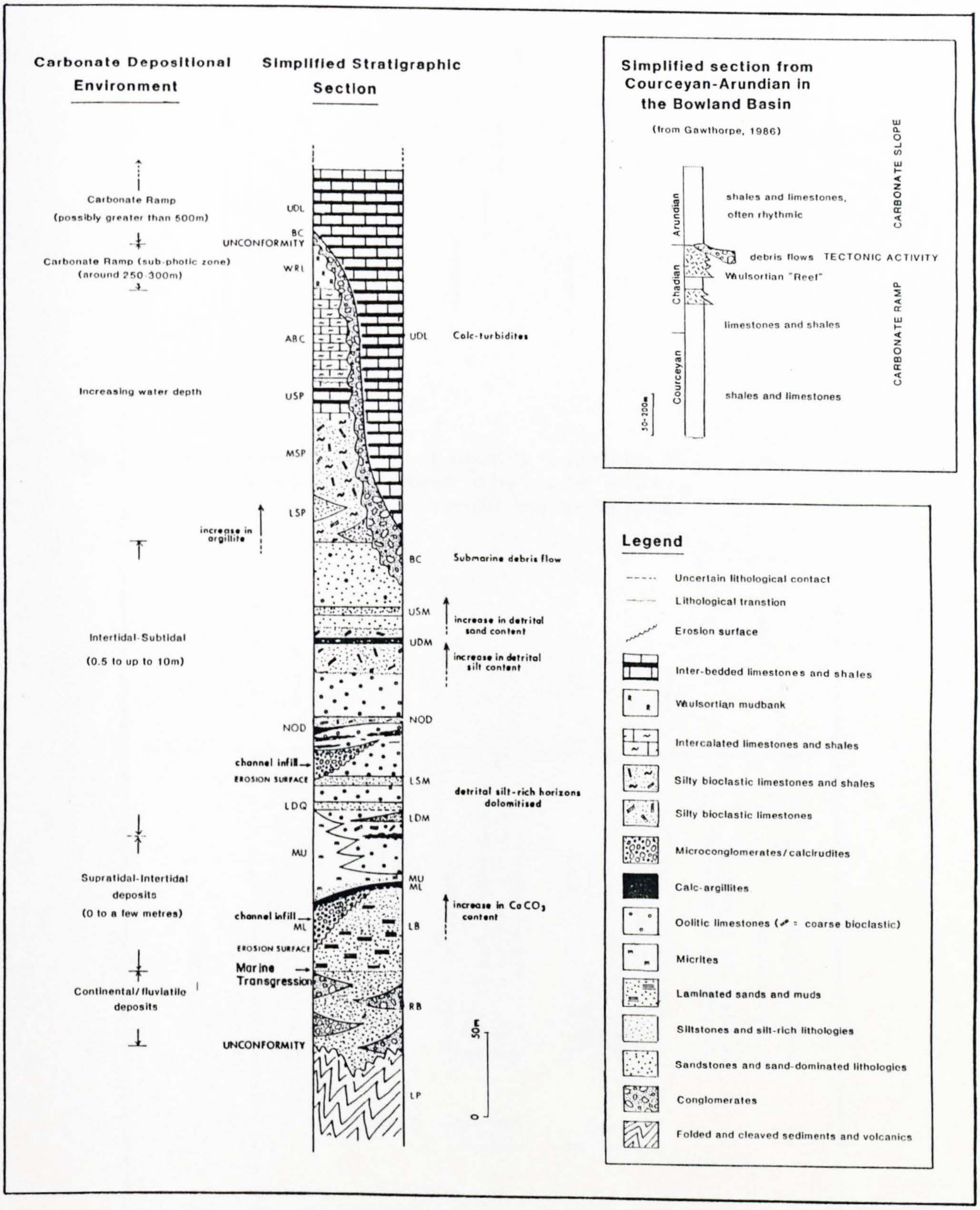

Carbonate Depositional Environment
Simplified Stratigraphic Section
Carbonate Ramp (possibly greater than 500m)
Carbonate Ramp (sub-photic zone) (around 250-300m)
Increasing water depth
increase in argillite
Intertidal-Subtidal (0.5 to up to 10m)
Supratidal-Intertidal deposits (0 to a few metres)
Continental/fluviatile deposits
UDL
BC
UNCONFORMITY
WRL
ABC
USP
MSP
LSP
NOD
channel infill
EROSION SURFACE
LDQ
MU
ML
Marine Transgression
UNCONFORMITY
UDL
Calc-turbidites
BC
Submarine debris flow
USM
increase in detrital sand content
UDM
increase in detrital silt content
NOD
LSM
detrital silt-rich horizons dolomitised
LDM
MU
ML
LB
increase in $CaCO_3$ content
RB
LP
50m
0
Simplified section from Courceyan-Arundian in the Bowland Basin
(from Gawthorpe, 1986)
Arundian
Chadian
Courceyan
shales and limestones, often rhythmic
debris flows
TECTONIC ACTIVITY
Waulsortian "Reef"
limestones and shales
shales and limestones
CARBONATE SLOPE
CARBONATE RAMP
50-200m
Legend
Uncertain lithological contact
Lithological transtion
Erosion surface
Inter-bedded limestones and shales
Waulsortian mudbank
Intercalated limestones and shales
Silty bioclastic limestones and shales
Silty bioclastic limestones
Microconglomerates/calcirudites
Calc-argillites
Oolitic limestones (= coarse bioclastic)
Micrites
Laminated sands and muds
Siltstones and silt-rich lithologies
Sandstones and sand-dominated lithologies
Conglomerates
Folded and cleaved sediments and volcanics

Figure 4.1 Simplified summary of the diagenetic stages within the Pale Beds limestones and dolomites at Navan.

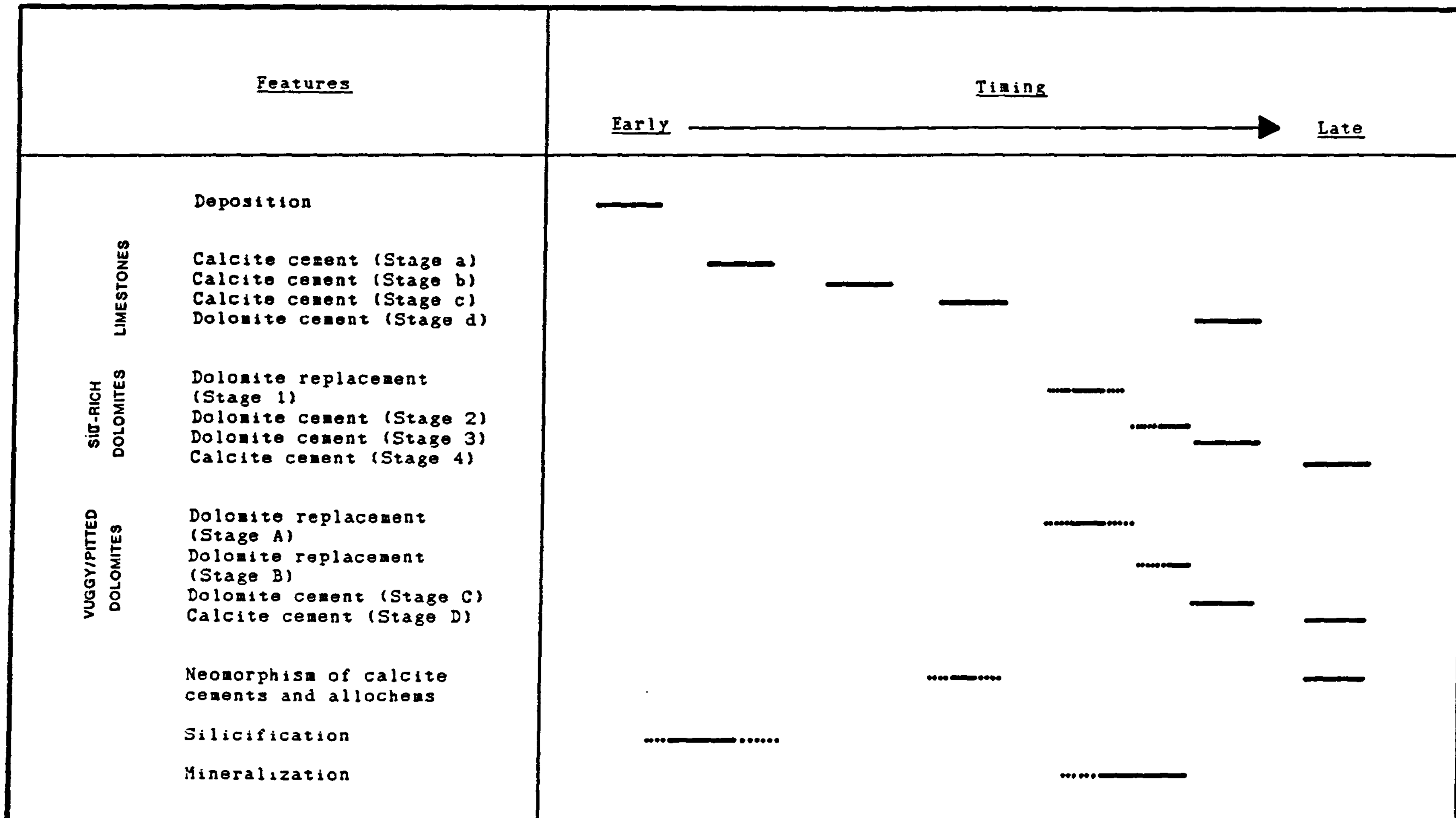
Features
Timing
Early
Late
Deposition
LIMESTONES
Calcite cement (Stage a)
Calcite cement (Stage b)
Calcite cement (Stage c)
Dolomite cement (Stage d)
SILT-RICH DOLOMITES
Dolomite replacement (Stage 1)
Dolomite cement (Stage 2)
Dolomite cement (Stage 3)
Calcite cement (Stage 4)
VUGGY/PITTED DOLOMITES
Dolomite replacement (Stage A)
Dolomite replacement (Stage B)
Dolomite cement (Stage C)
Calcite cement (Stage D)
Neomorphism of calcite cements and allochems
Silicification
Mineralization

Figure 4.2 Diagram illustrating the carbonate cement sequence in thin sections prepared from typical Pale Beds oolitic calcarenites; transmitted light vs cathodoluminescence.

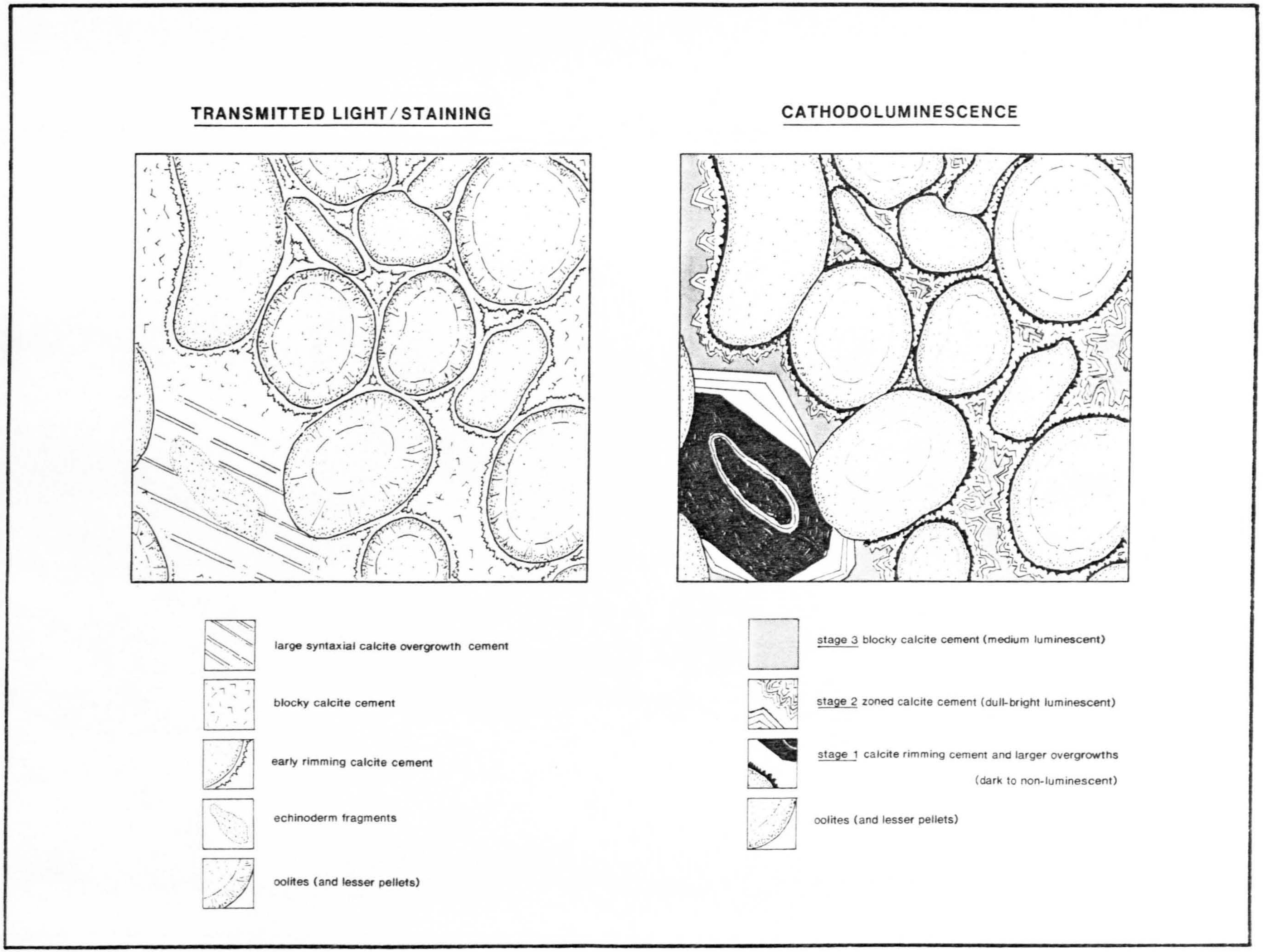
TRANSMITTED LIGHT/STAINING
CATHODOLUMINESCENCE
large syntaxial calcite overgrowth cement
blocky calcite cement
early rimming calcite cement
echinoderm fragments
oolites (and lesser pellets)
stage 3 blocky calcite cement (medium luminescent)
stage 2 zoned calcite cement (dull-bright luminescent)
stage 1 calcite rimming cement and larger overgrowths (dark to non-luminescent)
oolites (and lesser pellets)

Figure 4.3 Diagram illustrating the carbonate cement sequence in thin sections prepared from typical Pale Beds bioclastic calcarenites; transmitted light vs cathodoluminescence.

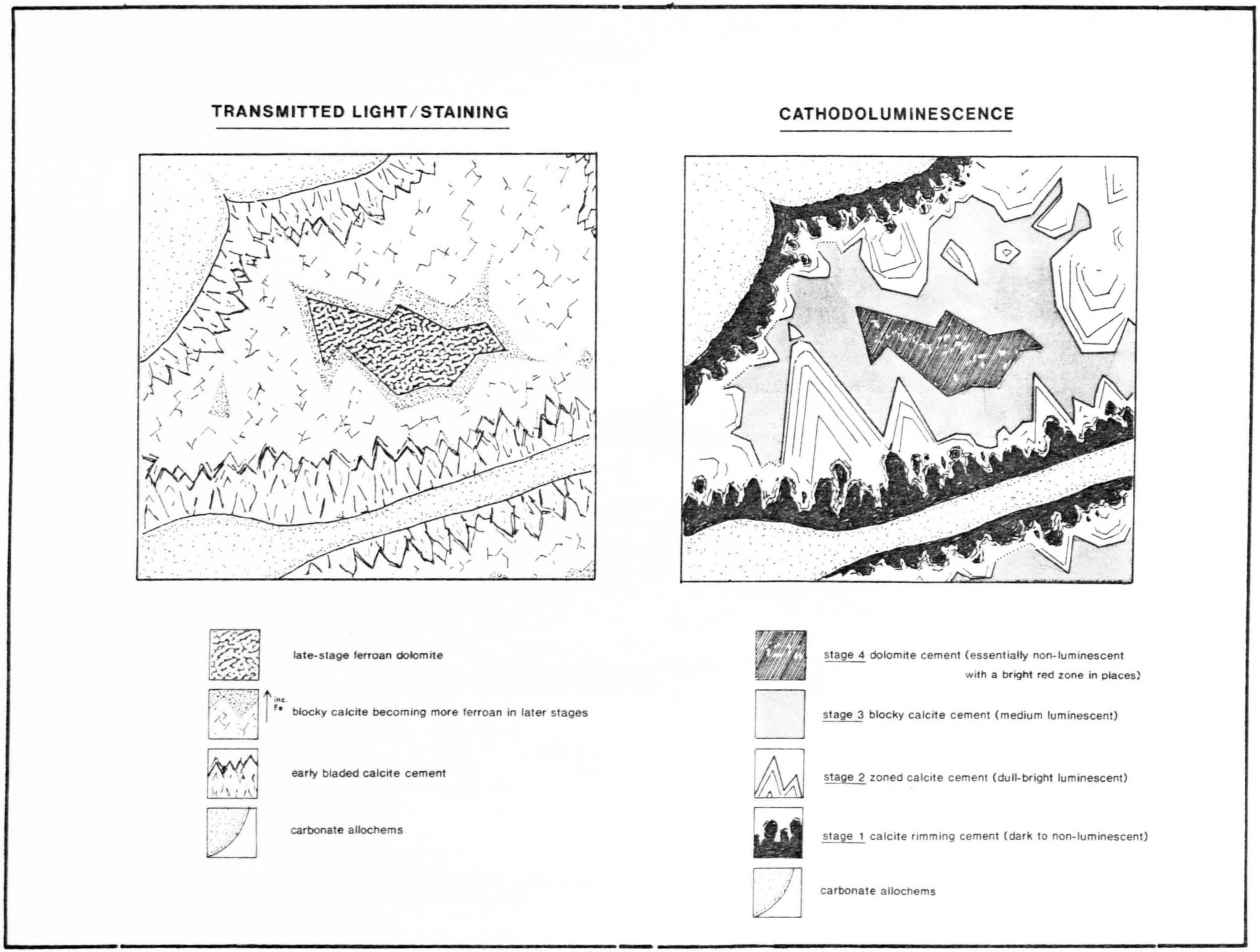
TRANSMITTED LIGHT/STAINING
CATHODOLUMINESCENCE
late-stage ferroan dolomite
inc. Fe
blocky calcite becoming more ferroan in later stages
early bladed calcite cement
carbonate allochems
stage 4 dolomite cement (essentially non-luminescent with a bright red zone in places)
stage 3 blocky calcite cement (medium luminescent)
stage 2 zoned calcite cement (dull-bright luminescent)
stage 1 calcite rimming cement (dark to non-luminescent)
carbonate allochems

Figure 5.1 The location in plan view of underground headings referred to in the text. The position of the faults is defined by their intersection with the base of the 5 Lens.

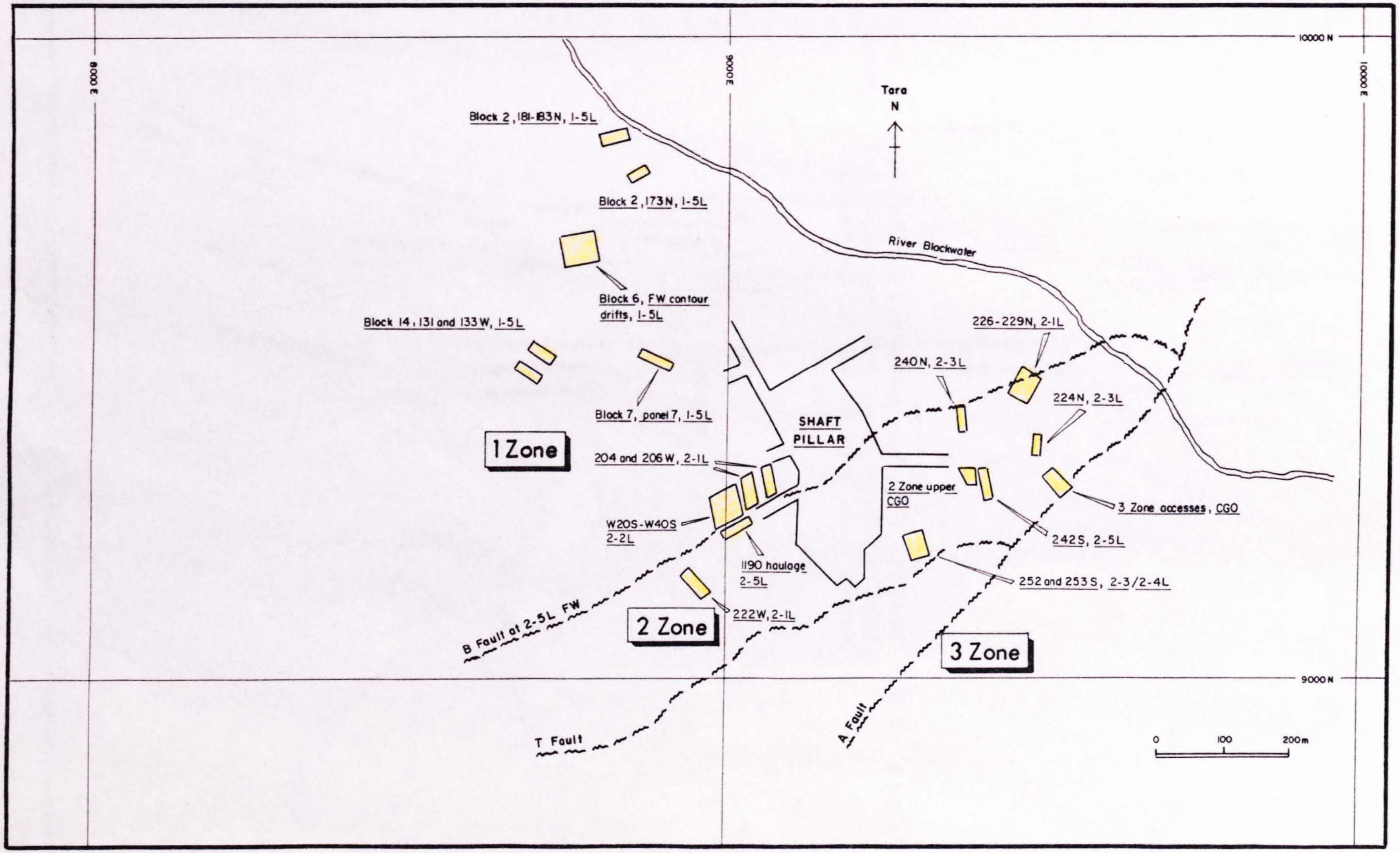
10000 N
9000 N
8000 E
9000 E
10000 E
Tara
N
River Blackwater
Block 2, 181-183N, 1-5L
Block 2, 173N, 1-5L
Block 6, FW contour drifts, 1-5L
Block 14, 131 and 133W, 1-5L
Block 7, panel 7, 1-5L
1 Zone
SHAFT PILLAR
204 and 206W, 2-1L
W20S-W40S 2-2L
1190 haulage 2-5L
222W, 2-1L
2 Zone
B Fault at 2-5L FW
T Fault
A Fault
226-229N, 2-1L
240N, 2-3L
224N, 2-3L
2 Zone upper CGO
3 Zone accesses, CGO
242S, 2-5L
252 and 253S, 2-3/2-4L
3 Zone
0
100
200m

Figure 5.2 Diagram from an underground heading in 2-1 Lens illustrating bedding-parallel, sphalerite replacement of calcarenites.

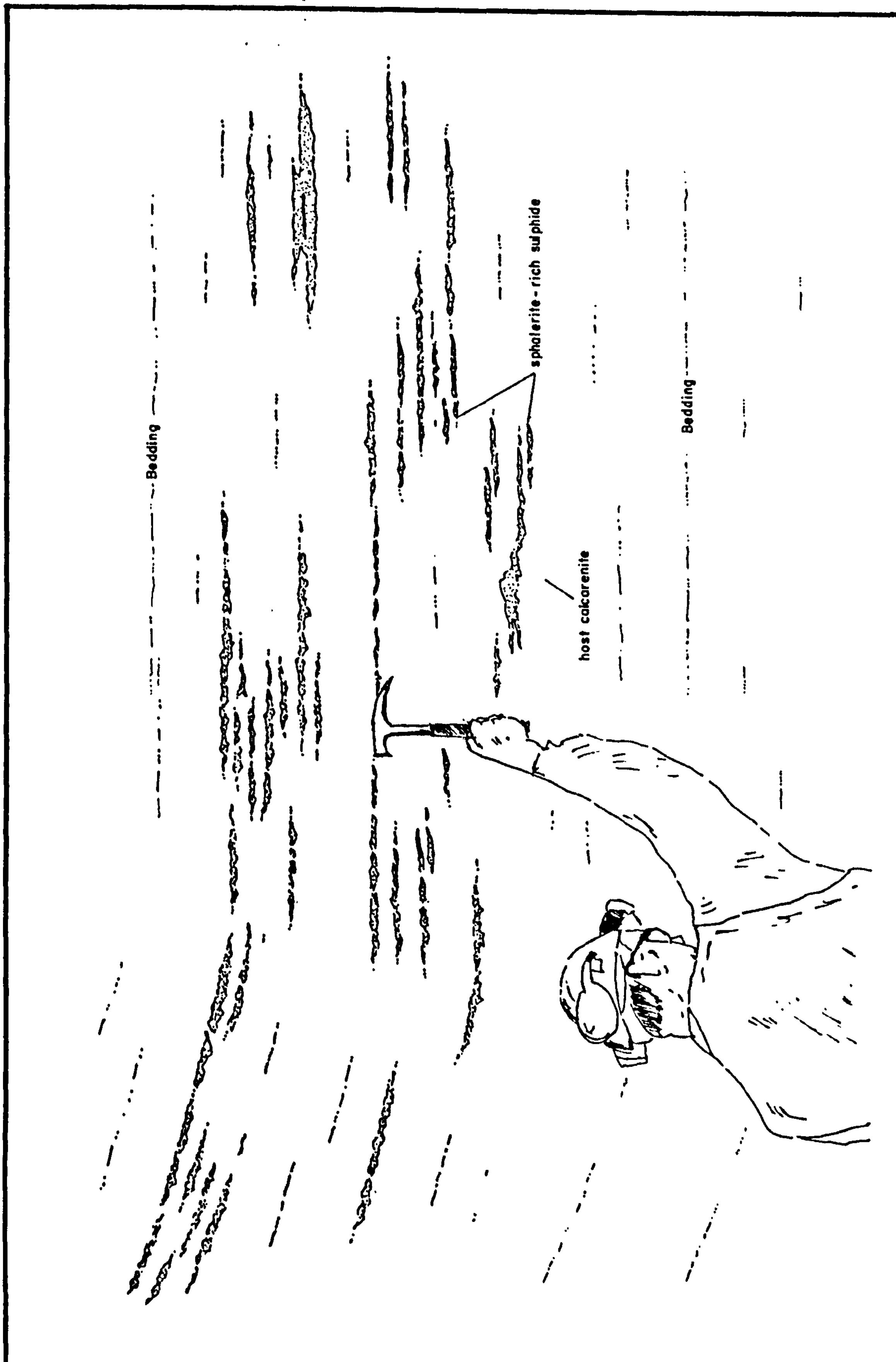
Bedding
sphalerite-rich sulphide
host calcarenite
Bedding

Figure 5.3 Diagram from an underground heading in 2-3 Lens (240N) illustrating bedding-parallel, sphalerite-rich replacement of calcarenites.

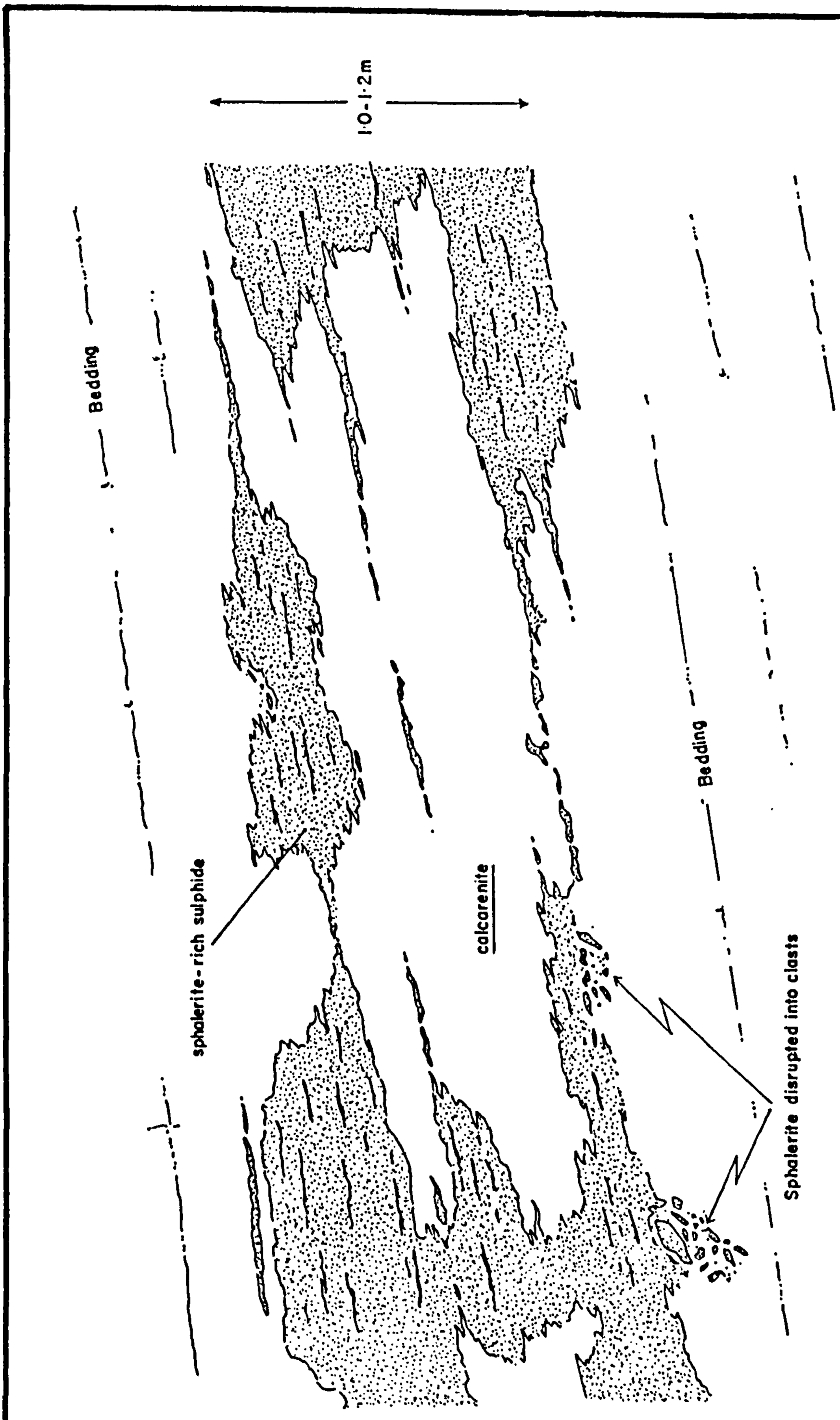
1·0-1·2m
Bedding
Bedding
sphalerite-rich sulphide
calcarenite
Sphalerite disrupted into clasts

Figure 5.4 Diagram from an underground heading in 2-1 Lens, (206W), illustrating sphalerite replacing calcarenites around a small bedding-parallel cavity, with the cavity itself infilled by laminated argillite/sphalerite and blocky calcite/dolomite.

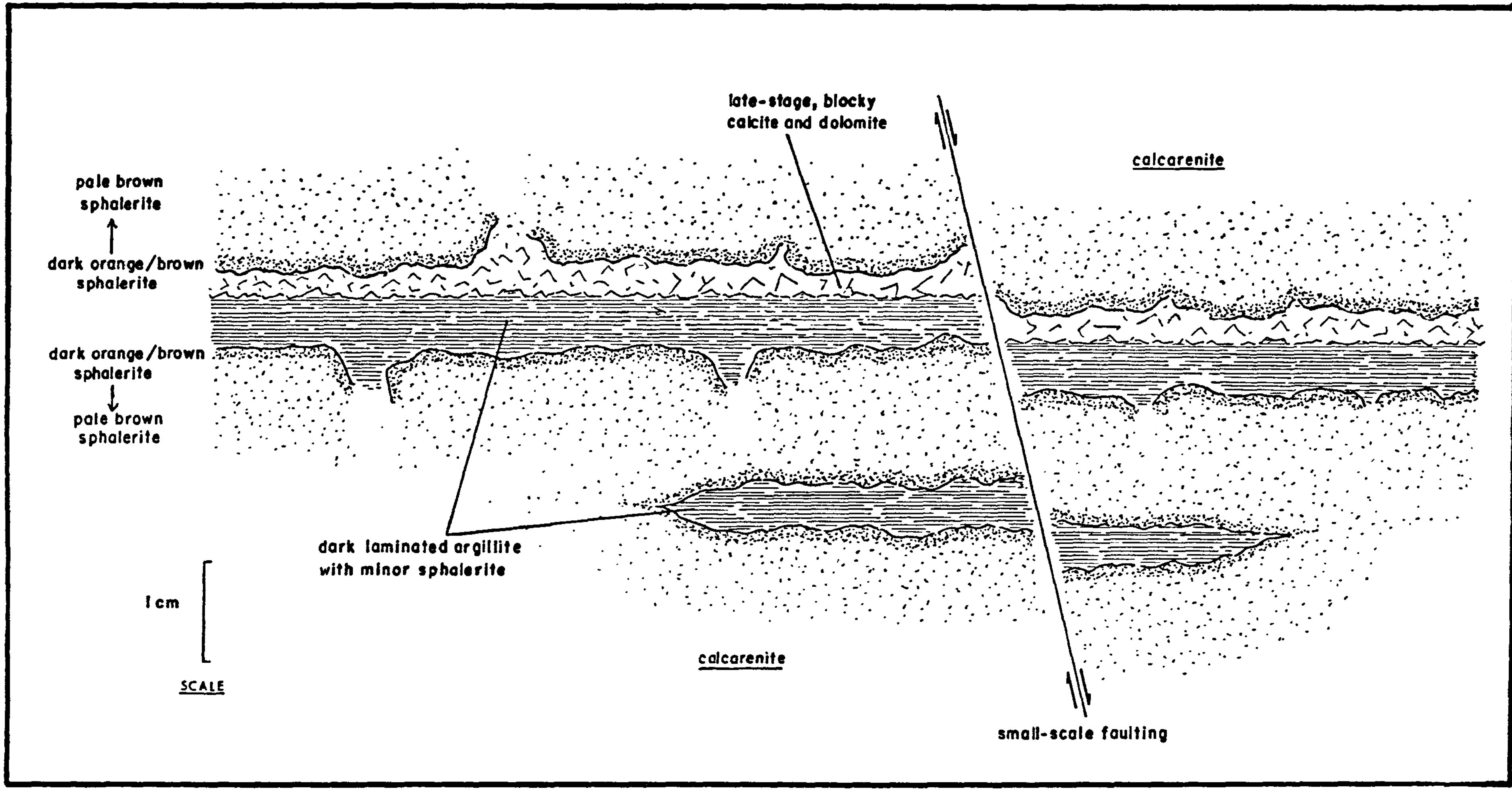
pale brown
sphalerite
dark orange/brown
sphalerite
dark orange/brown
sphalerite
pale brown
sphalerite
late-stage, blocky
calcite and dolomite
calcarenite
dark laminated argillite
with minor sphalerite
1 cm
SCALE
calcarenite
small-scale faulting

Figure 5.5a Diagram from an underground heading in 2-1 Lens (204W) illustrating stalactitic sulphides within a small, bedding-parallel cavity.

Figure 5.5b Diagram from the same underground heading as Figure 5.5a illustrating colloform and laminated sulphides within a small, bedding-parallel cavity.

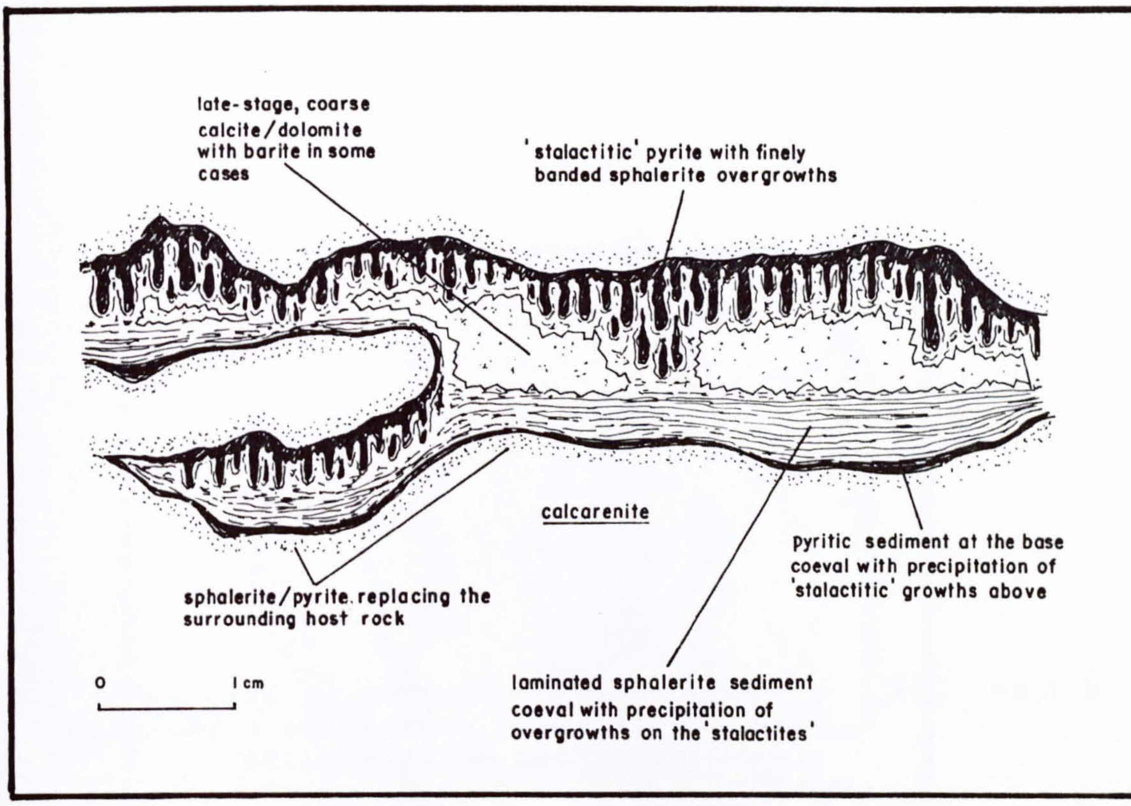
late-stage, coarse calcite/dolomite with barite in some cases
'stalactitic' pyrite with finely banded sphalerite overgrowths
calcarenite
pyritic sediment at the base coeval with precipitation of 'stalactitic' growths above
sphalerite/pyrite replacing the surrounding host rock
laminated sphalerite sediment coeval with precipitation of overgrowths on the 'stalactites'
0
1 cm

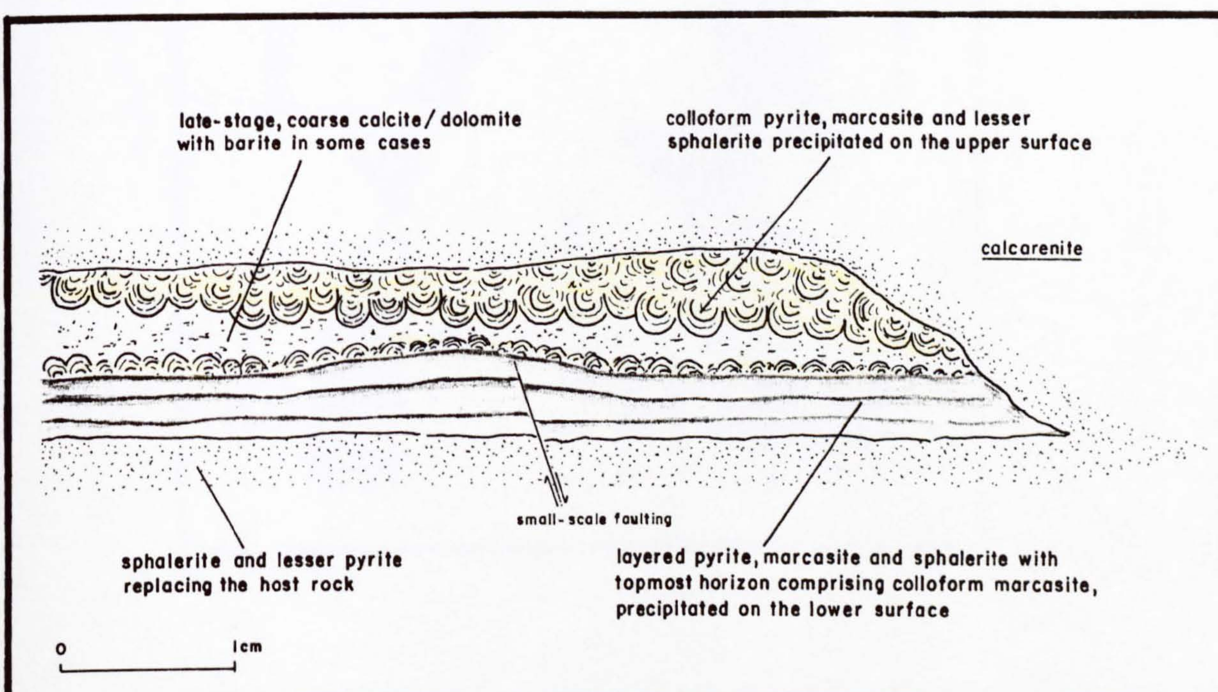
late-stage, coarse calcite/dolomite with barite in some cases
colloform pyrite, marcasite and lesser sphalerite precipitated on the upper surface
calcarenite
small-scale faulting
sphalerite and lesser pyrite replacing the host rock
layered pyrite, marcasite and sphalerite with topmost horizon comprising colloform marcasite, precipitated on the lower surface
0
1cm

Figure 5.6 Diagram from an underground heading in 2-3 Lens illustrating pull-apart structures within sulphides surrounded by calcarenites.

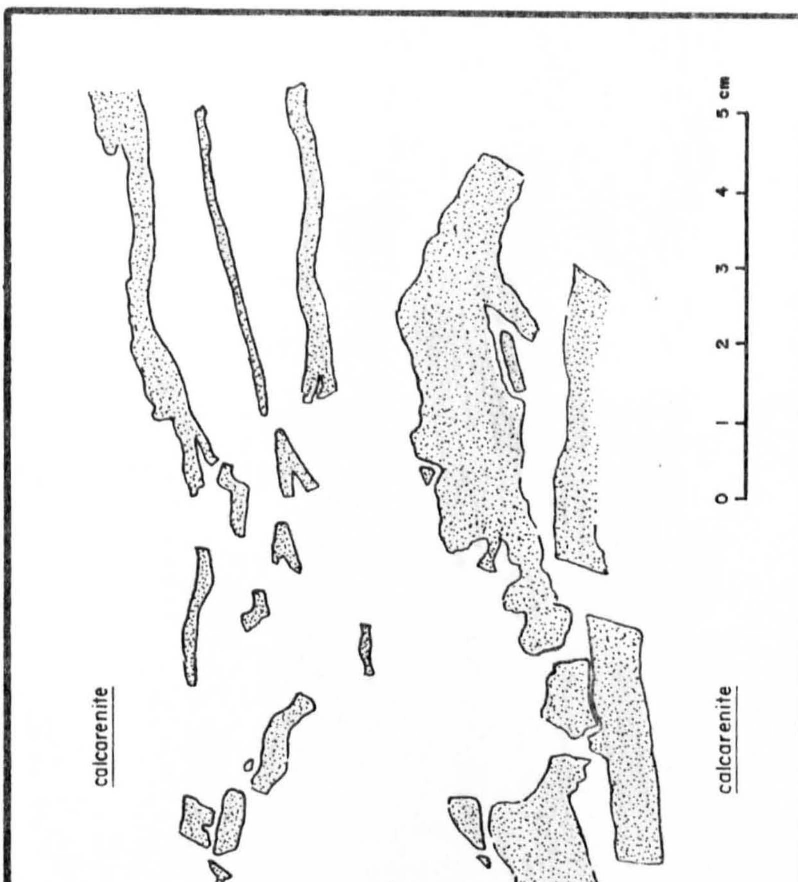
calcarenite
calcarenite
calcarenite
fine-grained ZnS
0 1 2 3 4 5 cm

Figure 5.7 Diagram from an underground heading in 1-5 Lens (173N) illustrating layered sulphides compacted around an unreplaced block of calcarenite.

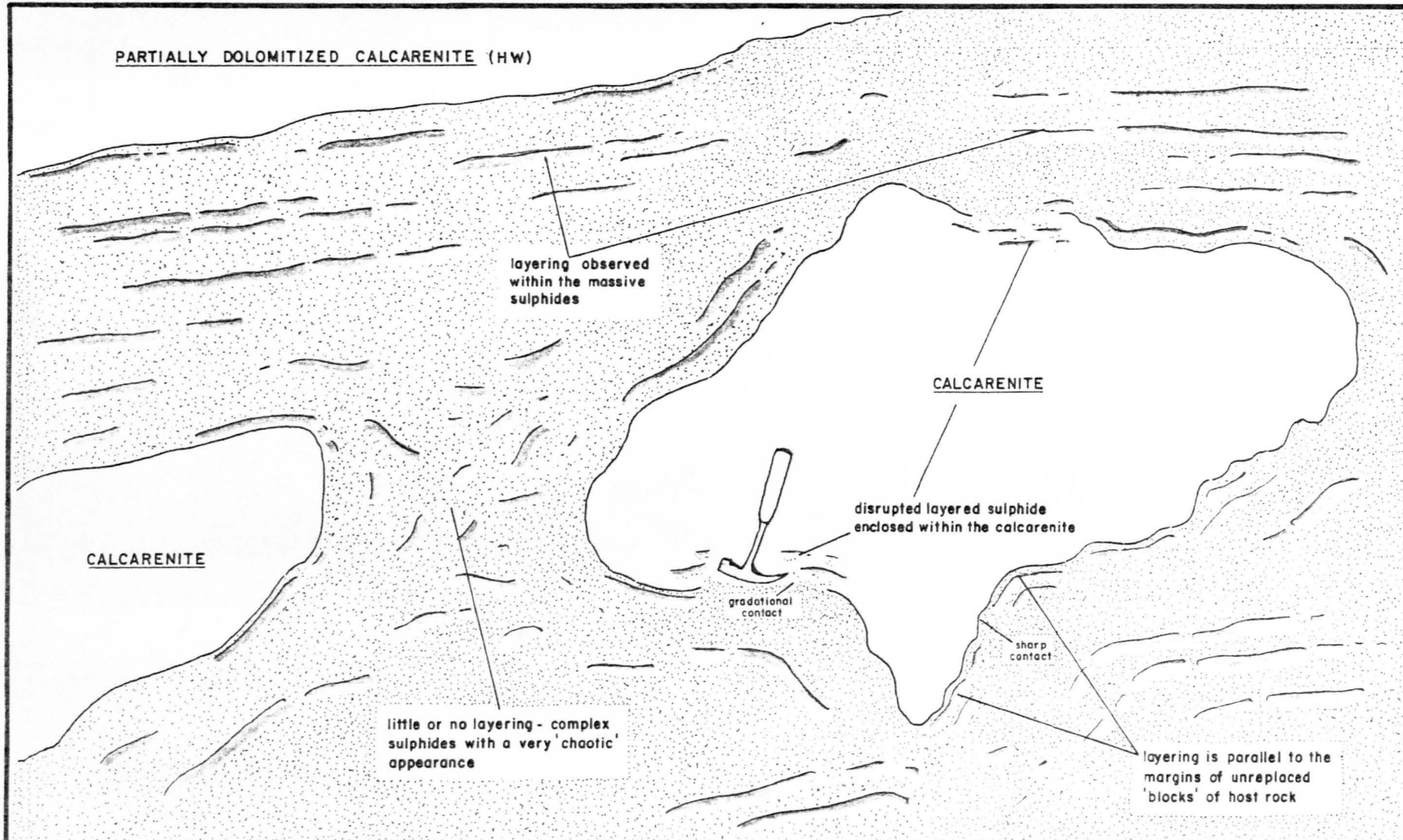
PARTIALLY DOLOMITIZED CALCARENITE (HW)
layering observed within the massive sulphides
CALCARENITE
disrupted layered sulphide enclosed within the calcarenite
CALCARENITE
gradational contact
sharp contact
little or no layering - complex sulphides with a very 'chaotic' appearance
layering is parallel to the margins of unreplaced 'blocks' of host rock

Figure 5.8 Diagram illustrating a mechanism to produce the features observed in Figure 5.7, during compaction of the stratigraphic section.

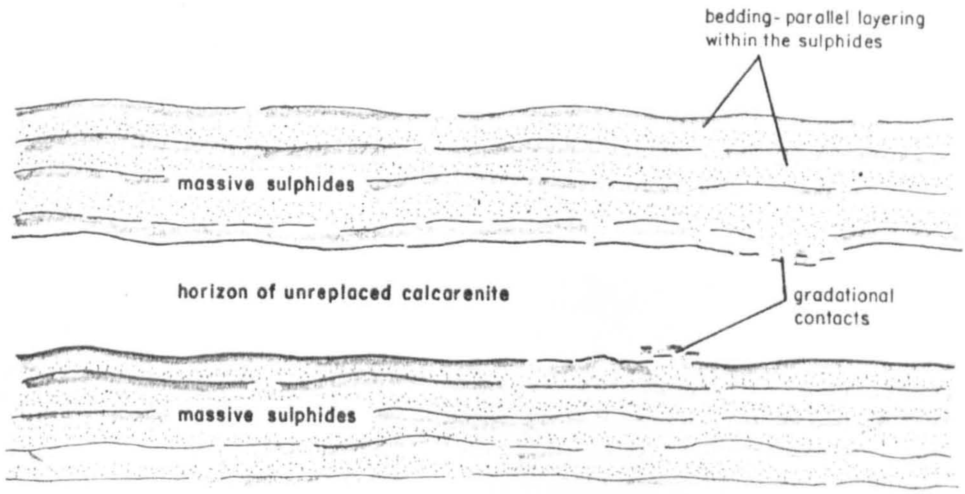

(a) Bedding-parallel replacement prior to compaction

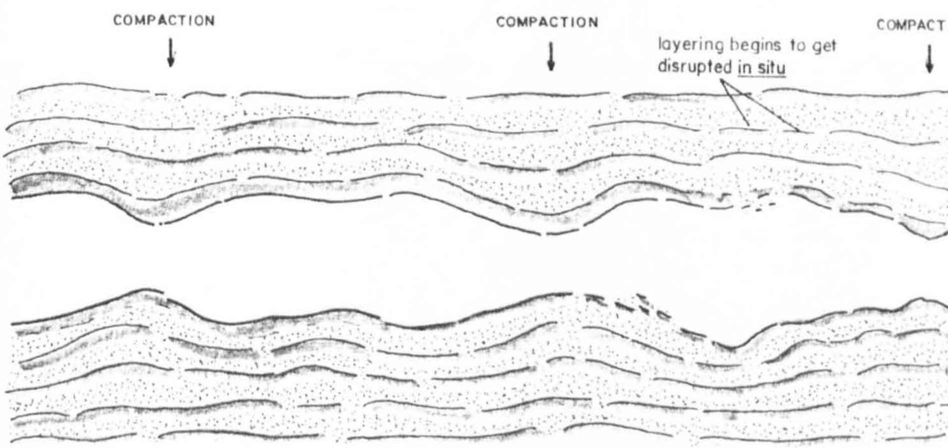

(b) Beginning of compaction and initiation of "boudinage-affect"

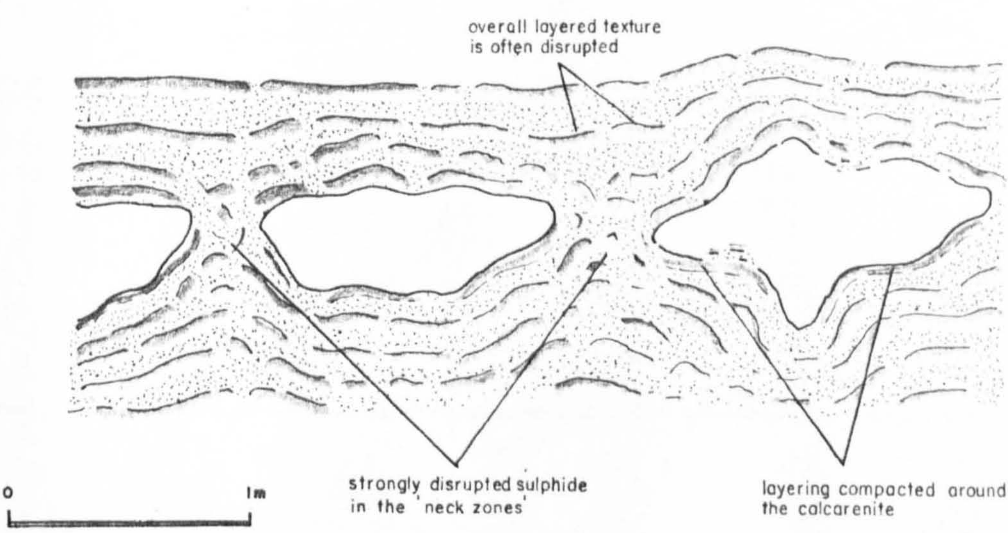

(c) Continual compaction gives rise to the presently observed situation

Figure 5.9 Diagram from an underground heading in 2-1 Lens illustrating a squashed or buckled, cross-cutting sulphide vein hosted in calcarenites, indicating that the vein formed while the calcarenites were still compacting.

Figure 5.10 Diagram from a handspecimen from 2-3 Lens (252/253S) illustrating collapsed sulphide clasts within a small, bedding-parallel cavity.

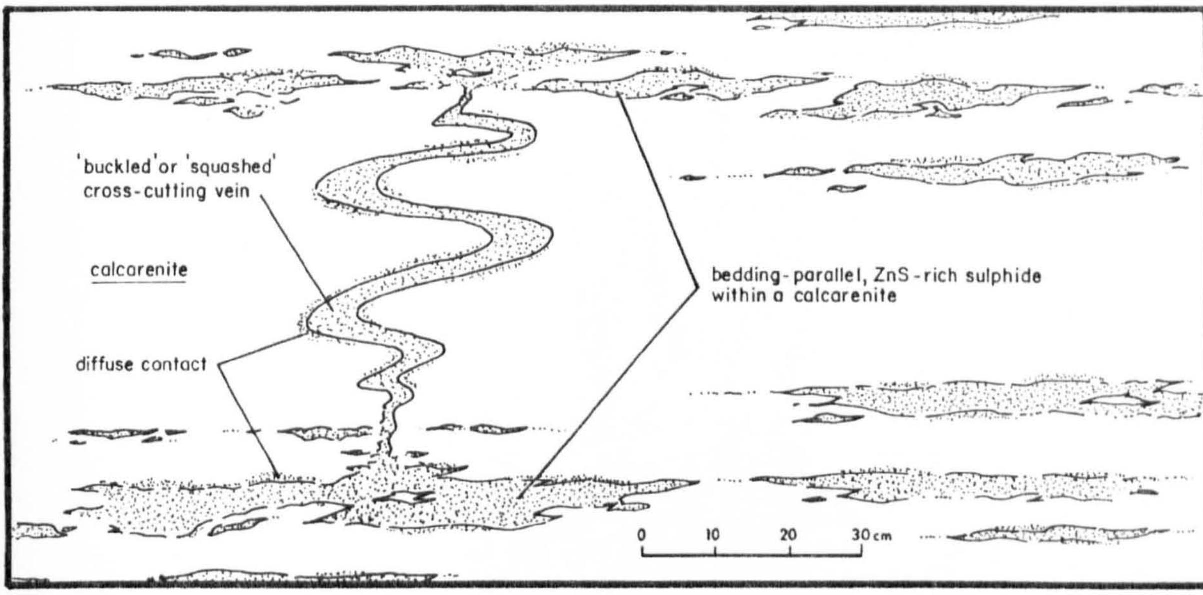
'buckled' or 'squashed'
cross-cutting vein
calcarenite
diffuse contact
bedding-parallel, ZnS-rich sulphide
within a calcarenite
0 10 20 30 cm

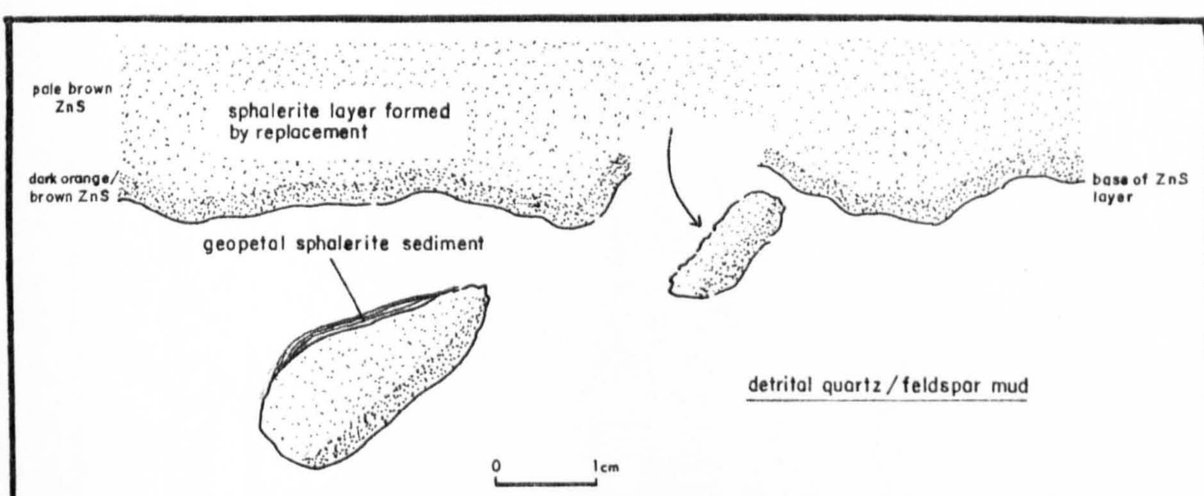
pale brown
ZnS
sphalerite layer formed
by replacement
dark orange/
brown ZnS
base of ZnS
layer
geopetal sphalerite sediment
detrital quartz / feldspar mud
0 1cm

Figure 5.11 Diagram from an underground heading in 2-4 Lens (252/253S) illustrating bedding-parallel sulphide stringers. The stringers consist of a thin veinlet of galena and sphalerite and a surrounding, diffuse halo dominated by sphalerite.

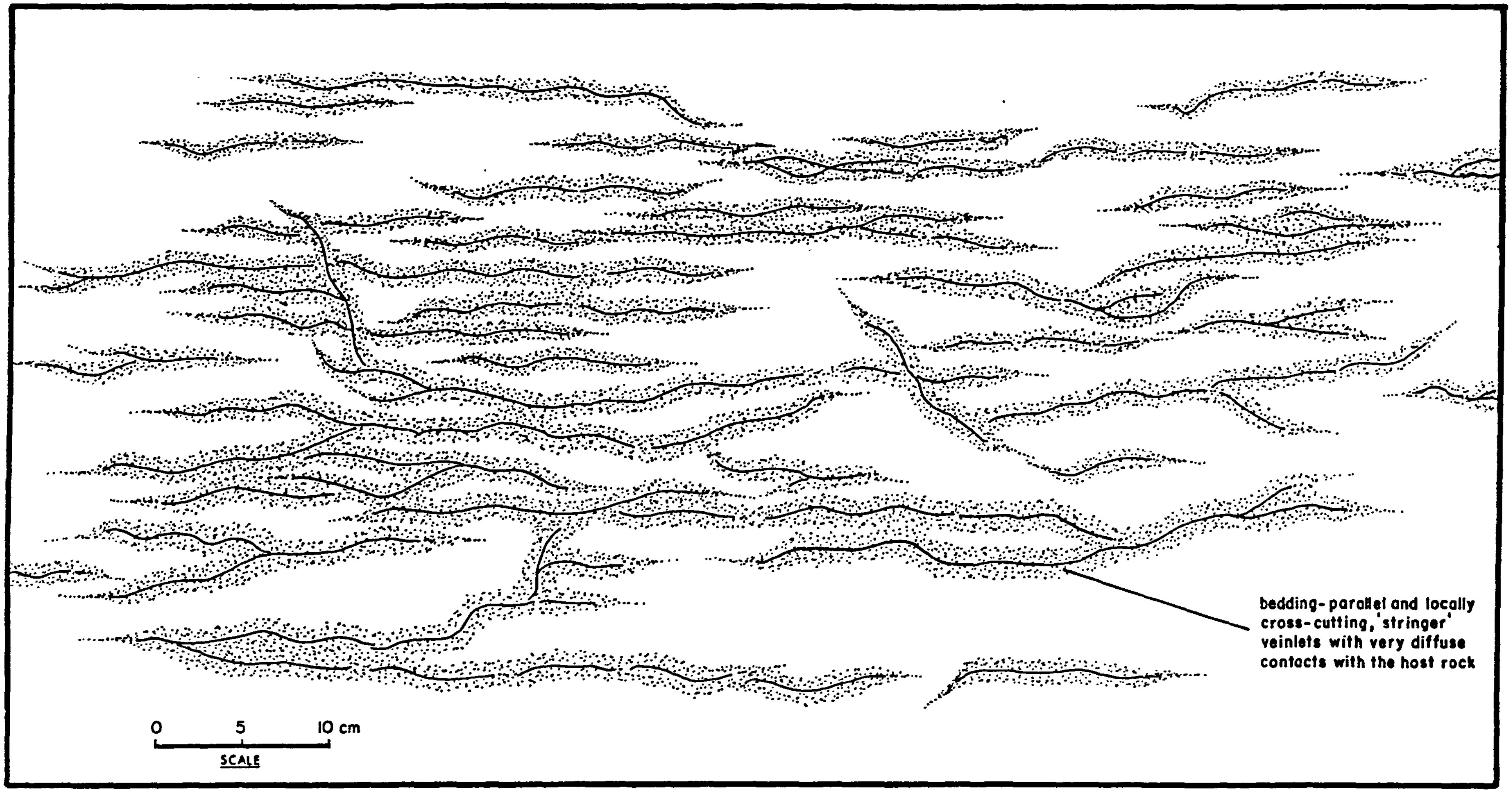
bedding-parallel and locally cross-cutting, 'stringer' veinlets with very diffuse contacts with the host rock
0 5 10 cm
SCALE

Figure 5.12a Diagram from a polished thin section prepared from the sphalerite halo around a bedding-parallel stringer veinlet (2-4 Lens, 252/253S), illustrating dolomite rhombs with sphalerite inclusions, in both reflected and cathodoluminescent light.

Figure 5.12b Reflected light diagram from the same polished thin section as Figure 5.12a, illustrating the relationships between sphalerite, authigenic dolomite and authigenic quartz overgrowths.

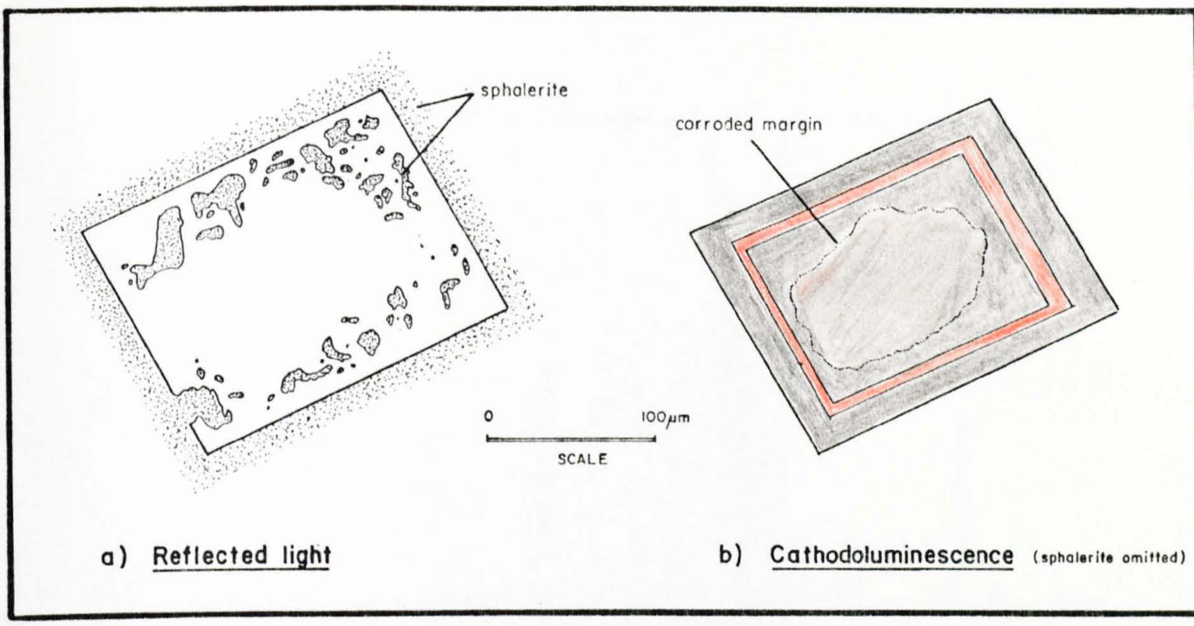
sphalerite
corroded margin
0
100μm
SCALE
a) Reflected light
b) Cathodoluminescence (sphalerite omitted)

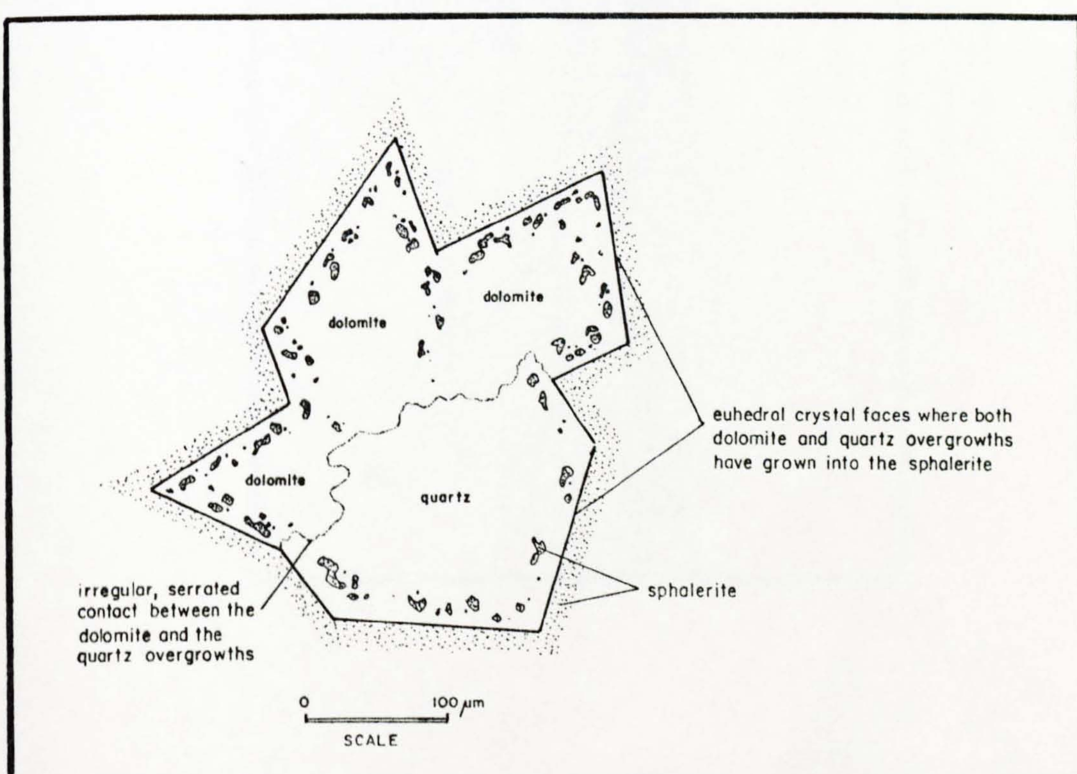
dolomite
dolomite
dolomite
quartz
euhedral crystal faces where both dolomite and quartz overgrowths have grown into the sphalerite
sphalerite
irregular, serrated contact between the dolomite and the quartz overgrowths
0
100μm
SCALE

Figure 5.13 Diagram from an underground heading in 2-2 Lens (W25S) mapped by mine geologists, illustrating the gross morphology of the massive sulphide horizon at the contact between an oolitic calcarenite and the overlying Nodular Marker.

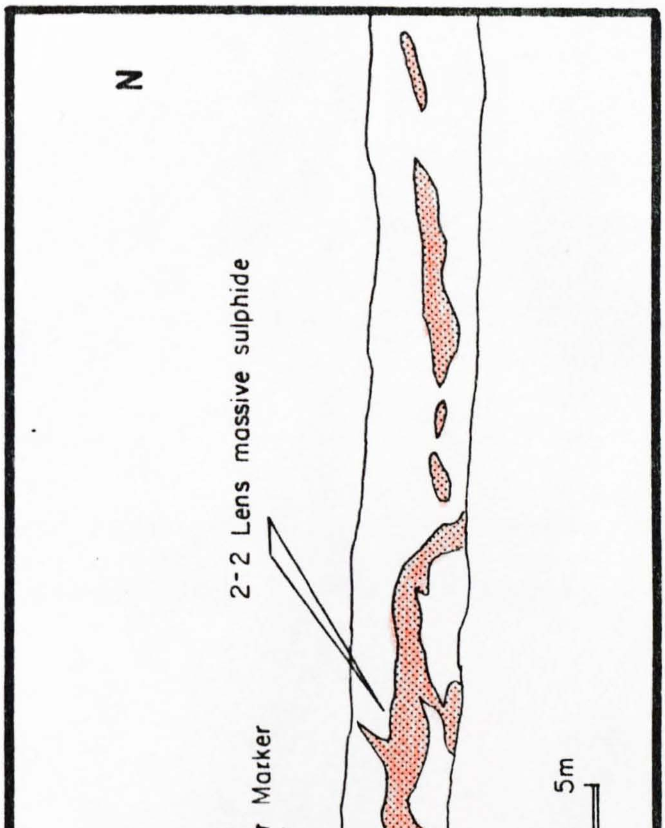
S
N
underground drift
Nodular Marker
2-2 Lens massive sulphide
oolitic calcarenite
0
5m

Figure 5.14 Diagrams from underground headings in 2-2 Lens (W20S-W40S) illustrating galena deposited within small cavity structures.

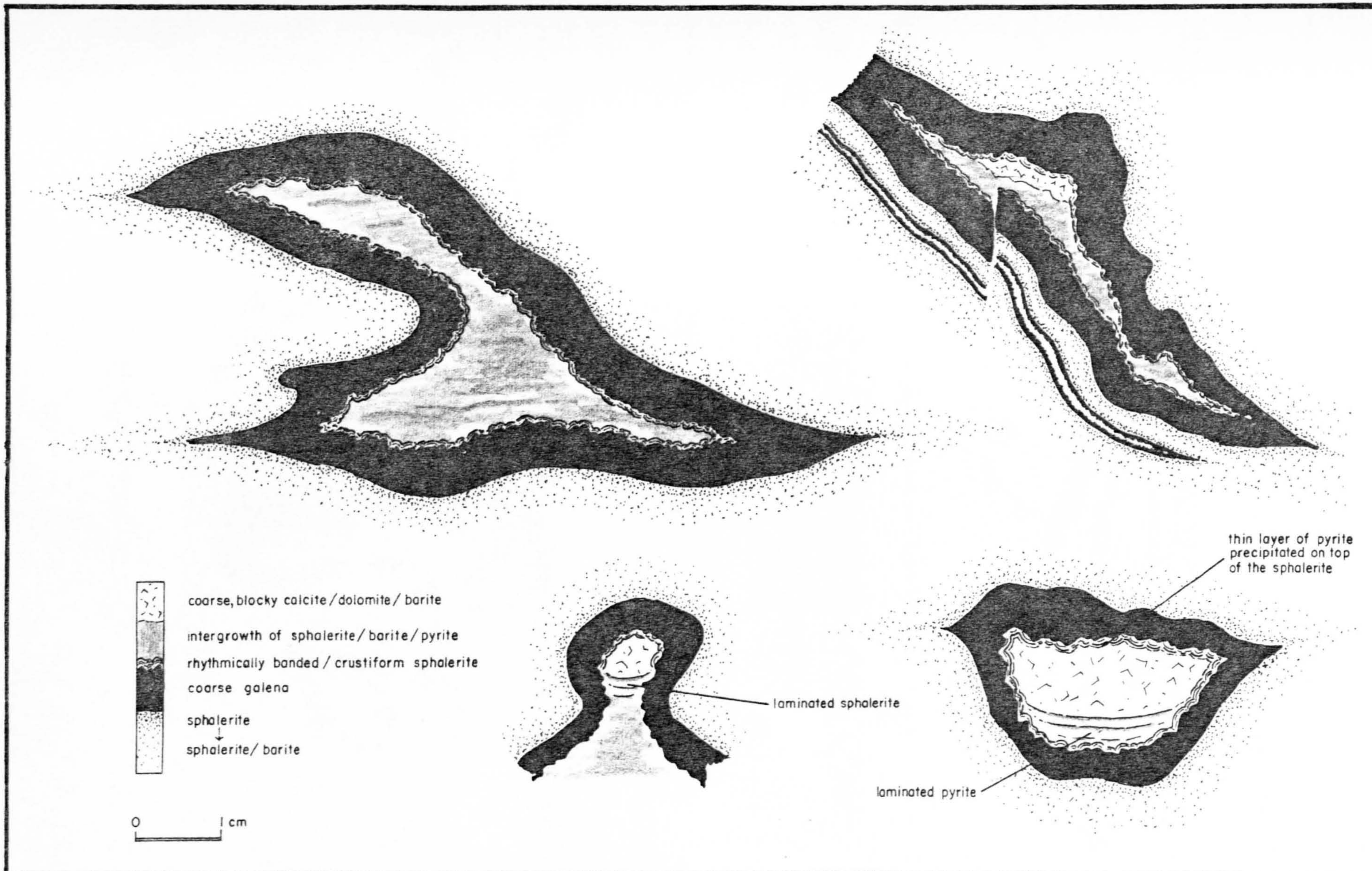
thin layer of pyrite precipitated on top of the sphalerite
coarse, blocky calcite / dolomite / barite
intergrowth of sphalerite / barite / pyrite
rhythmically banded / crustiform sphalerite
coarse galena
sphalerite
sphalerite / barite
laminated sphalerite
laminated pyrite
0
1 cm

Figure 5.15 Diagram illustrating a mechanism for producing contorted galena layers through slumping of the sulphides after initial deposition in small, bedding-parallel cavities.

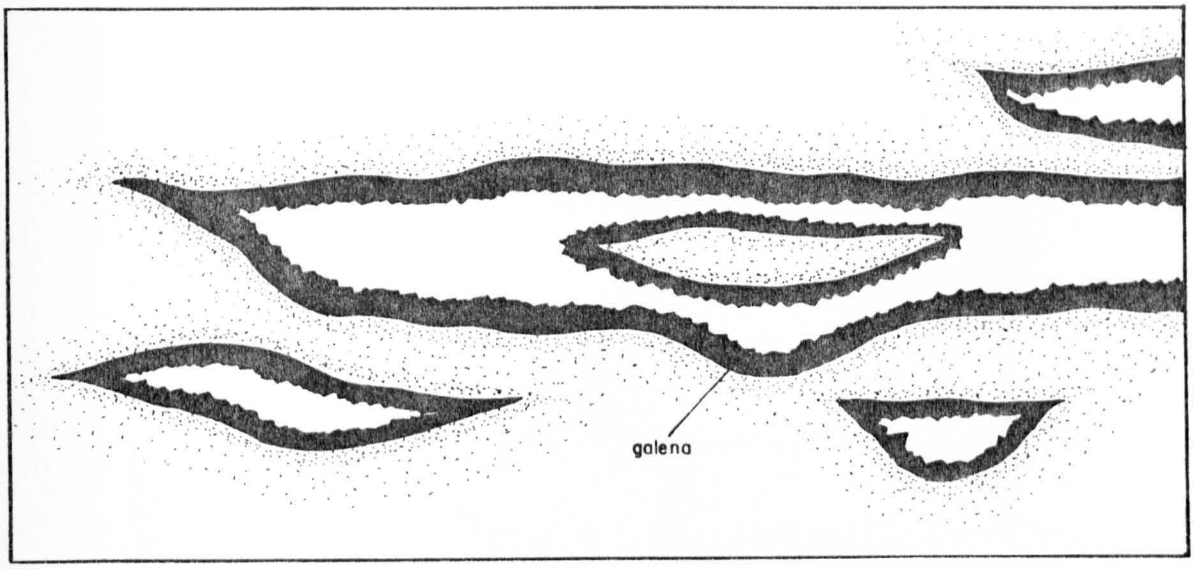

a) Initial infill of some form of small, bedding-parallel, "diagenetic?" spaces and replacement of surrounding carbonate

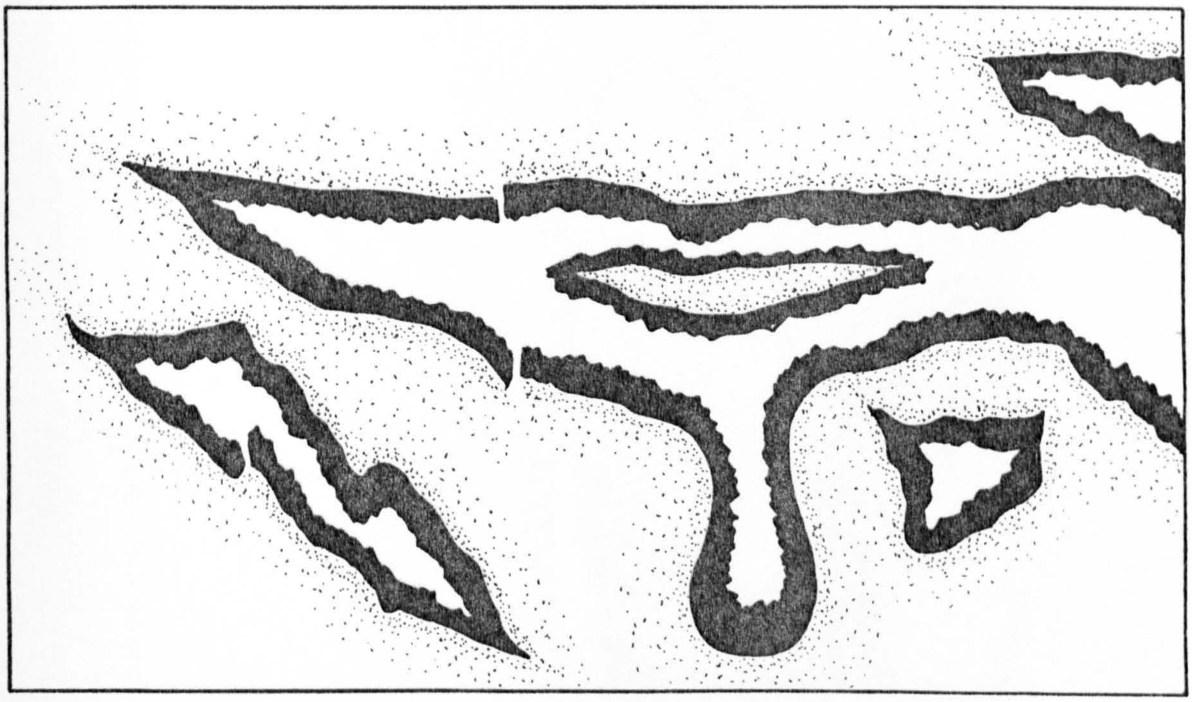

b) Subsequent "slumping" of the sulphides

Figure 5.16 Diagram illustrating a mechanism for producing contorted galena layers by the coating of clasts of host rock (which are subsequently totally replaced by sphalerite) in a cavity system.

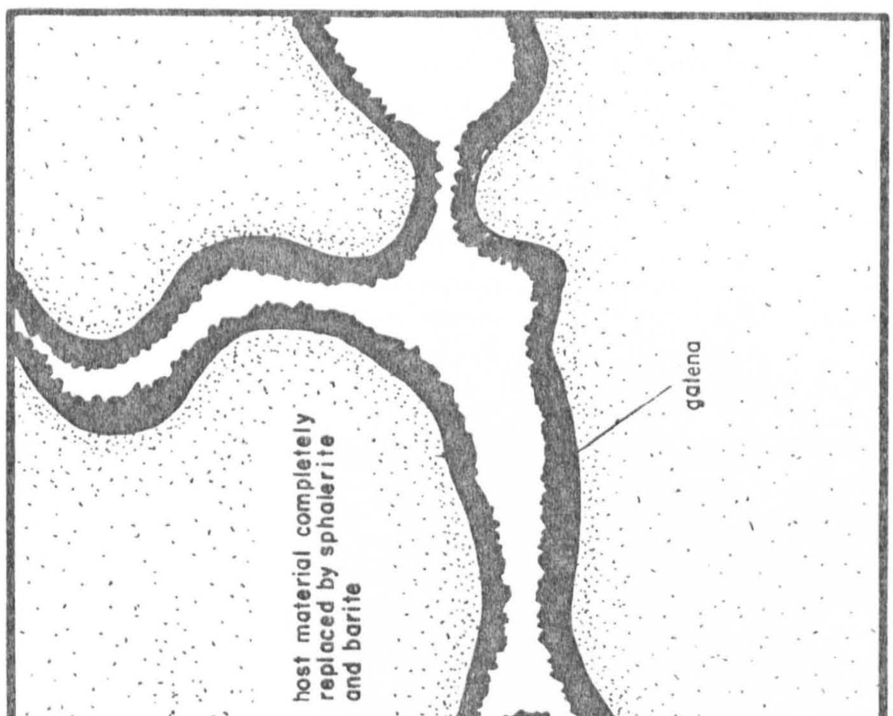
host material completely
replaced by sphalerite
and barite
galena

Figure 5.17 Diagram illustrating a mechanism for producing the funnel structure illustrated in Plate 5.23a by density slumping associated with extension and the initiation of fractures in the host lithologies.

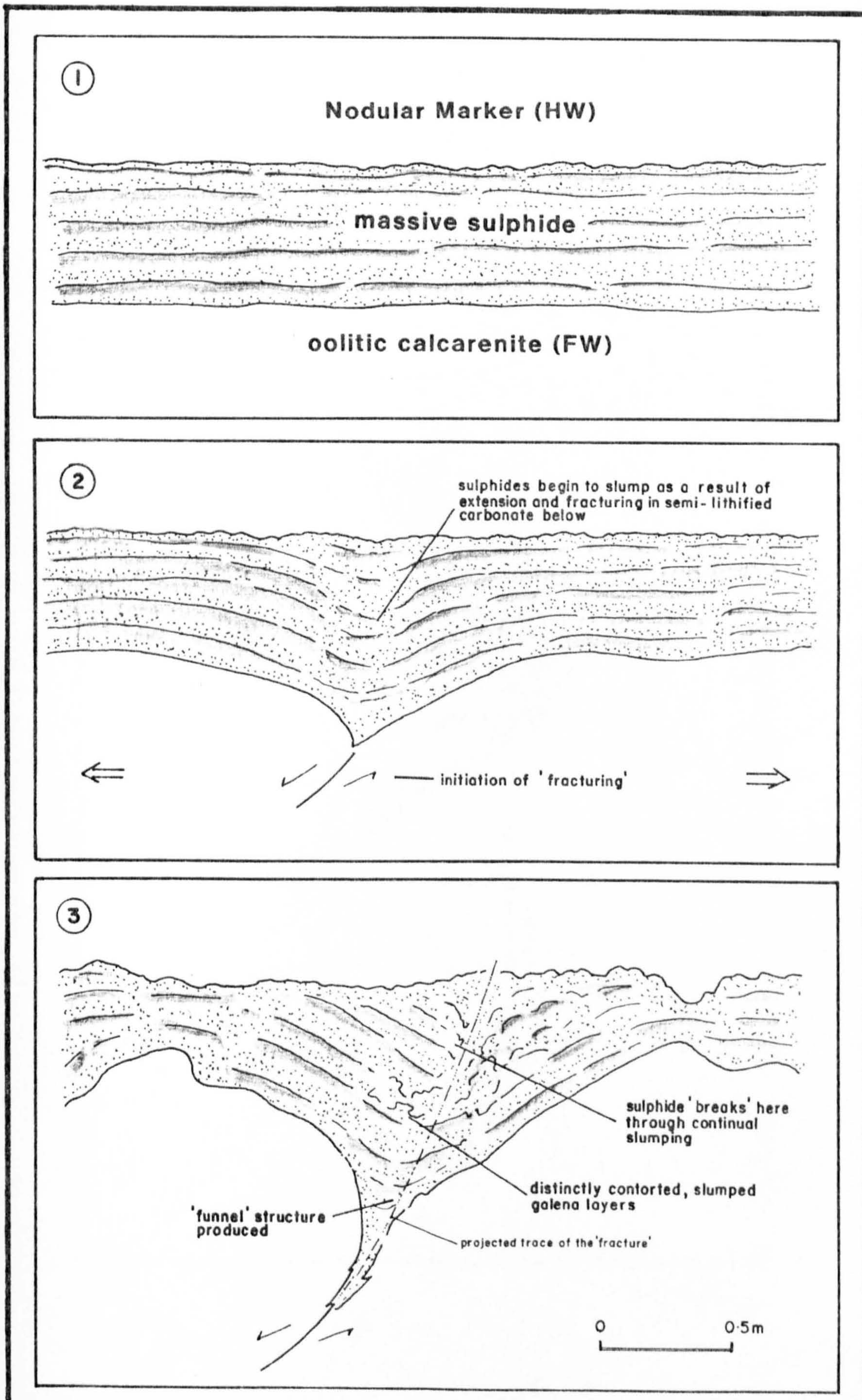
1
Nodular Marker (HW)
massive sulphide
oolitic calcarenite (FW)
2
sulphides begin to slump as a result of extension and fracturing in semi-lithified carbonate below
initiation of 'fracturing'
3
sulphide 'breaks' here through continual slumping
distinctly contorted, slumped galena layers
'funnel' structure produced
projected trace of the 'fracture'
0
0·5m

Figure 5.18 Diagram from an underground heading in 2-1 Lens (222W) illustrating dark argillite infilling a former depression at the base of a sulphide horizon.

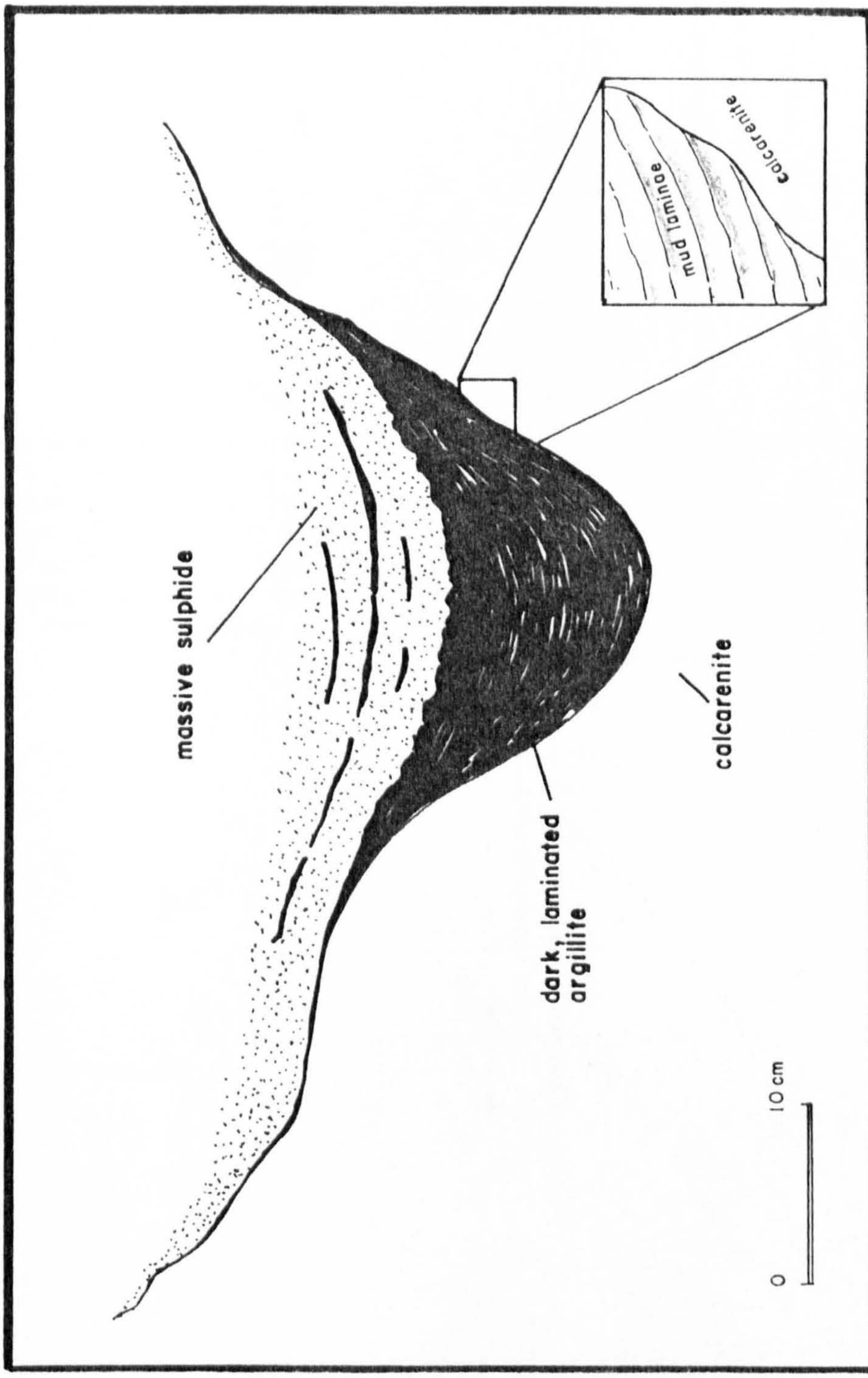
massive sulphide
dark, laminated argillite
calcarenite
mud laminae
calcarenite
0
10 cm

Figure 5.19 Diagram illustrating the mechanism for deposition of the internal sphalerite sediment involving rapid precipitation of fine-grained sphalerite in the ore fluid, possibly when the ore fluid encountered a supply of bacteriogenic H_2S. The sphalerite was subsequently deposited out of suspension.

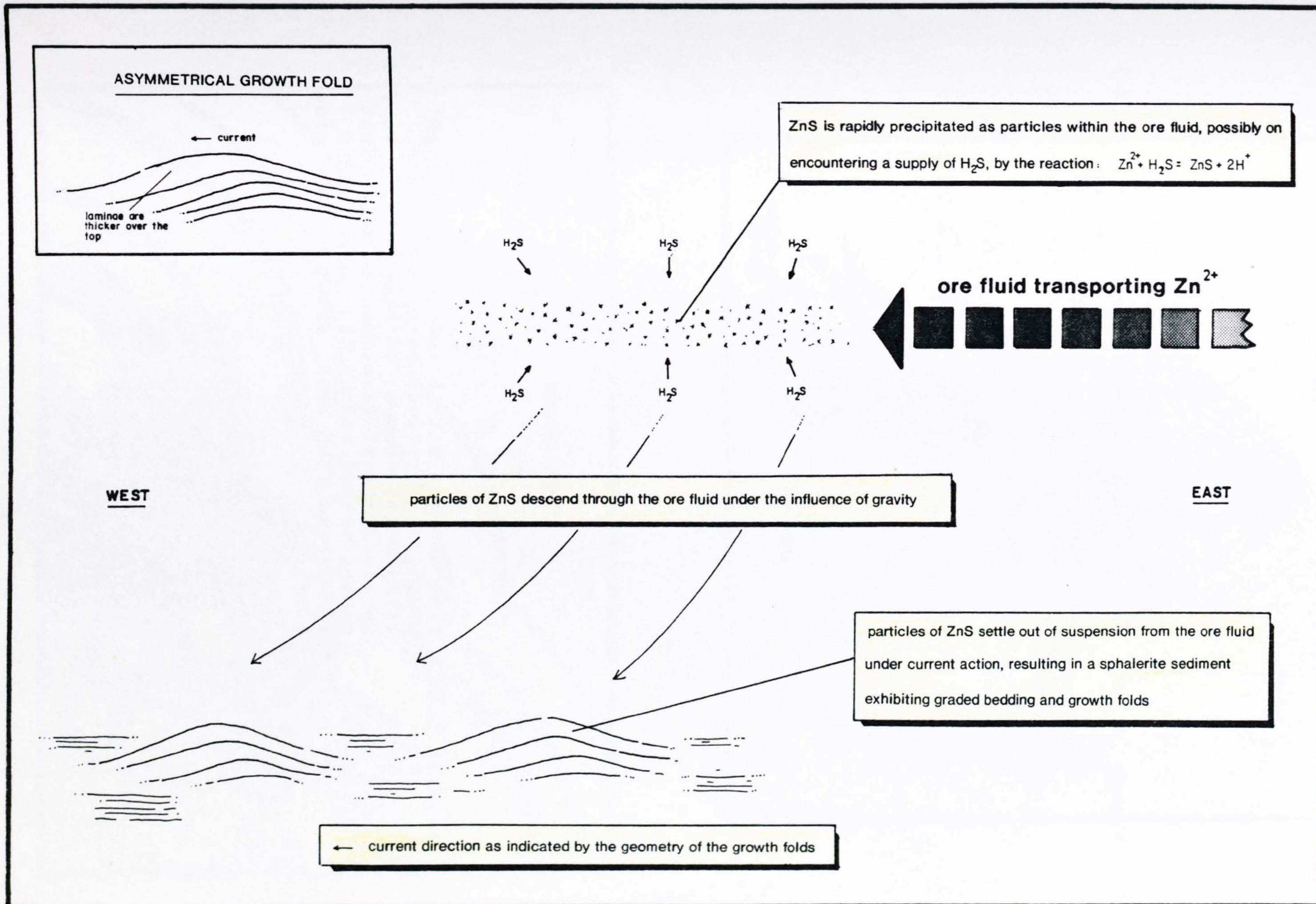
ASYMMETRICAL GROWTH FOLD
← current
laminae are thicker over the top
ZnS is rapidly precipitated as particles within the ore fluid, possibly on encountering a supply of H_2S, by the reaction: $Zn^{2+} + H_2S = ZnS + 2H^+$
H_2S
H_2S
H_2S
ore fluid transporting Zn^{2+}
H_2S
H_2S
H_2S
WEST
particles of ZnS descend through the ore fluid under the influence of gravity
EAST
particles of ZnS settle out of suspension from the ore fluid under current action, resulting in a sphalerite sediment exhibiting graded bedding and growth folds
← current direction as indicated by the geometry of the growth folds

Figure 5.20 Diagram from an underground heading in 2-1 Lens (229N) illustrating a complex assemblage of sulphide clasts with occassional clasts of host rock.

Figure 5.21 Diagram from a thin section under transmitted light illustrating late-stage calcite replacement of rhythmically banded sphalerite best-developed at re-entrant angles within the rhythmically banded sphalerite (1-5 Lens, Block 6, FW contour drifts).

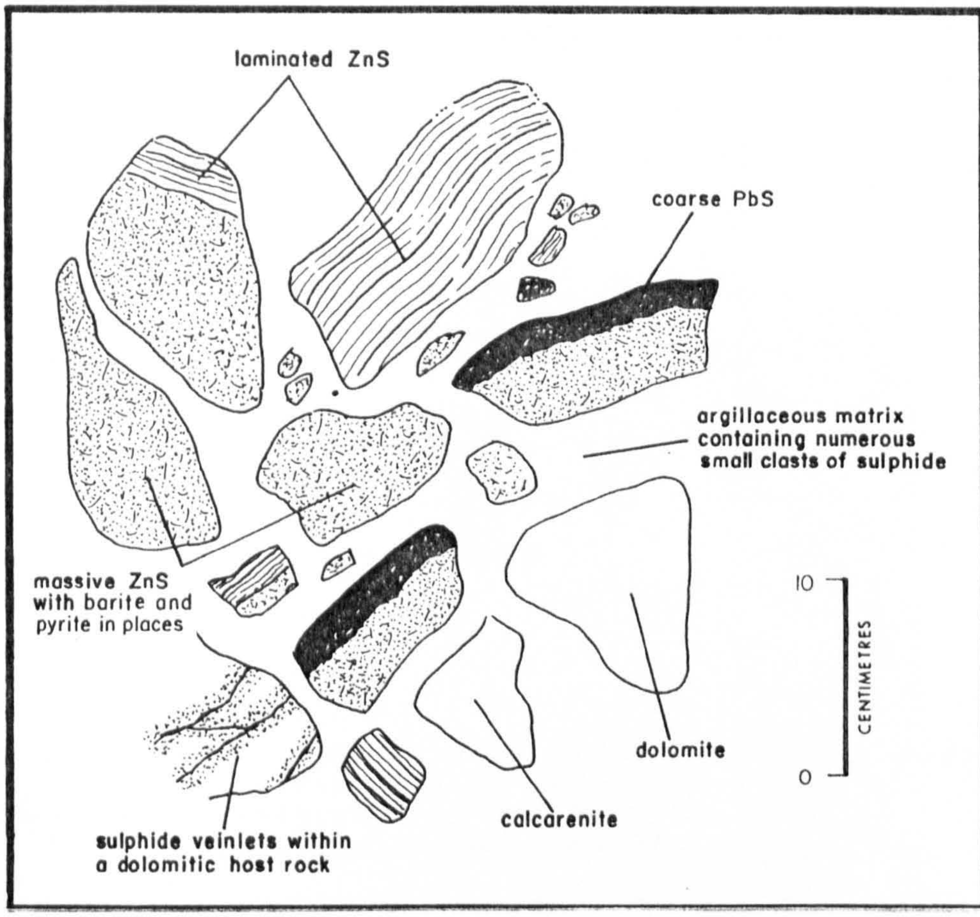
laminated ZnS
coarse PbS
argillaceous matrix
containing numerous
small clasts of sulphide
massive ZnS
with barite and
pyrite in places
10
CENTIMETRES
0
dolomite
calcarenite
sulphide veinlets within
a dolomitic host rock

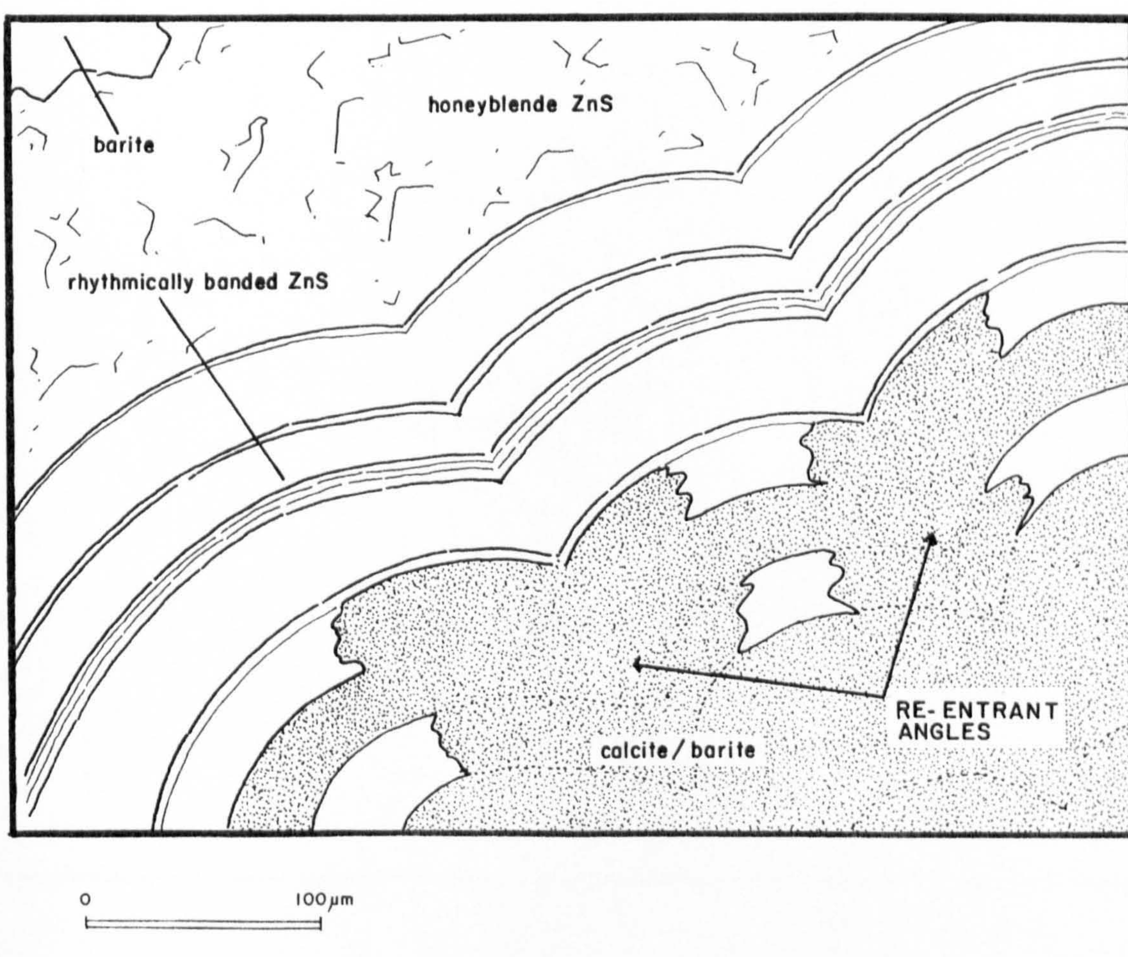
barite
honeyblende ZnS
rhythmically banded ZnS
RE-ENTRANT
ANGLES
calcite/barite
0
100μm

Figure 5.22 Diagrams of drillcore illustrating sulphides at the contact between a micrite and an overlying dolomite, with some collapse of the dolomite (1-5 Lens FW).

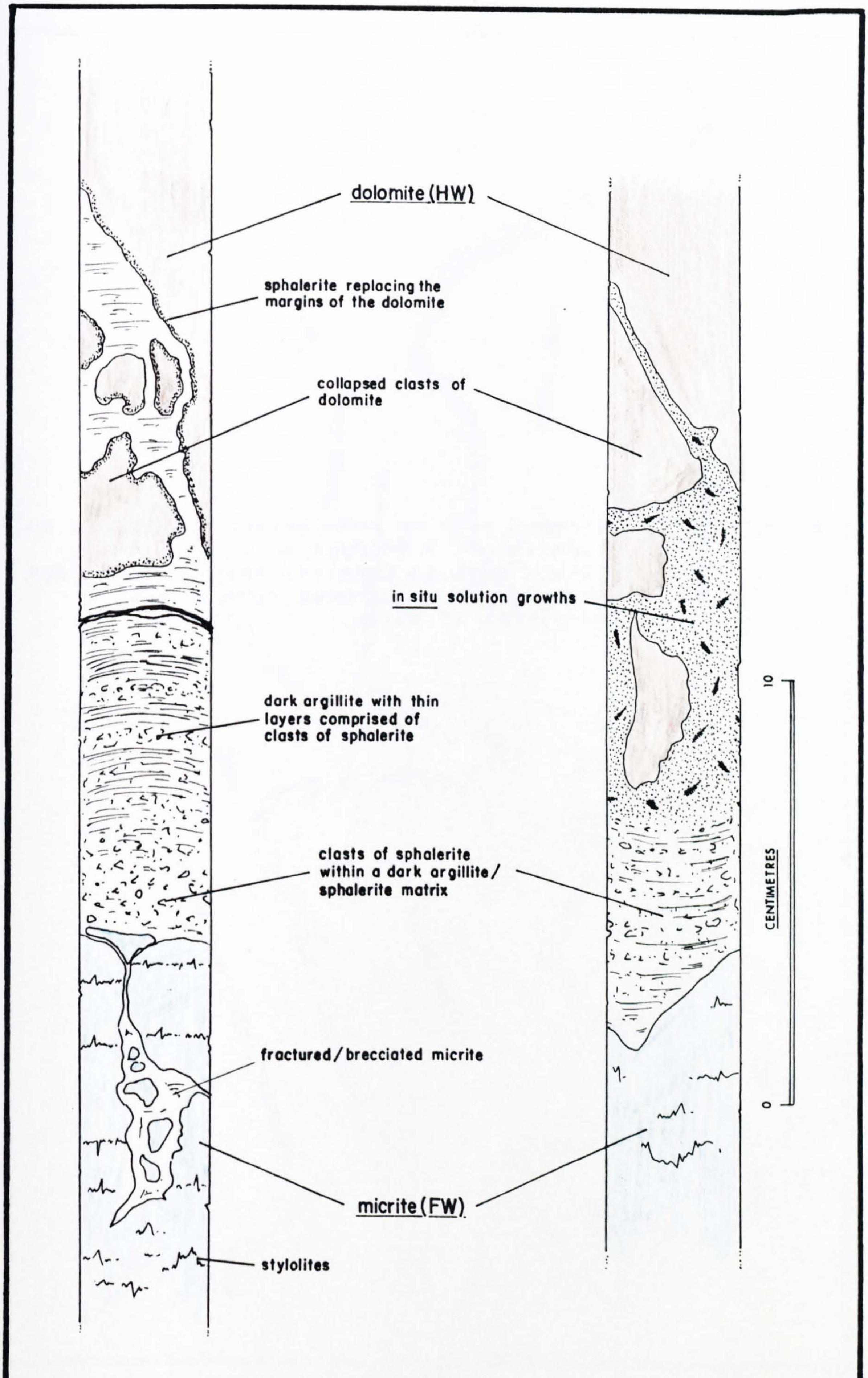
dolomite (HW)
sphalerite replacing the margins of the dolomite
collapsed clasts of dolomite
in situ solution growths
dark argillite with thin layers comprised of clasts of sphalerite
clasts of sphalerite within a dark argillite/ sphalerite matrix
fractured/brecciated micrite
micrite (FW)
stylolites
10
0
CENTIMETRES

Figure 5.23 Diagram from an underground heading in 1-5 Lens (Block 6 FW contour drift) illustrating bedding-parallel massive sulphides at the contact between micrite and overlying dolomite.

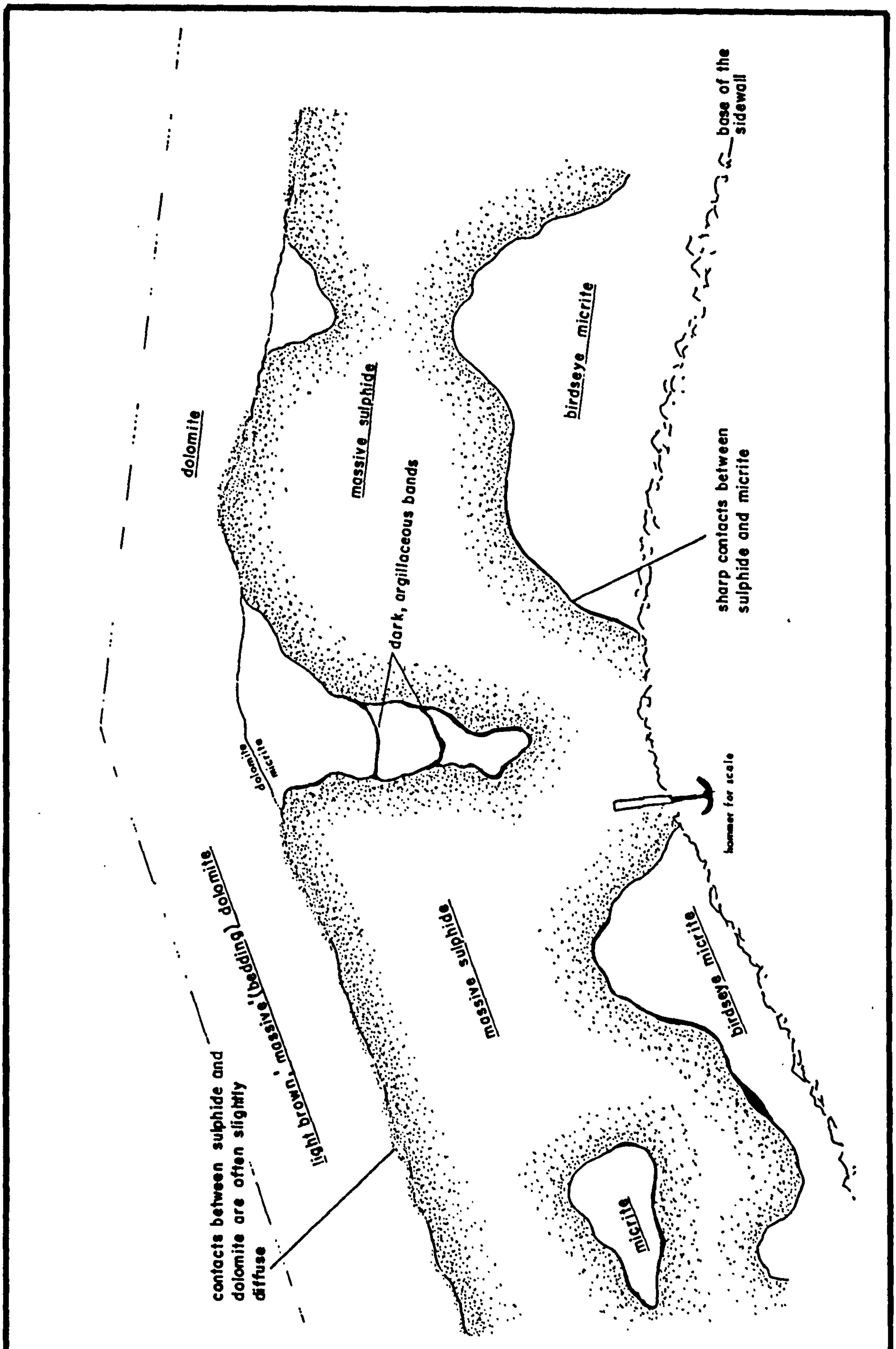
dolomite
massive sulphide
birdseye micrite
base of the sidewall
sharp contacts between sulphide and micrite
dark, argillaceous bands
dolomite
micrite
hammer for scale
light brown, massive (bedding) dolomite
massive sulphide
birdseye micrite
micrite
contacts between sulphide and dolomite are often slightly diffuse

Figure 5.24 Diagram from an underground heading in 1-5 Lens (Block 6 FW contour drift) illustrating bedding-parallel massive sulphides within the micrites.

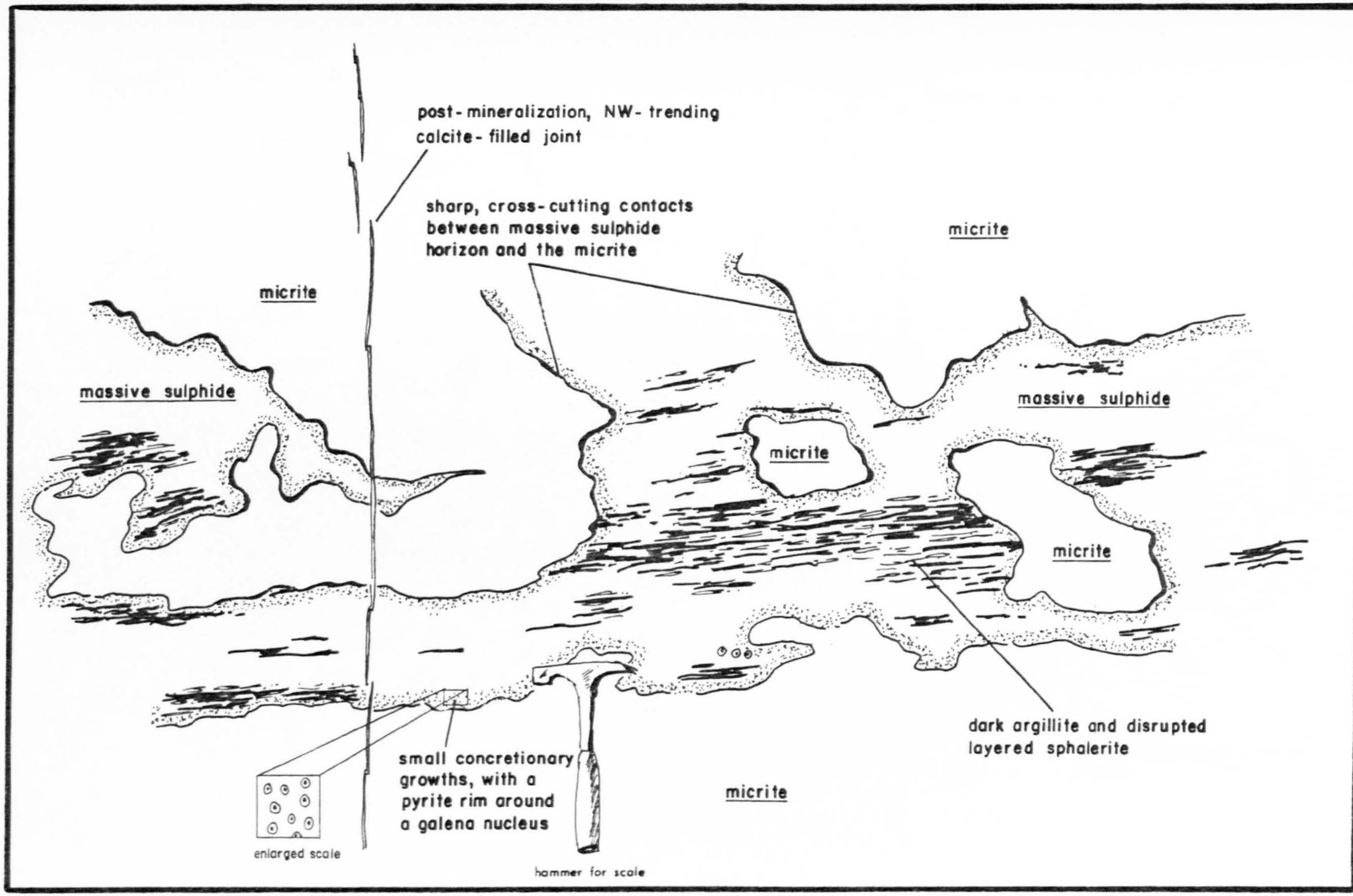
post-mineralization, NW-trending
calcite-filled joint
sharp, cross-cutting contacts
between massive sulphide
horizon and the micrite
micrite
micrite
massive sulphide
massive sulphide
micrite
micrite
dark argillite and disrupted
layered sphalerite
small concretionary
growths, with a
pyrite rim around
a galena nucleus
micrite
enlarged scale
hammer for scale

Figure 5.25 Diagram from an underground heading in 1-5 Lens (Block 6 FW contour drift) illustrating complex, chaotic clasts within bedding-parallel massive sulphides.

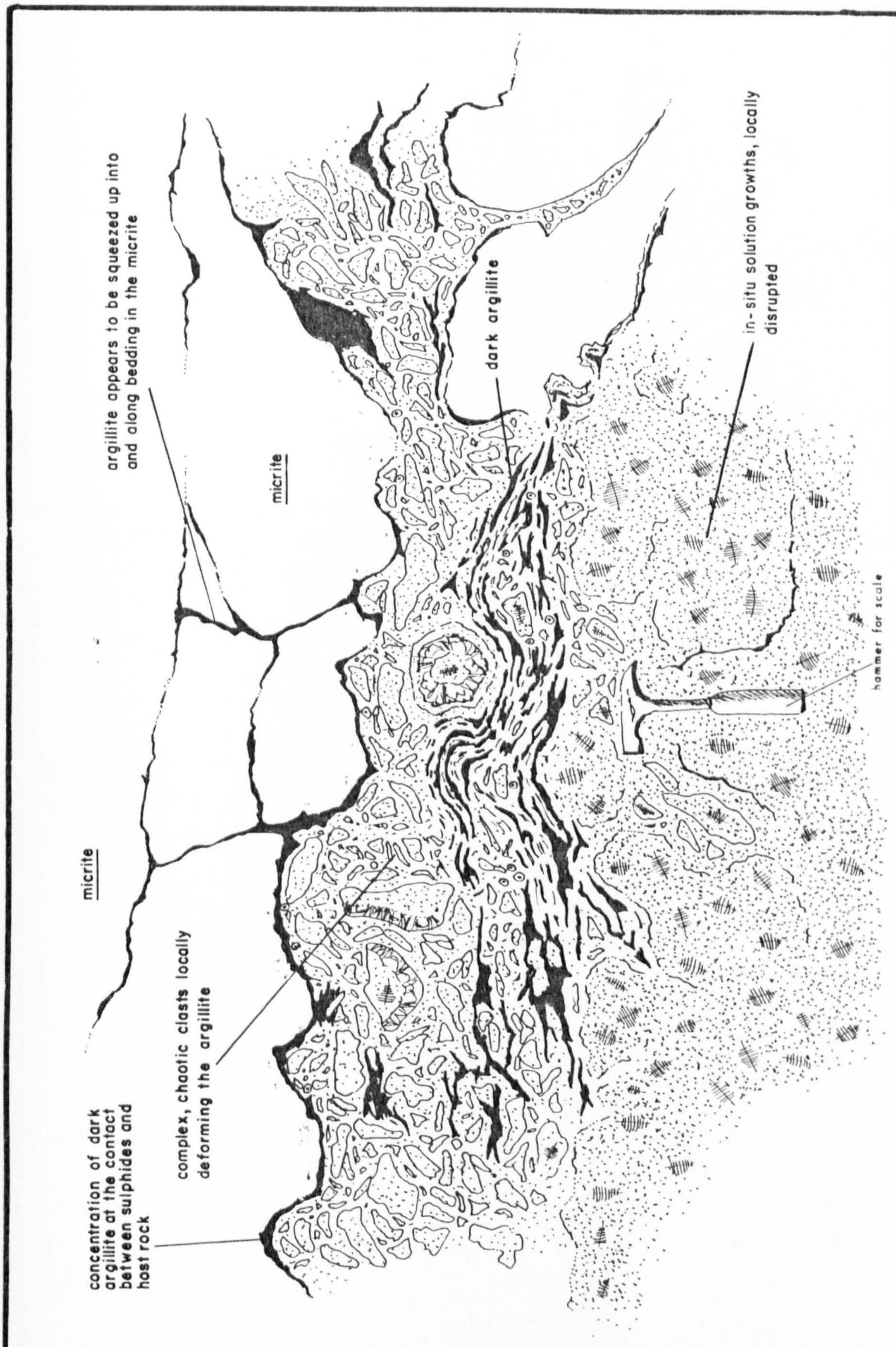

concentration of dark argillite at the contact between sulphides and host rock
complex, chaotic clasts locally deforming the argillite
micrite
micrite
argillite appears to be squeezed up into and along bedding in the micrite
dark argillite
hammer for scale
in-situ solution growths, locally disrupted

Figure 5.26 Diagram from an underground heading in 1-5 Lens (133W) illustrating complex, chaotic sulphide clasts in cross-cutting mineralization within the micrites.

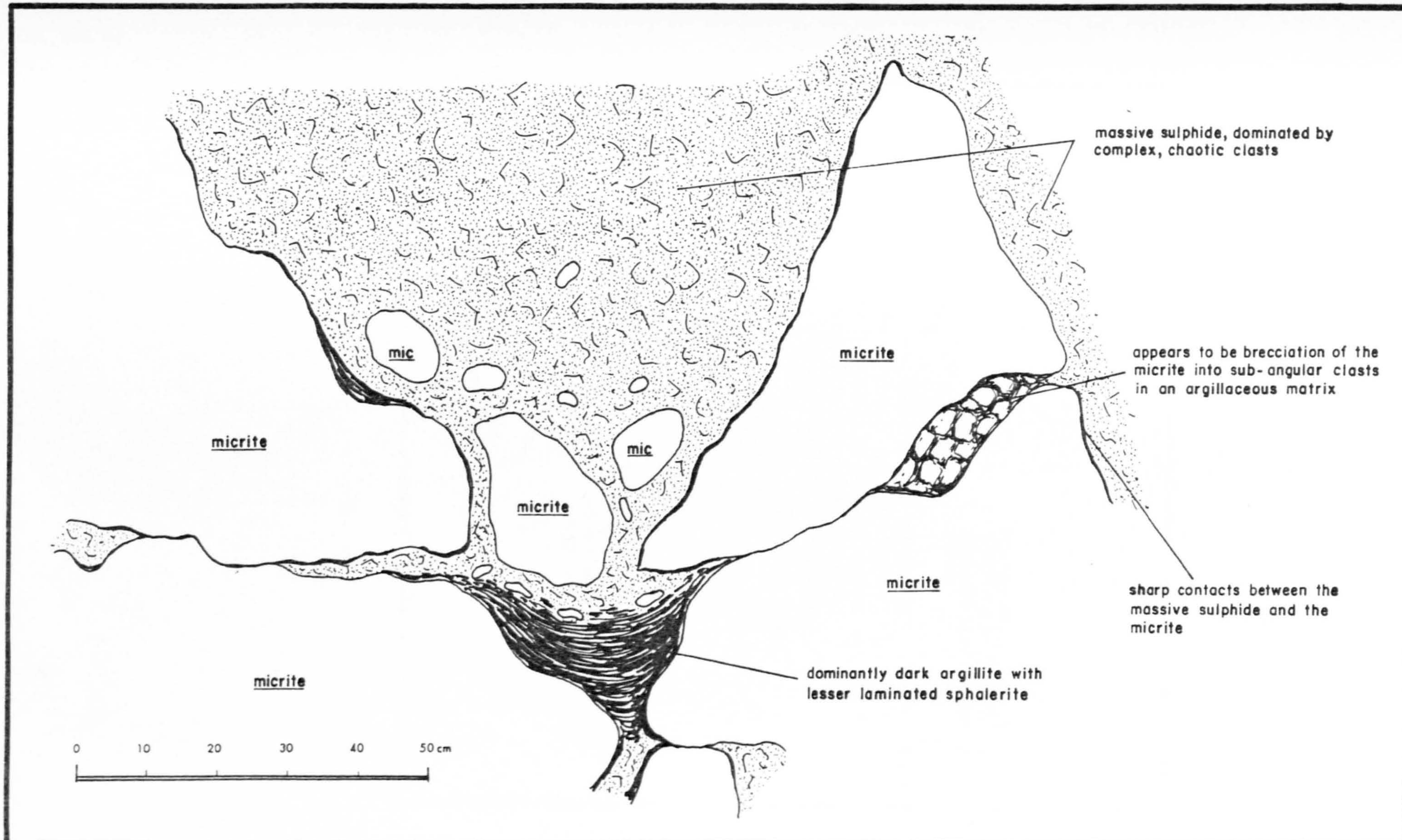
massive sulphide, dominated by complex, chaotic clasts
mic
micrite
mic
micrite
micrite
appears to be brecciation of the micrite into sub-angular clasts in an argillaceous matrix
micrite
sharp contacts between the massive sulphide and the micrite
dominantly dark argillite with lesser laminated sphalerite
micrite
0 10 20 30 40 50 cm

Figure 5.27 Diagram of drillcore from 1-5 Lens illustrating disrupted layers of symmetrically banded rhythmic sphalerite within the matrix around clasts of sulphide and micrite.

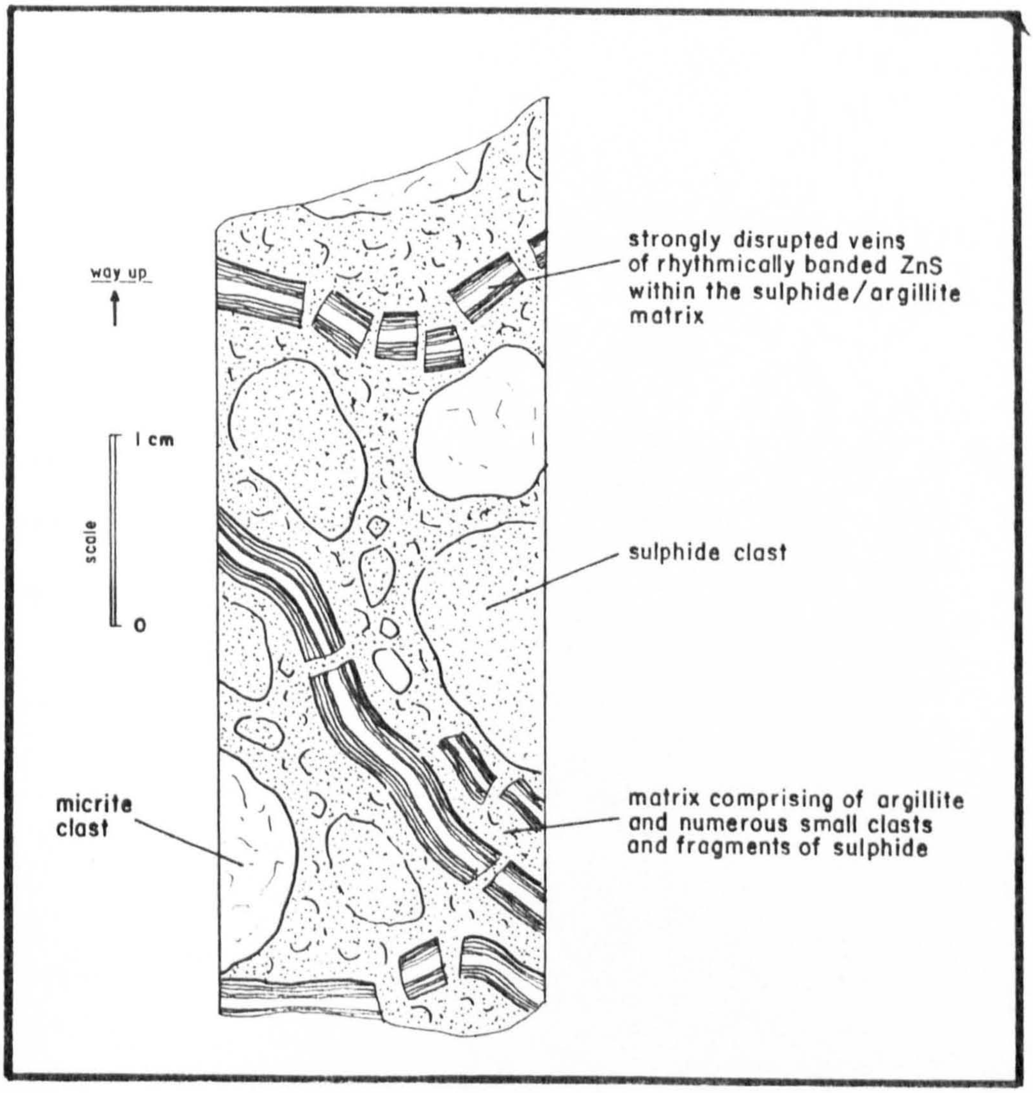

way up
1 cm
scale
0
strongly disrupted veins of rhythmically banded ZnS within the sulphide/argillite matrix
sulphide clast
micrite clast
matrix comprising of argillite and numerous small clasts and fragments of sulphide

Figure 5.28a Diagram illustrating initial fracturing of the micrites as mechanism for explaining the style of mineralization in the micrites.

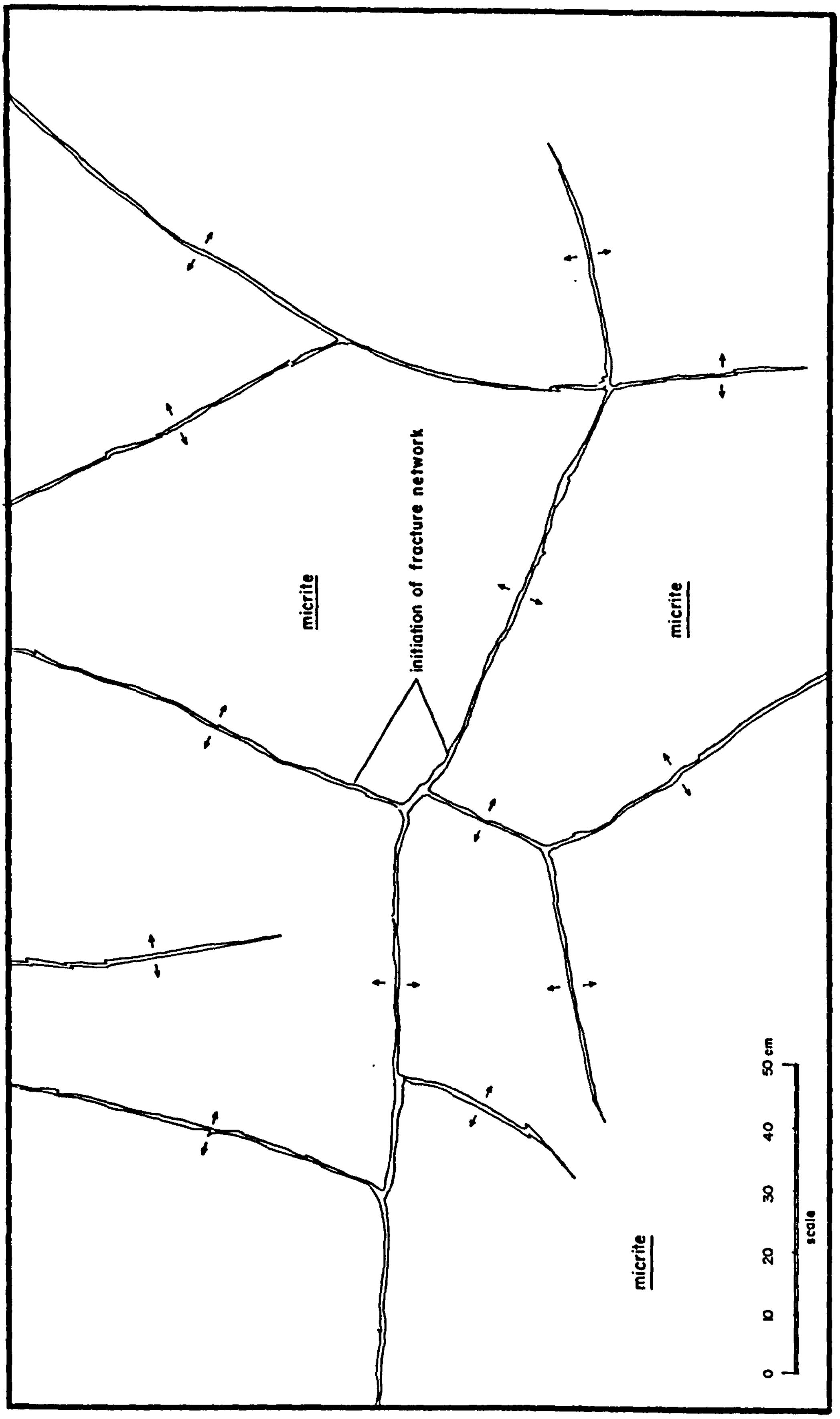
micrite
initiation of fracture network
micrite
micrite
0 10 20 30 40 50 cm
scale

Figure 5.28b Diagram illustrating sulphide deposition and disruption during continual extension of the micrites.

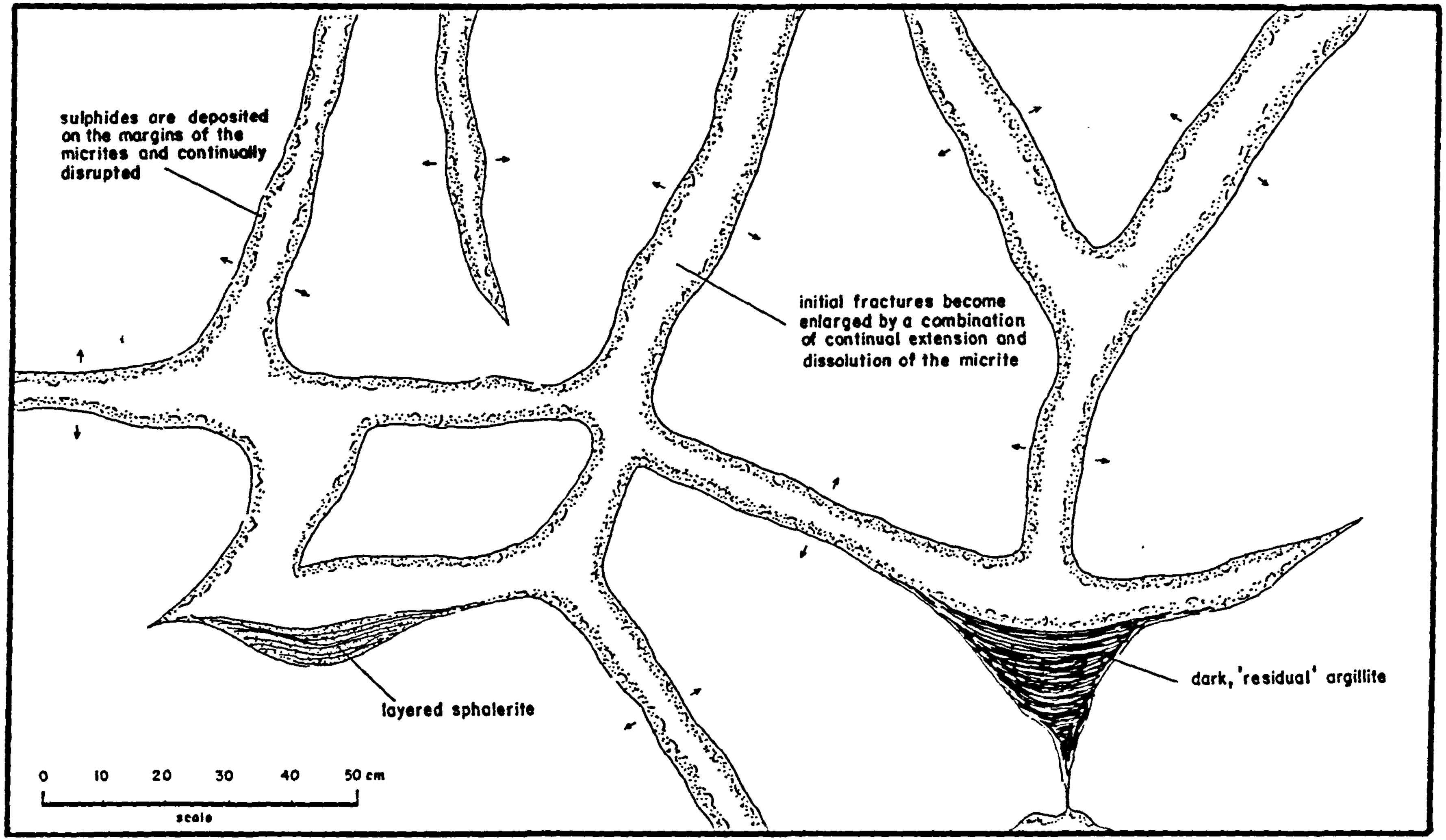
sulphides are deposited on the margins of the micrites and continually disrupted
initial fractures become enlarged by a combination of continual extension and dissolution of the micrite
layered sphalerite
dark, 'residual' argillite
0 10 20 30 40 50 cm
scale

Figure 5.28c Diagram illustrating the presently observed features of mineralization within the micrites.

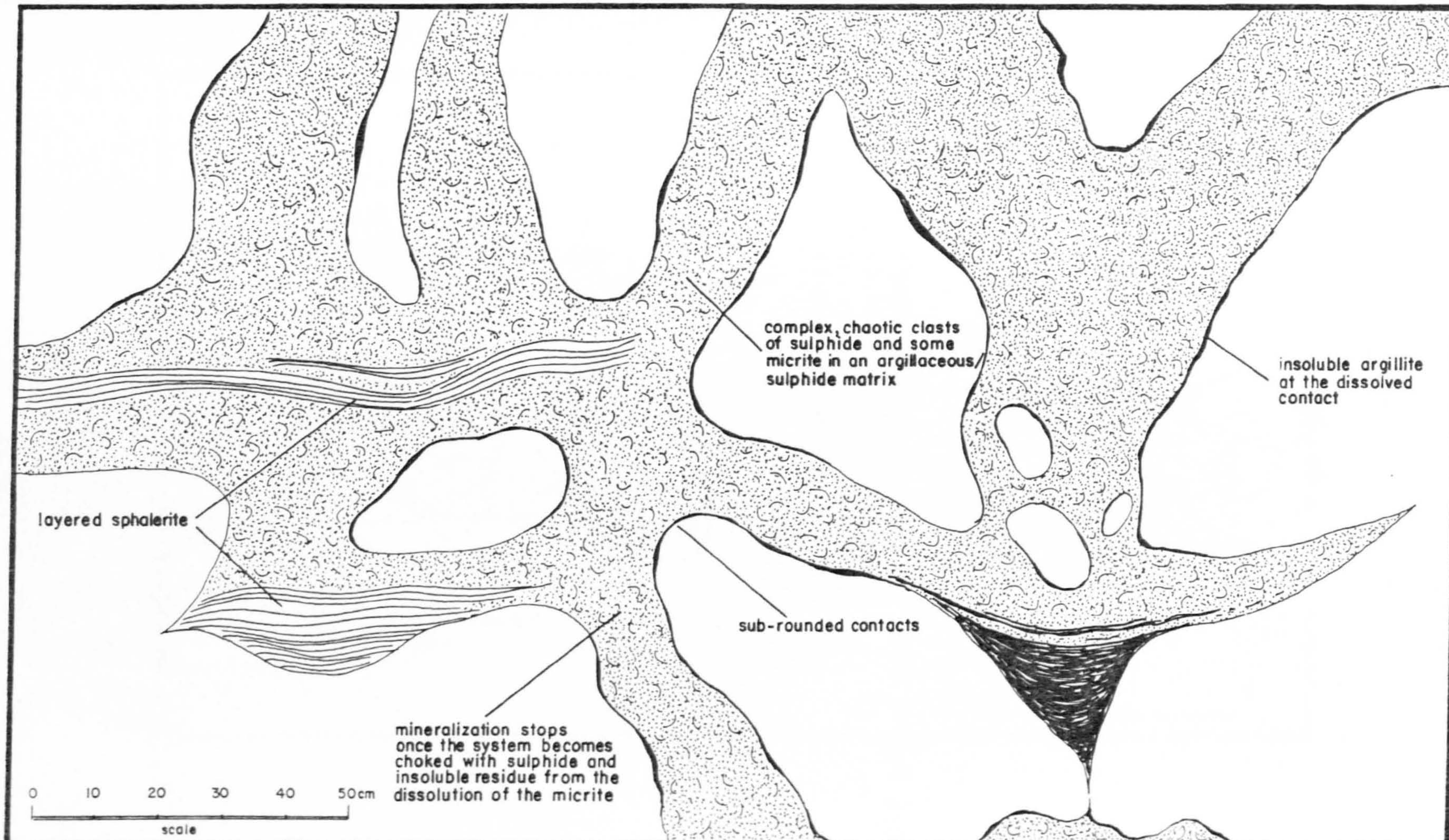
complex, chaotic clasts of sulphide and some micrite in an argillaceous/ sulphide matrix
insoluble argillite at the dissolved contact
layered sphalerite
sub-rounded contacts
mineralization stops once the system becomes choked with sulphide and insoluble residue from the dissolution of the micrite
0 10 20 30 40 50cm
scale

Figure 5.29 Diagram from an underground heading in 1-5 Lens illustrating a sulphide vein cross-cutting the micrite and dying out on encountering an overlying dolomitic horizon.

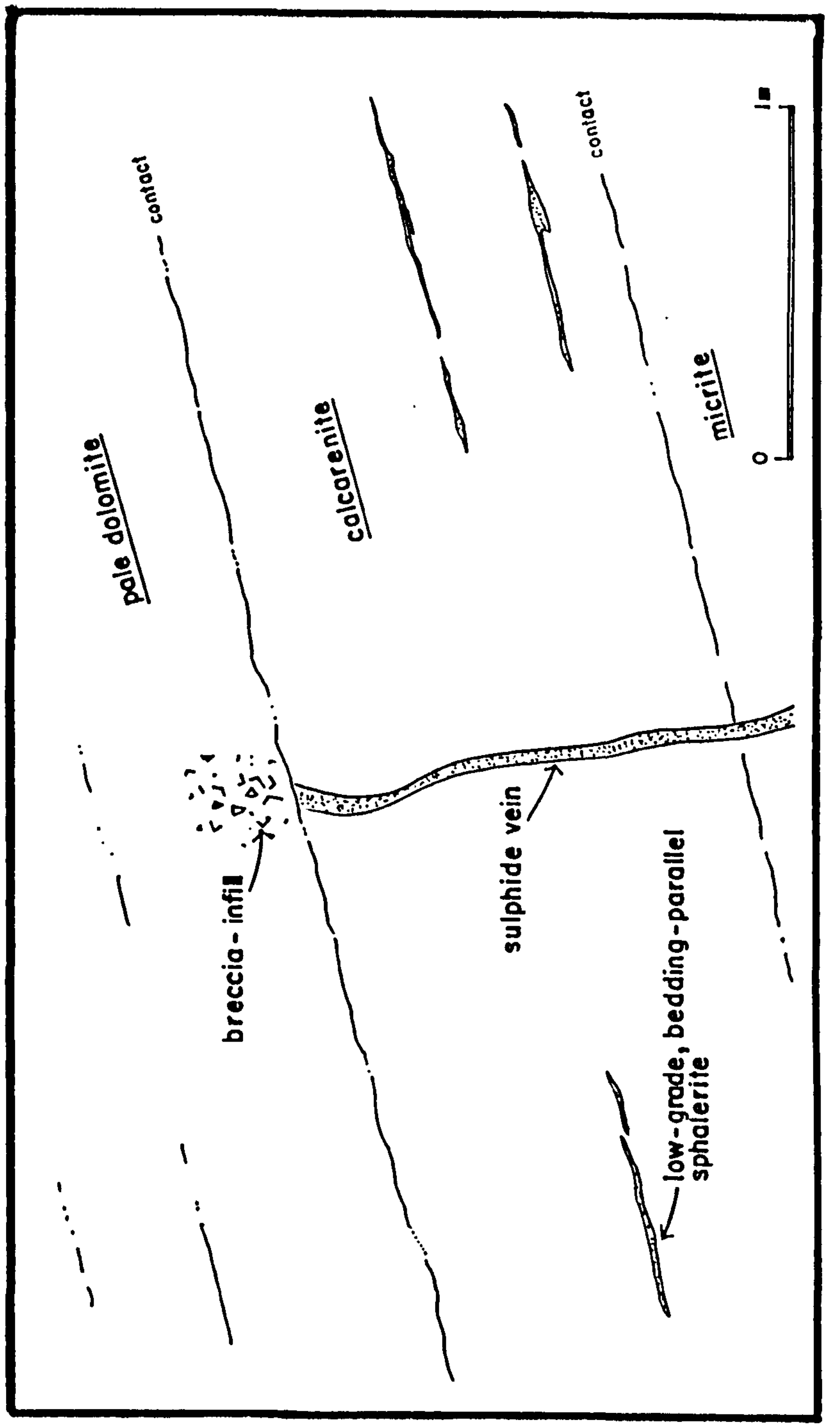

pale dolomite
calcarenite
micrite
contact
contact
breccia- infill
sulphide vein
low-grade, bedding-parallel
sphalerite
0
1m

Figure 5.30 Diagram from an underground heading in 1-5 Lens (Block 6 FW contour drift) illustrating layered birdseyes within micrites truncated by the footwall of a massive sulphide horizon.

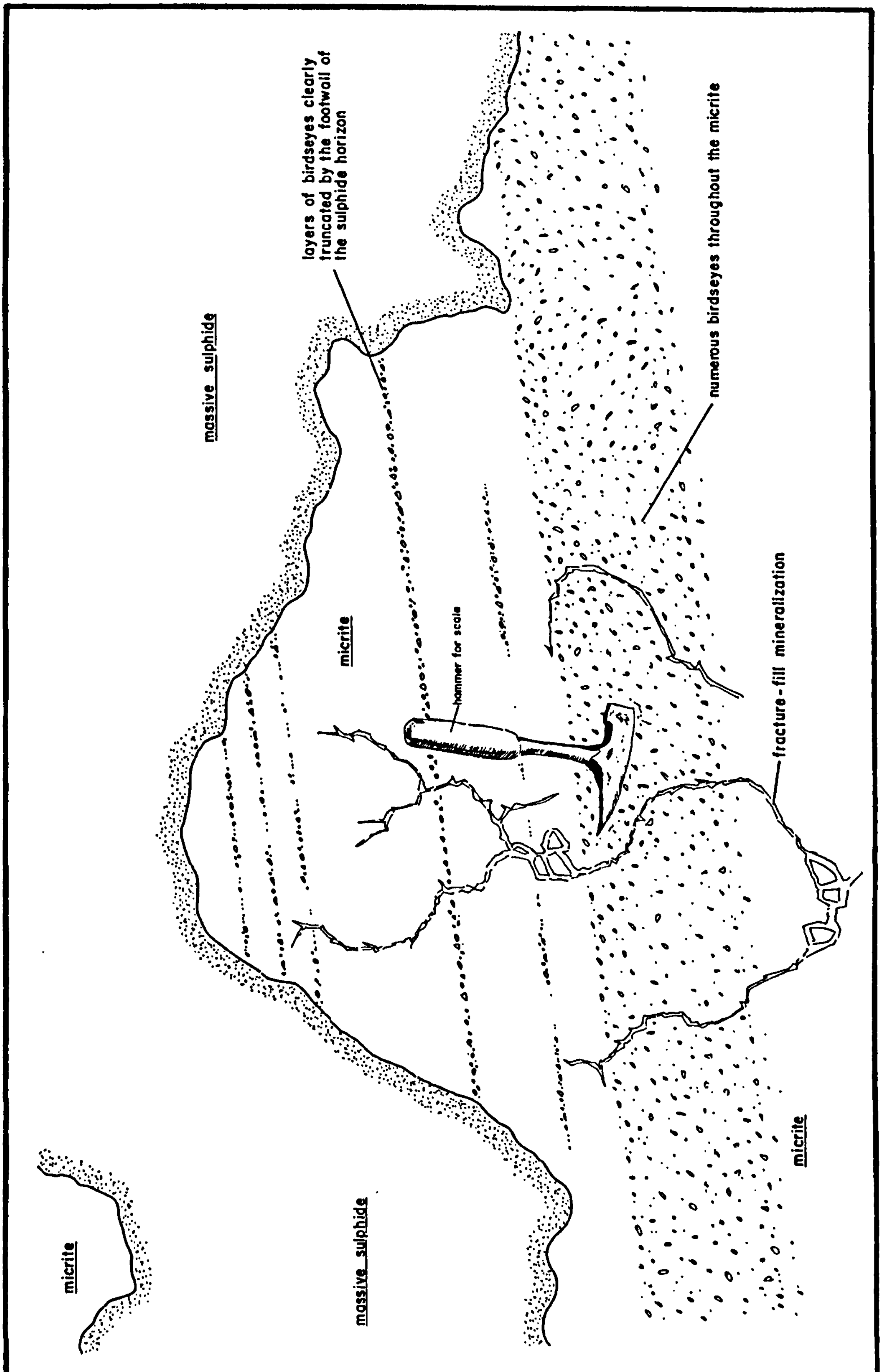
micrite
massive sulphide
massive sulphide
layers of birdseyes clearly truncated by the footwall of the sulphide horizon
micrite
hammer for scale
numerous birdseyes throughout the micrite
fracture-fill mineralization
micrite

Figure 5.31 Diagram from an underground heading in 1-5 Lens (Block 6 FW contour drift) illustrating a dark stylolitic micrite directly above a massive sulphide horizon.

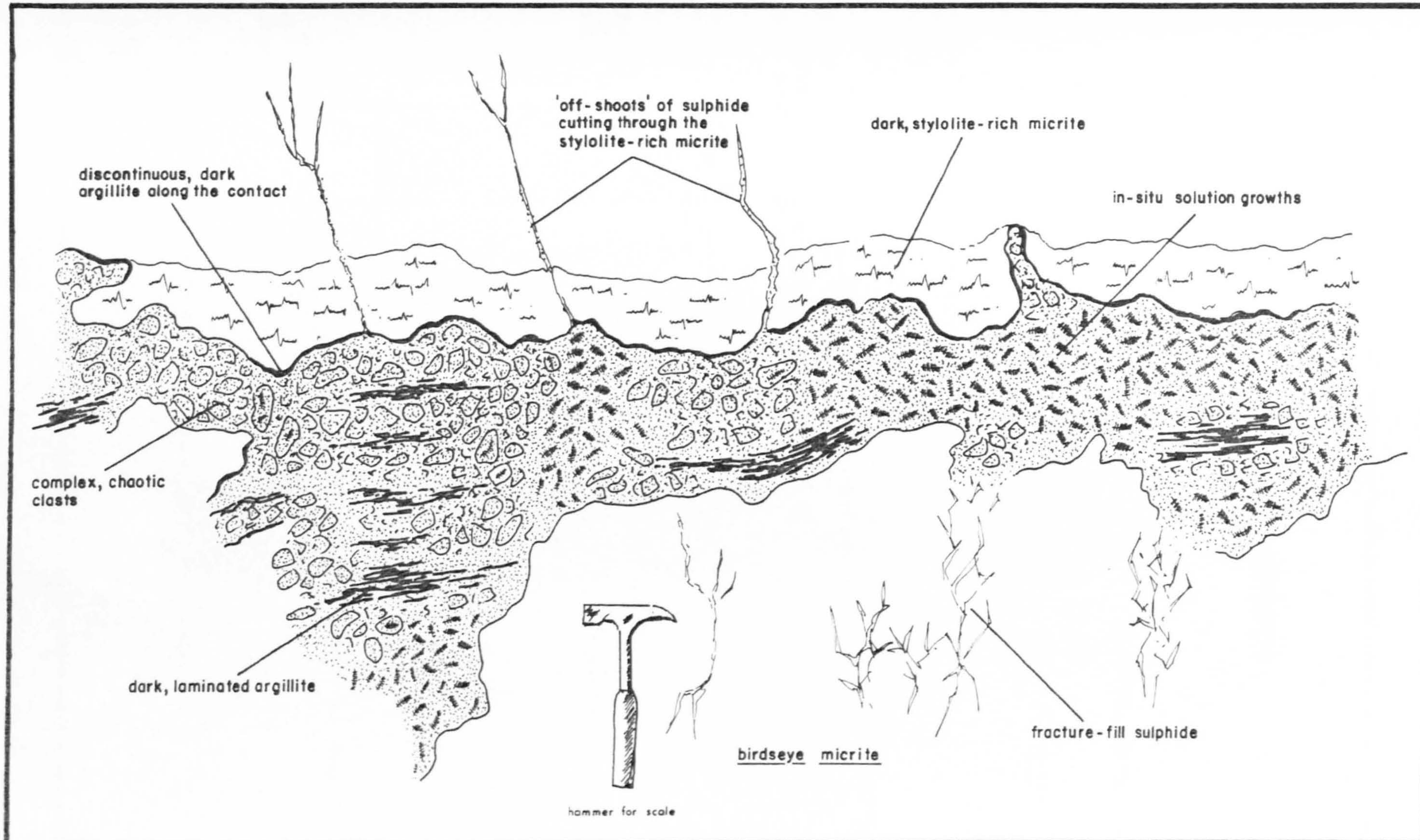
'off-shoots' of sulphide cutting through the stylolite-rich micrite
dark, stylolite-rich micrite
discontinuous, dark argillite along the contact
in-situ solution growths
complex, chaotic clasts
dark, laminated argillite
fracture-fill sulphide
birdseye micrite
hammer for scale

Figure 5.32 Diagram compiled from observations made on thin sections prepared from 2-5 Lens (242S, 1315 and 1330 levels) illustrating the sequence of sphalerite and galena deposition in both transmitted light and cathodoluminescence.

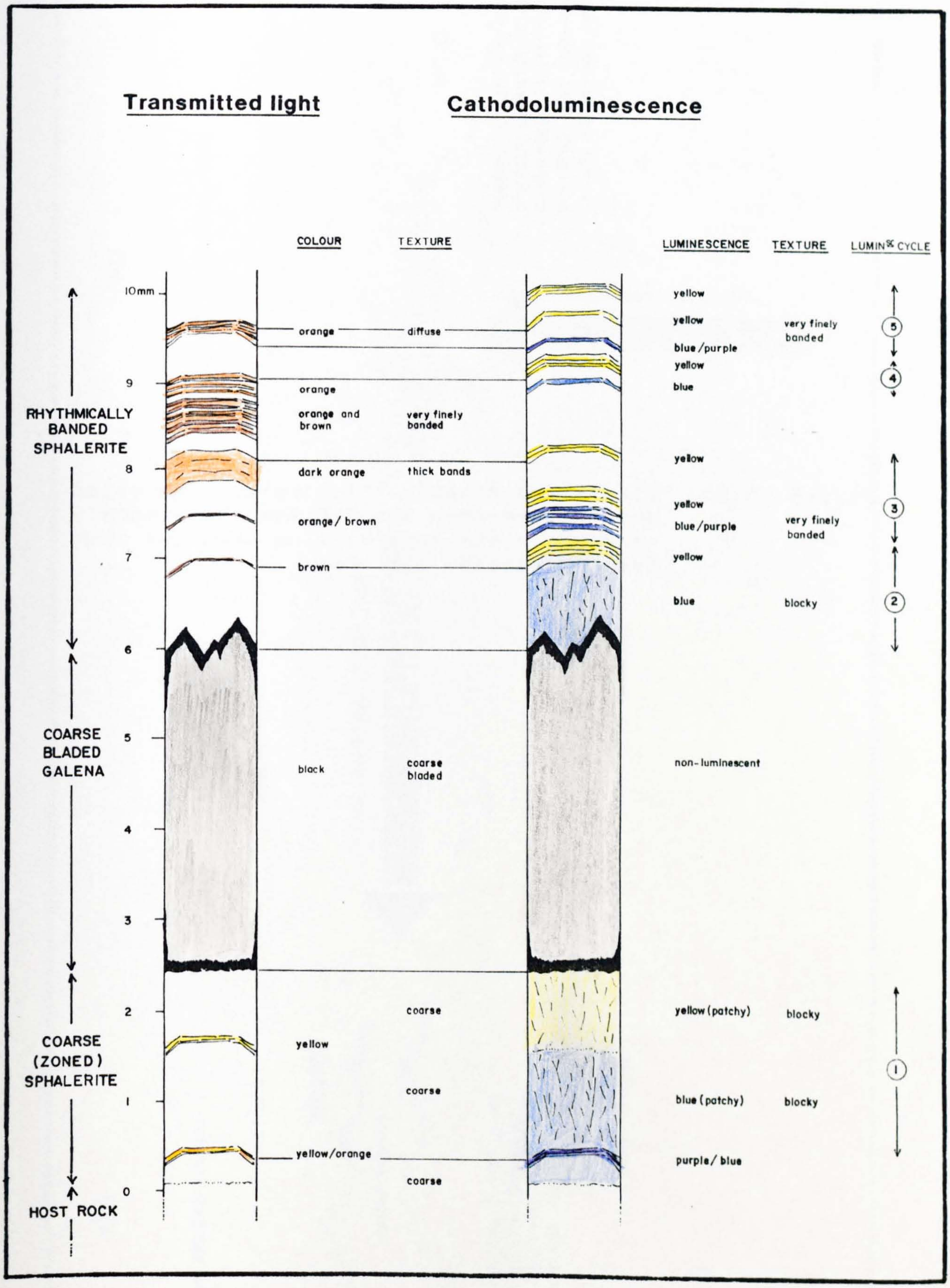
Transmitted light
Cathodoluminescence
COLOUR
TEXTURE
LUMINESCENCE
TEXTURE
LUMIN% CYCLE
10mm
9
8
7
6
5
4
3
2
1
0
RHYTHMICALLY BANDED SPHALERITE
COARSE BLADED GALENA
COARSE (ZONED) SPHALERITE
HOST ROCK
orange
diffuse
orange
orange and brown
very finely banded
dark orange
thick bands
orange / brown
brown
black
coarse bladed
coarse
yellow
coarse
yellow/orange
coarse
yellow
yellow
very finely banded
blue / purple
yellow
blue
yellow
yellow
blue / purple
very finely banded
yellow
blue
blocky
non-luminescent
yellow (patchy)
blocky
blue (patchy)
blocky
purple / blue
5
4
3
2
1

Figure 5.33 Simplified diagram illustrating the relationships between the 2-5 Lens FW mineralization in the central mine area and that further towards the west.

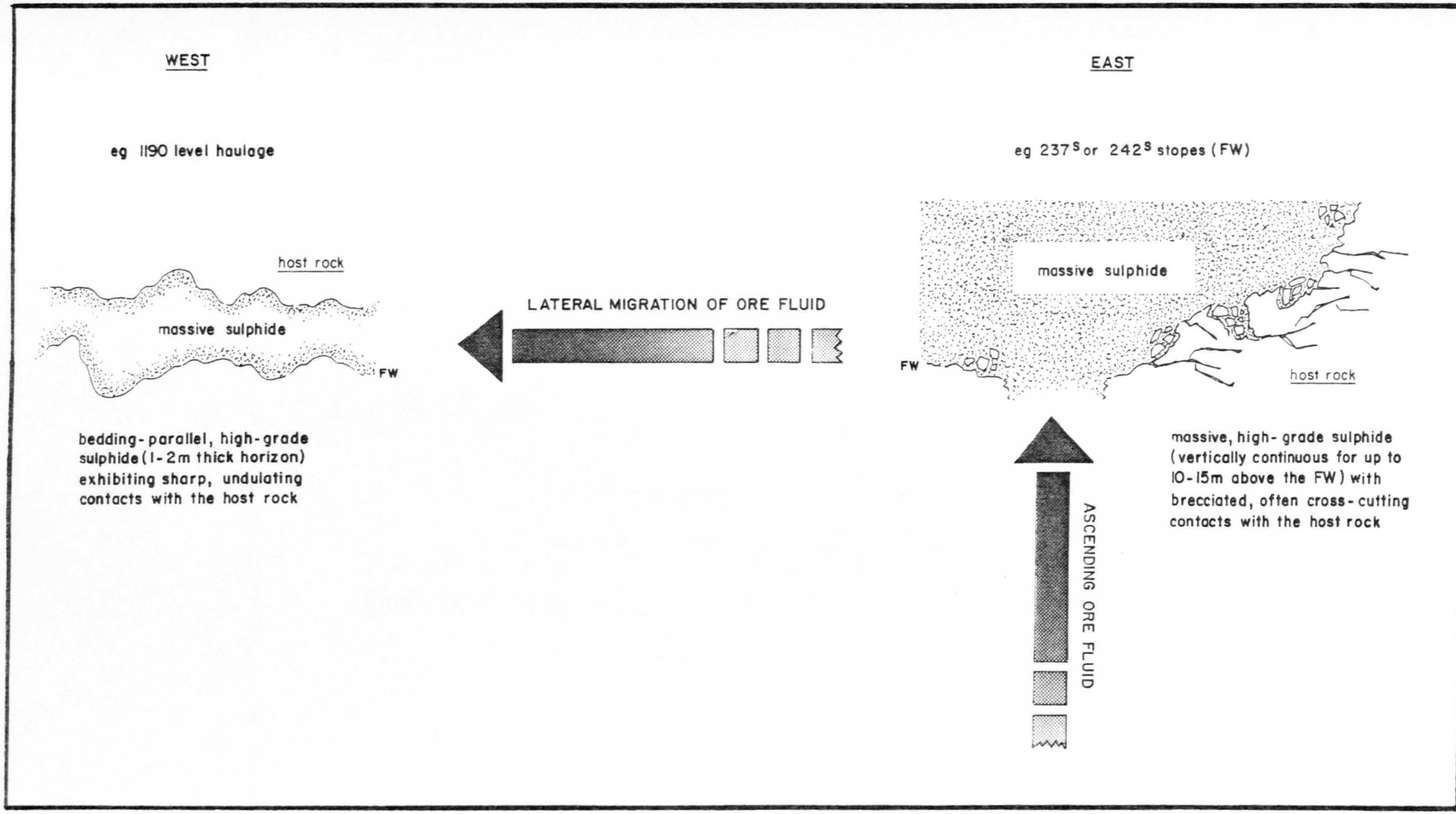
WEST
eg 1190 level haulage
host rock
massive sulphide
FW
bedding-parallel, high-grade sulphide (1-2m thick horizon) exhibiting sharp, undulating contacts with the host rock
LATERAL MIGRATION OF ORE FLUID
EAST
eg 237S or 242S stopes (FW)
massive sulphide
FW
host rock
ASCENDING ORE FLUID
massive, high-grade sulphide (vertically continuous for up to 10-15m above the FW) with brecciated, often cross-cutting contacts with the host rock

Figure 5.34 Diagram illustrating and explaining the apparent relationships between different styles of mineralization in a heading in 2-4 Lens (252/253S).

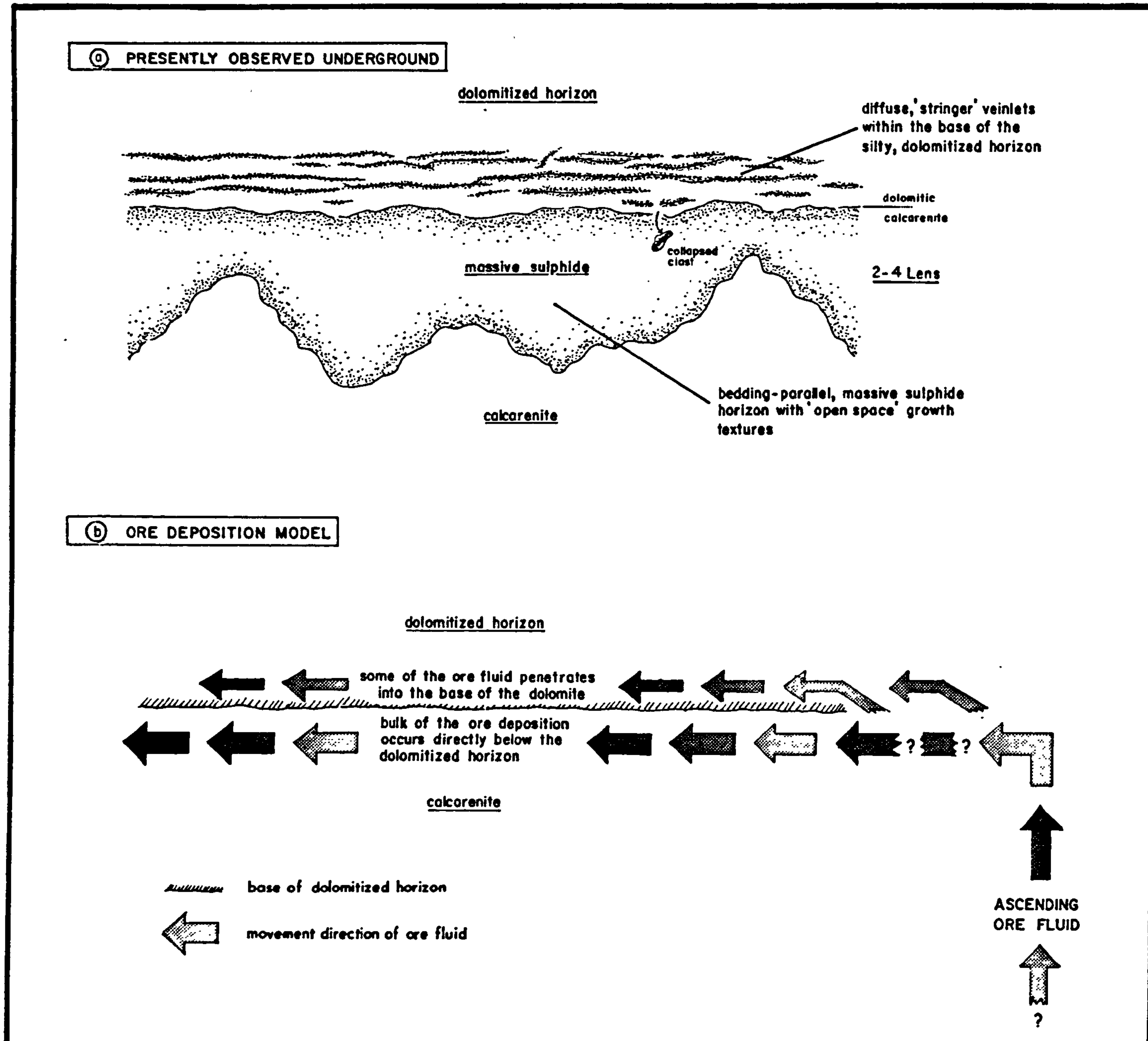

ⓐ PRESENTLY OBSERVED UNDERGROUND
dolomitized horizon
diffuse, 'stringer' veinlets within the base of the silty, dolomitized horizon
dolomitic calcarenite
collapsed clast
massive sulphide
2-4 Lens
bedding-parallel, massive sulphide horizon with 'open space' growth textures
calcarenite
ⓑ ORE DEPOSITION MODEL
dolomitized horizon
some of the ore fluid penetrates into the base of the dolomite
bulk of the ore deposition occurs directly below the dolomitized horizon
?
?
calcarenite
base of dolomitized horizon
movement direction of ore fluid
ASCENDING ORE FLUID
?

Figure 5.35 Simplified diagram illustrating and explaining the relationships between styles of mineralization in 2-2/1-2 Lenses.

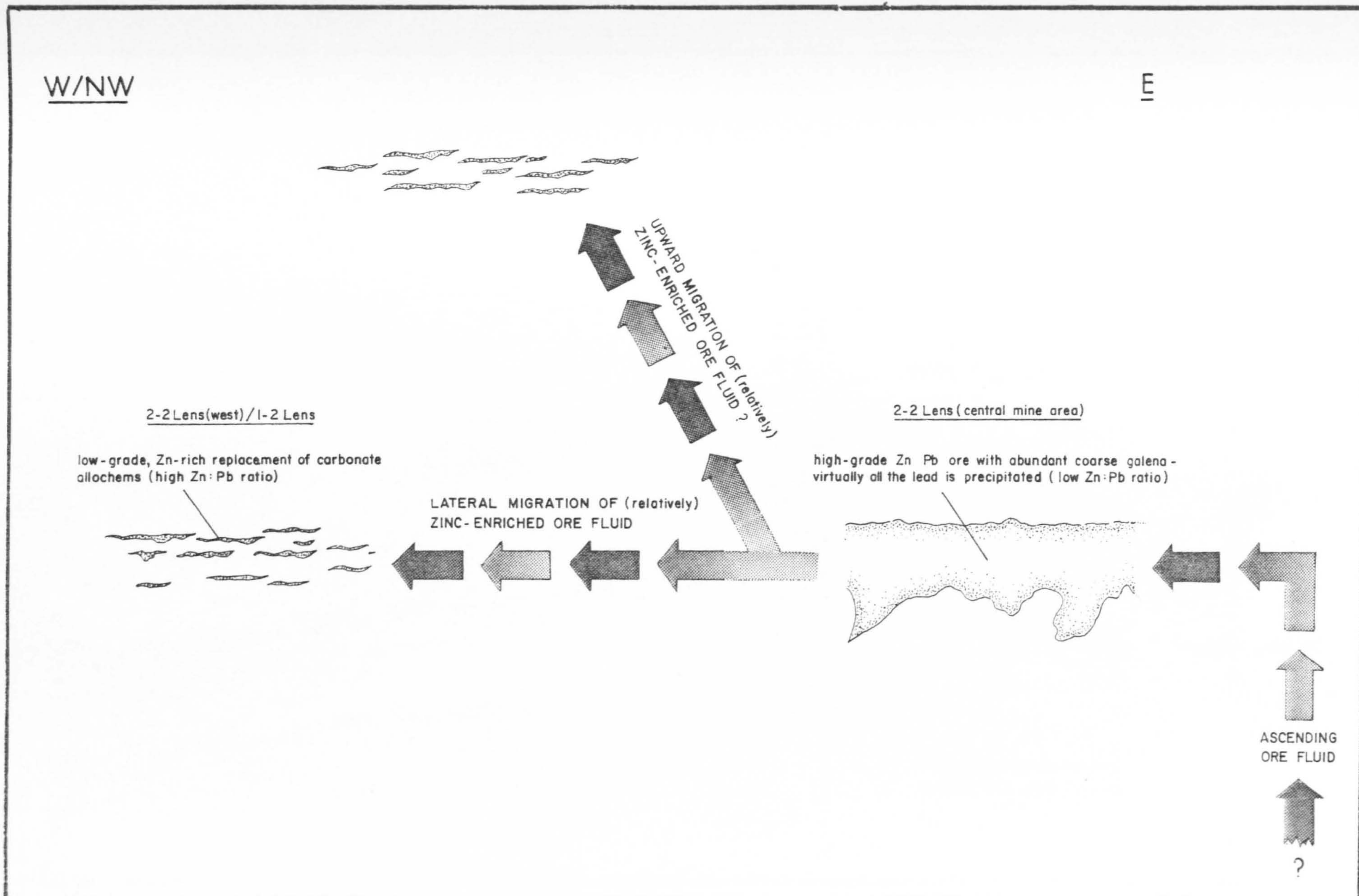

W/NW
E
UPWARD MIGRATION OF (relatively)
ZINC-ENRICHED ORE FLUID ?
2-2 Lens(west)/I-2 Lens
low-grade, Zn-rich replacement of carbonate
allochems (high Zn:Pb ratio)
LATERAL MIGRATION OF (relatively)
ZINC-ENRICHED ORE FLUID
2-2 Lens (central mine area)
high-grade Zn Pb ore with abundant coarse galena -
virtually all the lead is precipitated (low Zn:Pb ratio)
ASCENDING
ORE FLUID
?

Figure 5.36 Simplified diagram illustrating the relationships between different styles of mineralization in 2-1 Lens west.

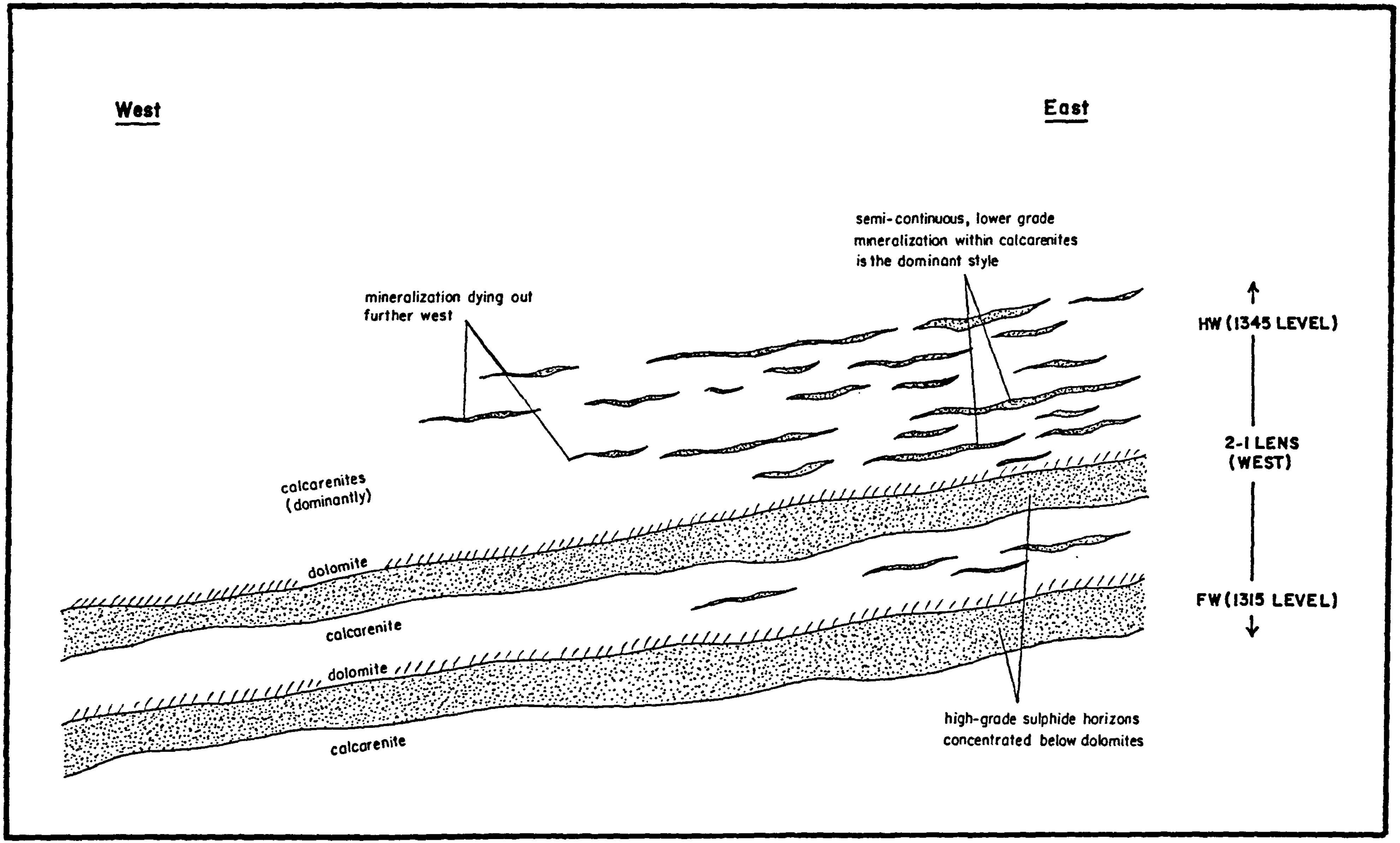
West
East
semi-continuous, lower grade
mineralization within calcarenites
is the dominant style
mineralization dying out
further west
HW (1345 LEVEL)
2-1 LENS
(WEST)
FW (1315 LEVEL)
calcarenites
(dominantly)
dolomite
calcarenite
dolomite
calcarenite
high-grade sulphide horizons
concentrated below dolomites

Figure 5.37a Diagram illustrating the accumulation of sulphides adjacent to the F3 Fault.

Figure 5.37b Diagram illustrating the accumulation of sulphides adjacent to the F2 Fault.

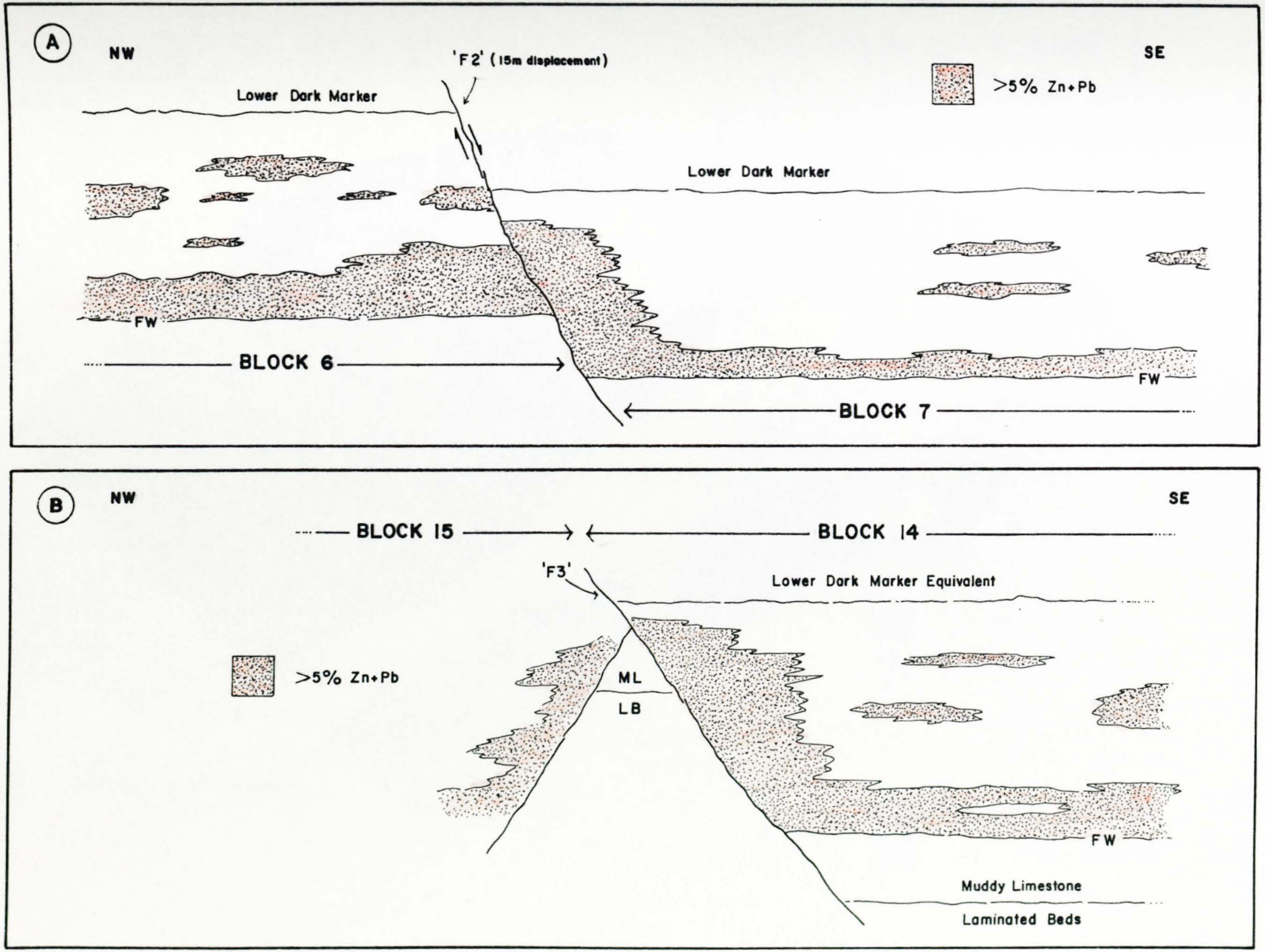
A
NW
SE
'F2' (15m displacement)
>5% Zn+Pb
Lower Dark Marker
Lower Dark Marker
FW
BLOCK 6
FW
BLOCK 7
B
NW
SE
BLOCK 15
BLOCK 14
'F3'
Lower Dark Marker Equivalent
>5% Zn+Pb
ML
LB
FW
Muddy Limestone
Laminated Beds

Figure 5.38 Diagram showing Zn + Pb contours in the 5 Lens, supplied by Tara Mines computer graphics (from Andrew and Ashton, 1985).

Zn+Pb DISTRIBUTION IN 5 LENS - TARA MINES, NAVAN

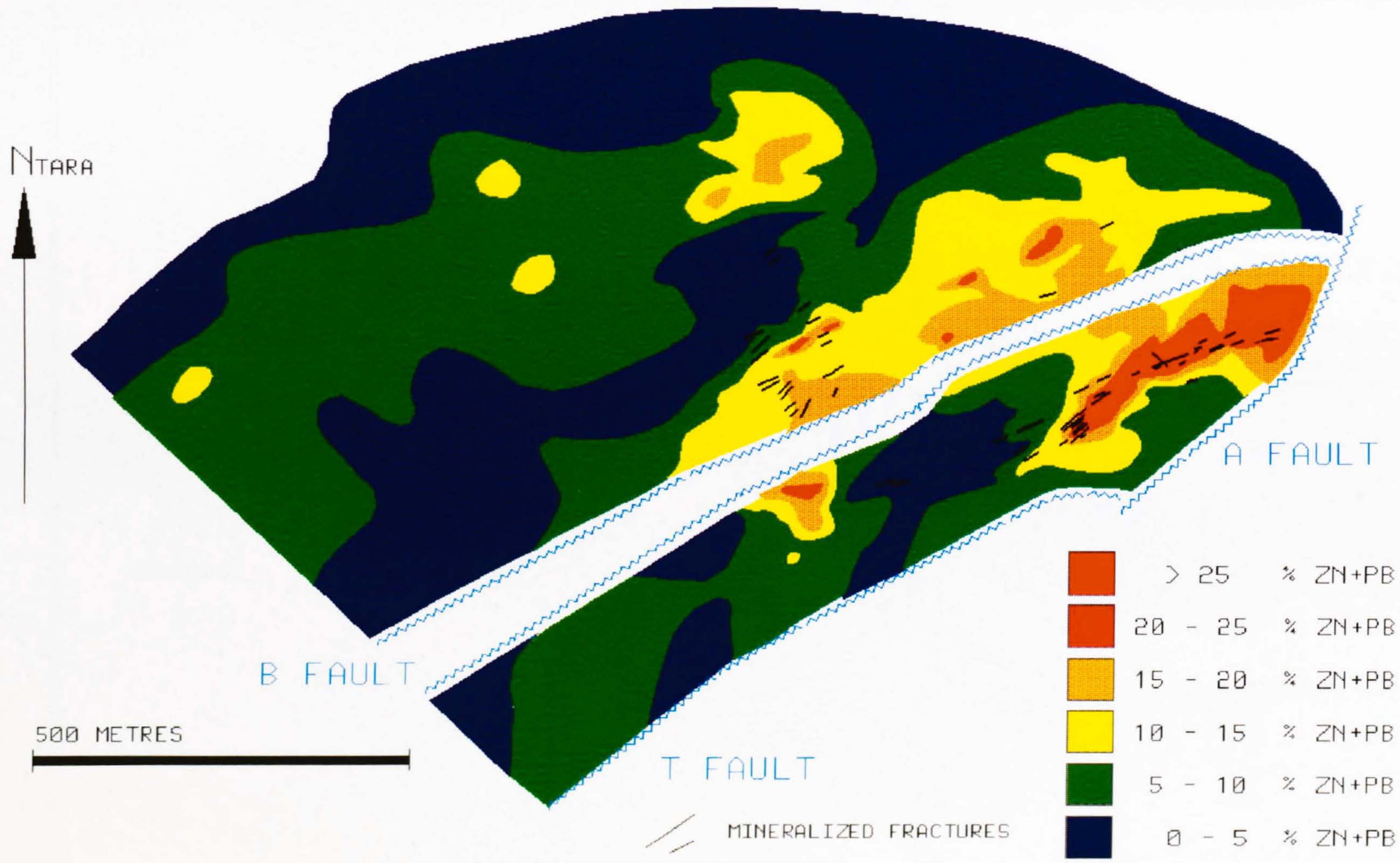

Figure 5.39 Diagram from an underground heading in the Conglomerate Group Ore (3 Zone access drift, 1390 level) illustrating massive and laminated pyrite.

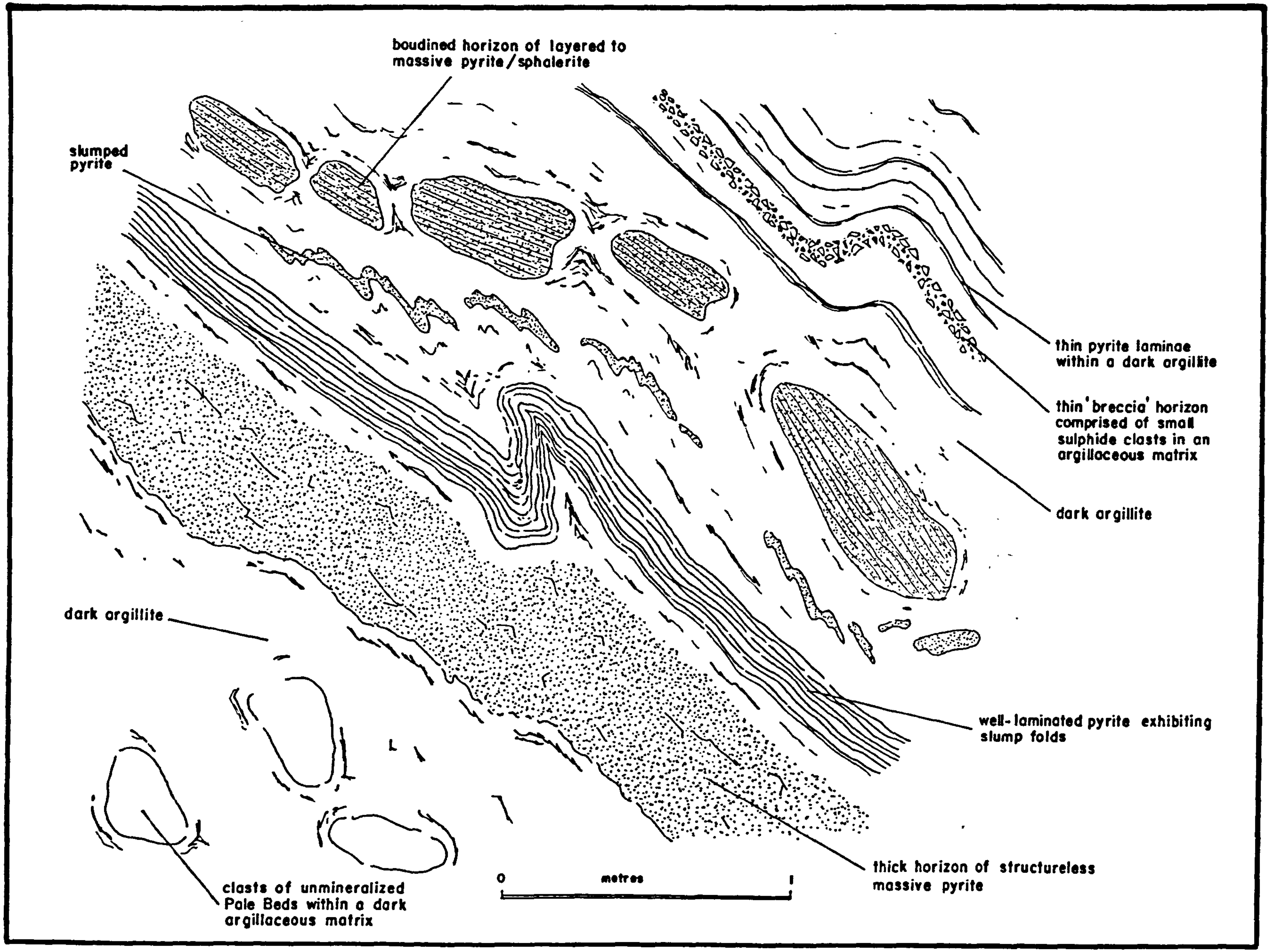
boudined horizon of layered to massive pyrite/sphalerite
slumped pyrite
thin pyrite laminae within a dark argillite
thin 'breccia' horizon comprised of small sulphide clasts in an argillaceous matrix
dark argillite
dark argillite
well-laminated pyrite exhibiting slump folds
thick horizon of structureless massive pyrite
clasts of unmineralized Pale Beds within a dark argillaceous matrix
0
metres
1

Figure 6.1 Diagram illustrating the influence of fo_2 and pH on the sulphur isotopic composition of H_2S in an ore fluid; Temperature = 250°C, $\delta^{34}S_{\Sigma S}$ = 0°/oo (from Ohmoto, 1972).

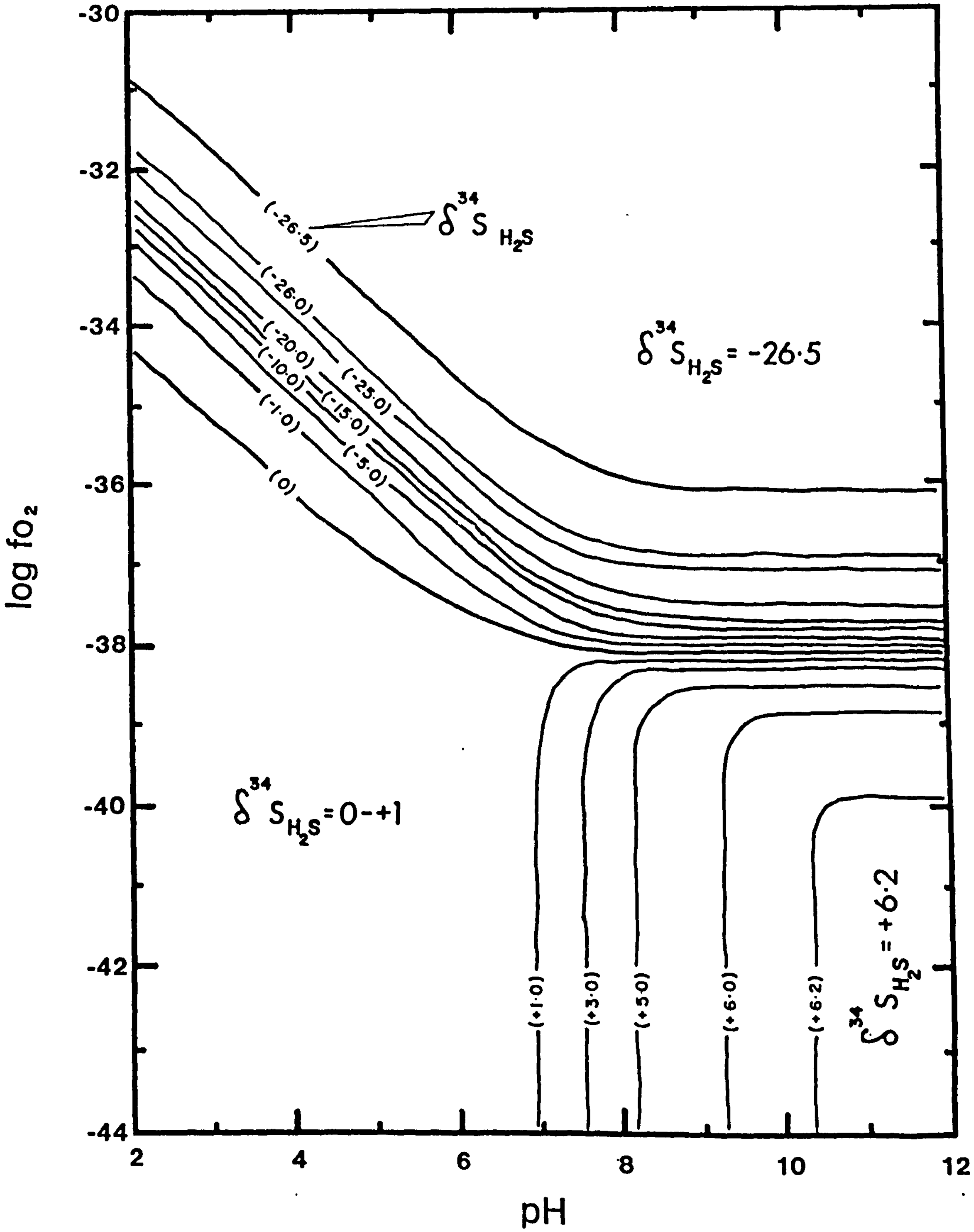

log fo2
pH
-30
-32
-34
-36
-38
-40
-42
-44
2
4
6
8
10
12
δ34S H2S
δ34S H2S = -26·5
δ34S H2S = 0-+1
δ34S H2S = +6·2
(-26·5)
(-26·0)
(-25·0)
(-20·0)
(-15·0)
(-10·0)
(-5·0)
(-1·0)
(0)
(+1·0)
(+3·0)
(+5·0)
(+6·0)
(+6·2)

Figure 6.2a Diagram illustrating the influence of the SO_4^{2-}/H_2S ratio on the sulphur isotopic composition of galena and sphalerite deposited from an ore fluid with $\delta^{34}S_{\Sigma S} = 0^o/_{oo}$, at 200°C (from Rye and Ohmoto, 1974).

Figure 6.2b Graph illustrating the influence of a changing SO_4^{2-}/H_2S ratio on the sulphur isotopic composition of SO_4^{2-}, H_2S, ZnS and PbS in a closed system at 200°C, $\delta^{34}S_{\Sigma S} = 0^o/_{oo}$.

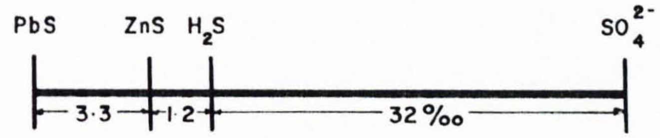

A

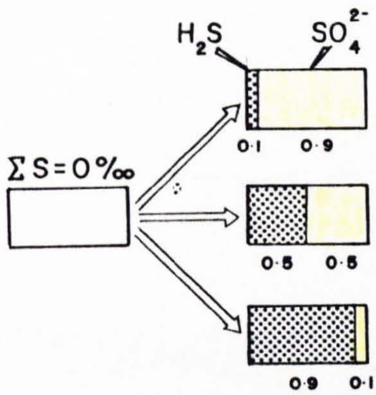

$\delta^{34}S$			
H_2S	SO_4^{2-}	ZnS	PbS
-28·8	3·2	-30·0	-33·3
-16·0	16·0	-17·2	-20·5
-3·2	28·8	-4·4	-7·7

B

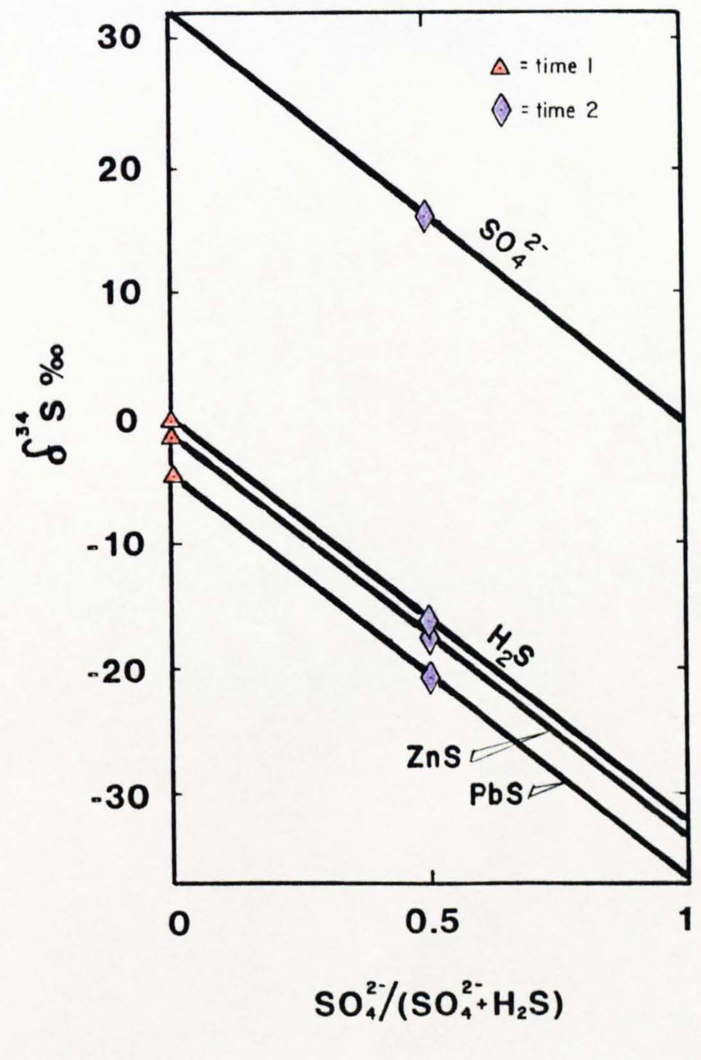

Figure 6.3 Graph illustrating the isotopic composition of SO_4^{2-} and H_2S during closed system bacteriogenic reduction with a fractionation between the starting SO_4^{2-} and the H_2S produced of around 25°/oo. The graph assumes that the H_2S produced is continually removed from the system during the reduction process.

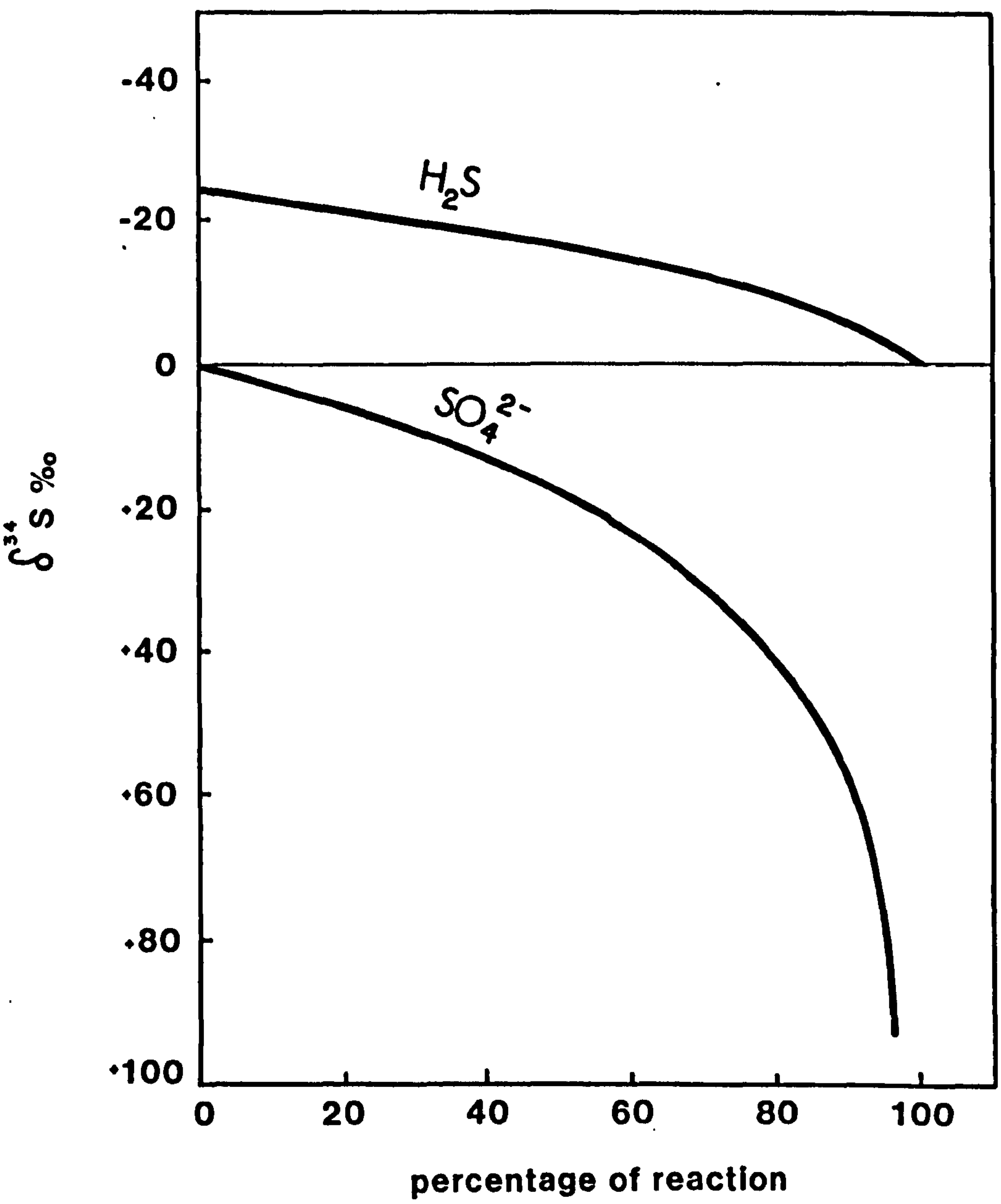
-40
-20
0
+20
+40
+60
+80
+100
$\delta^{34}S$ ‰
H_2S
SO_4^{2-}
0
20
40
60
80
100
percentage of reaction

Figure 6.4 Diagram illustrating the secular variation in the sulphur isotopic composition of seawater sulphate through time as determined from evaporites preserved in the stratigraphic record (adapted from Claypool et al., 1980).

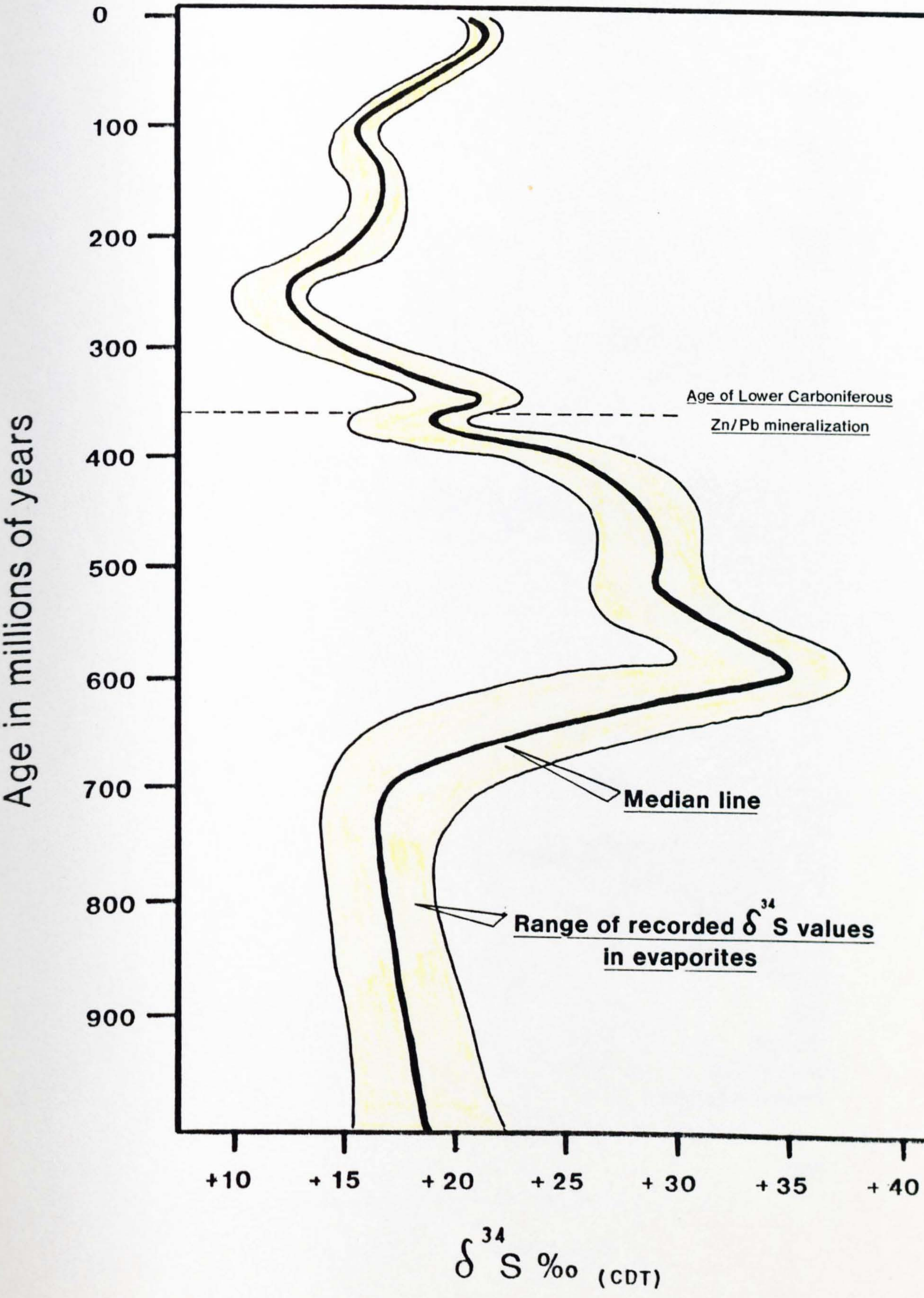

Age in millions of years
0
100
200
300
400
500
600
700
800
900
Age of Lower Carboniferous
Zn/Pb mineralization
Median line
Range of recorded $\delta^{34}S$ values
in evaporites
+10
+ 15
+ 20
+ 25
+ 30
+ 35
+ 40
$\delta^{34}S$ ‰ (CDT)

Figure 6.5 Histogram of the sulphur isotopic composition of all sulphides and sulphates analyzed from the Navan deposit.

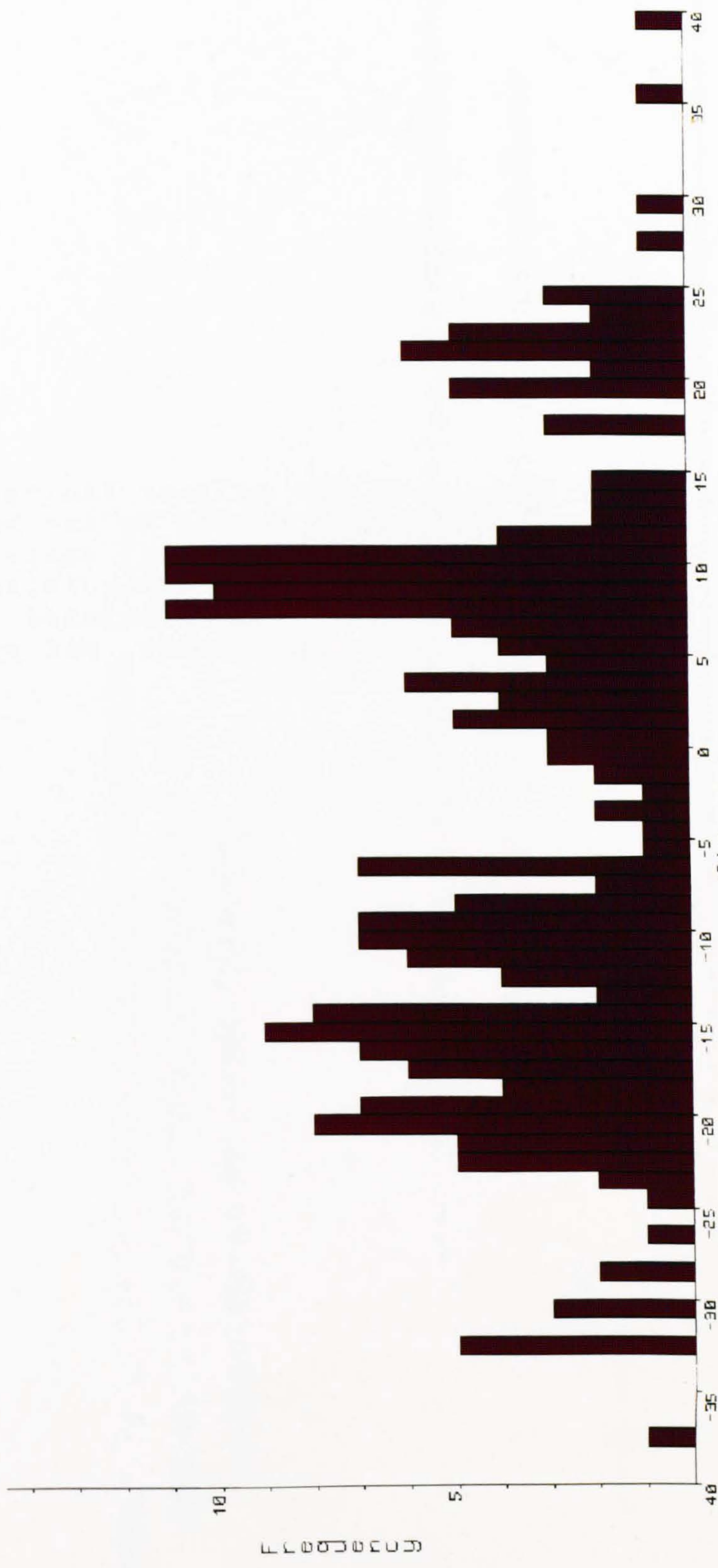
Frequency
10
5
0
-40
-35
-30
-25
-20
-15
-10
-5
0
5
10
15
20
25
30
35
40
$\delta^{34}S$ ‰ (CDT)

Figure 6.6 Summary of the sulphur isotopic composition of sphalerite formed by the bedding-parallel replacement of semi-lithified calcarenites, pyrite/marcasite in bedding-parallel cavities associated with the sphalerite replacement, and pyrite in the CGO (Table 6.2a).

Range in the Isotopic Composition of Laminated and Massive Pyrite in the Conglomerate Group Ore, Navan Mine

Range in the Isotopic Composition of Sulphides Deposited by Replacement of a Semi-lithified Carbonate Host, and Local Bedding-parallel Veining, Navan Mine

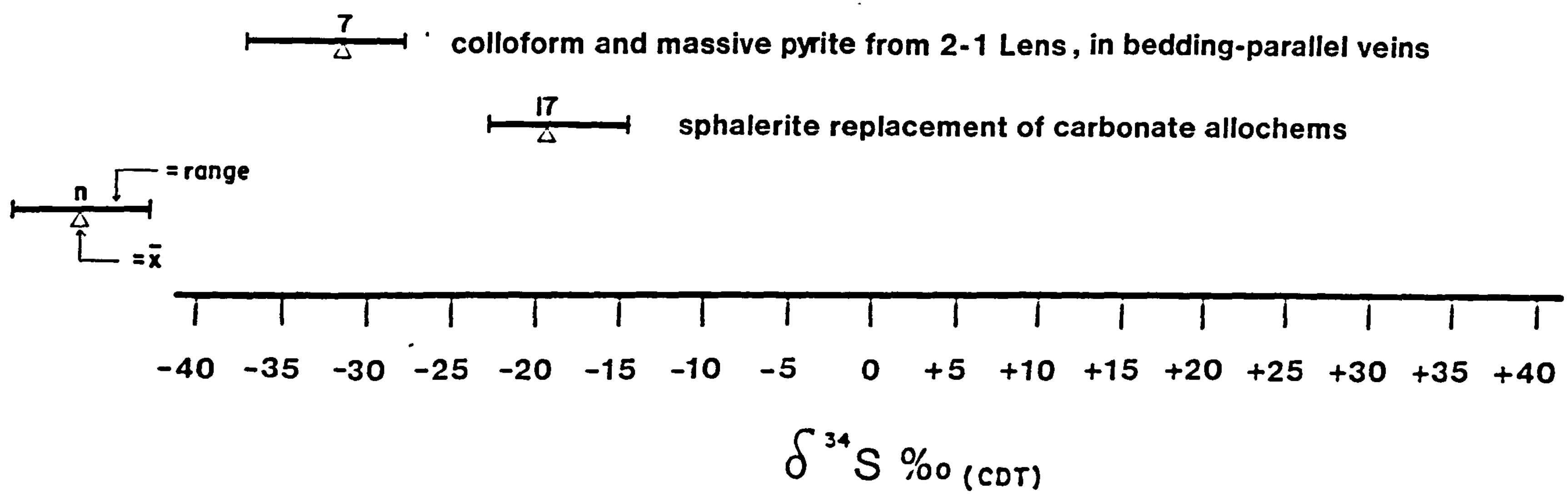

Figure 6.7 Histogram of the sulphur isotopic composition of bedding-parallel sphalerite replacement of allochems, pyrite/marcasite deposited within associated small, bedding-parallel cavities, and pyrite in the CGO (Table 6.2a).

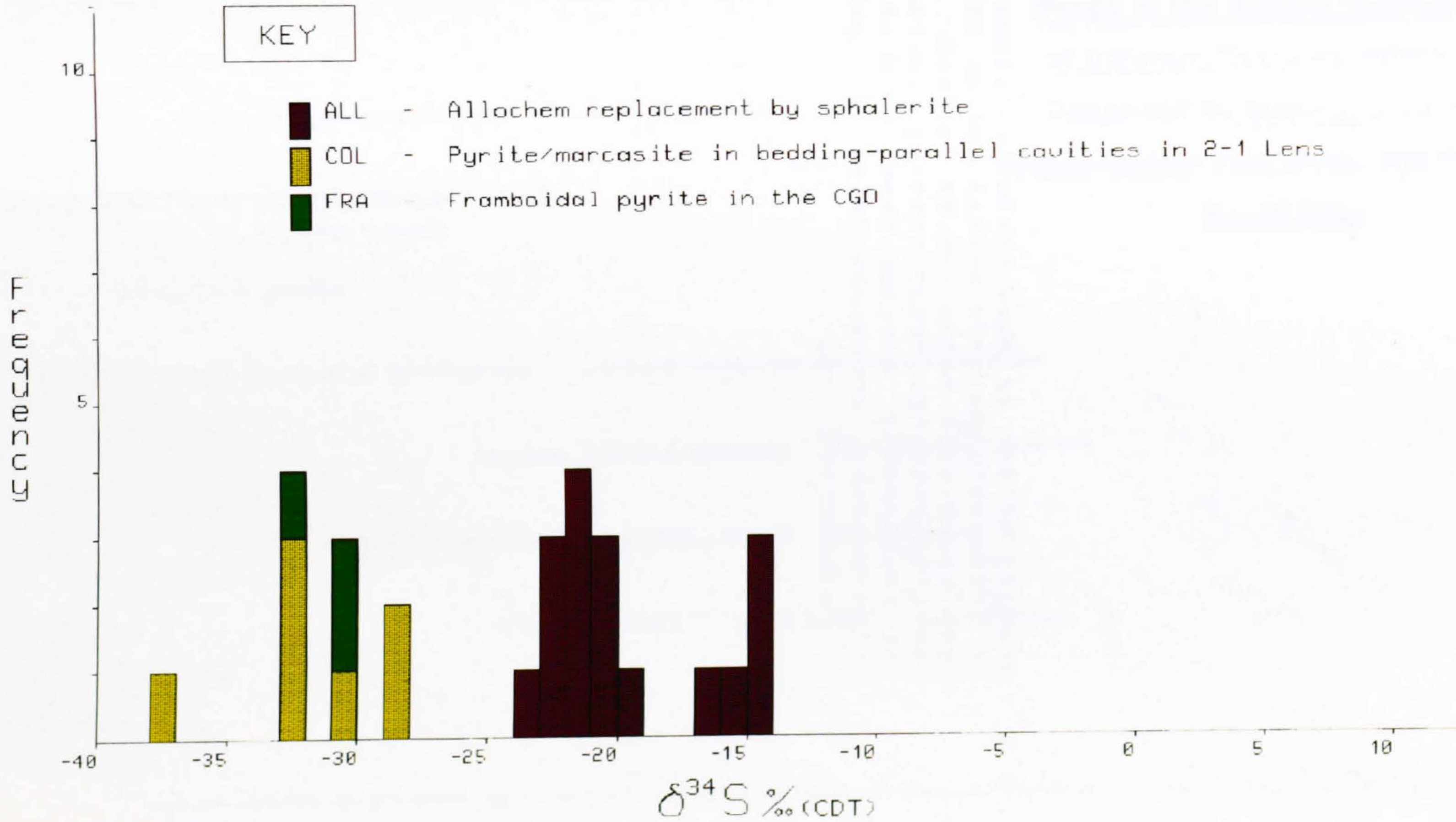
KEY
ALL - Allochem replacement by sphalerite
COL - Pyrite/marcasite in bedding-parallel cavities in 2-1 Lens
FRA - Framboidal pyrite in the CGO
Frequency
10
5
-40
-35
-30
-25
-20
-15
-10
-5
0
5
10
δ34S ‰ (CDT)

Figure 6.8 Summary of the sulphur isotopic composition of different textures within coarse galena/sphalerite ores deposited by bedding-parallel veining, cross-cutting fracturing, and replacement. Similar textures within cross-cutting, cockscomb veins are included for comparison.

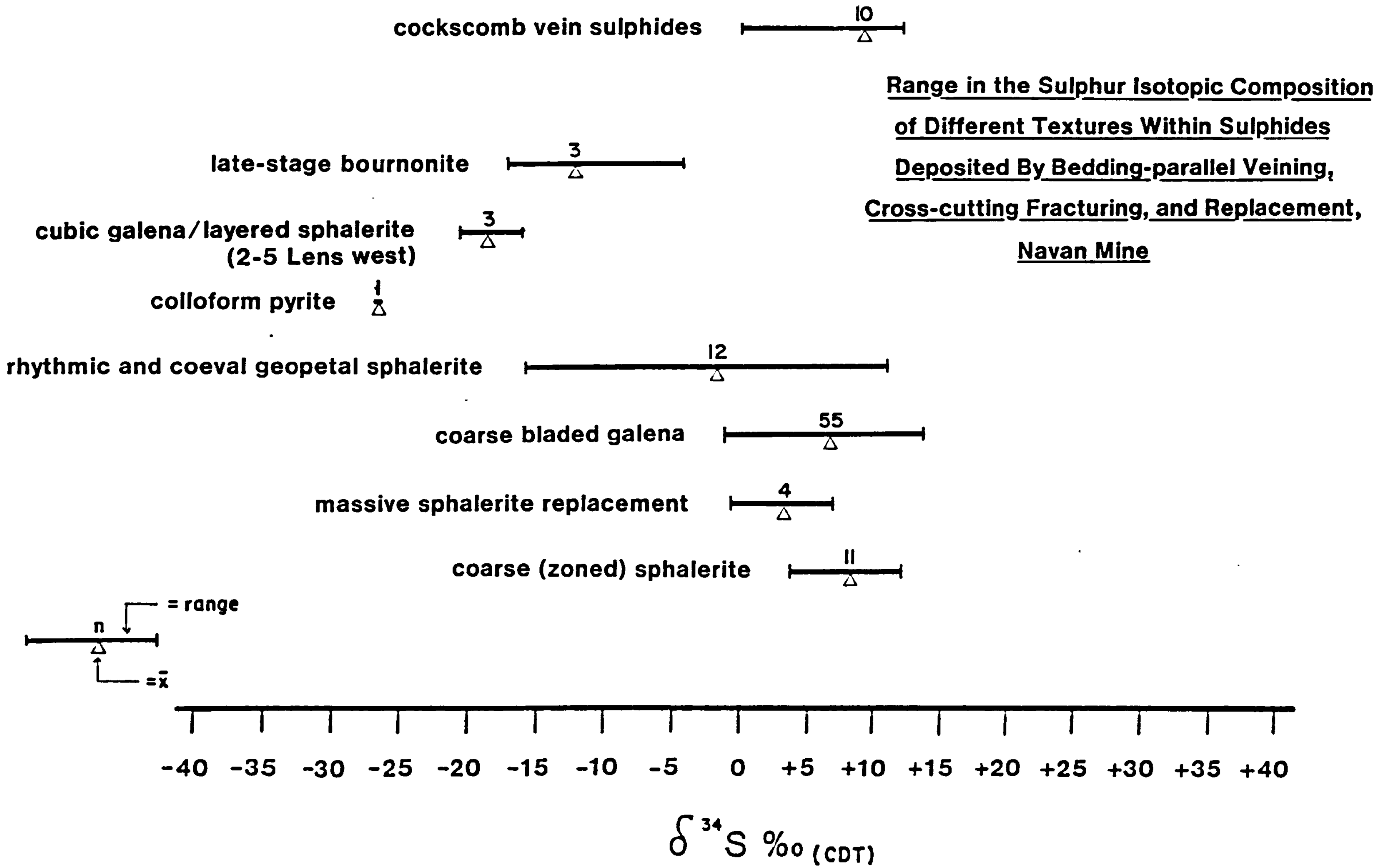

Range in the Sulphur Isotopic Composition of Different Textures Within Sulphides Deposited By Bedding-parallel Veining, Cross-cutting Fracturing, and Replacement, Navan Mine

Figure 6.9 Histogram of the sulphur isotopic composition of different textures within sulphides deposited by bedding-parallel veining, cross-cutting fracturing, and replacement (Table 6.2b).

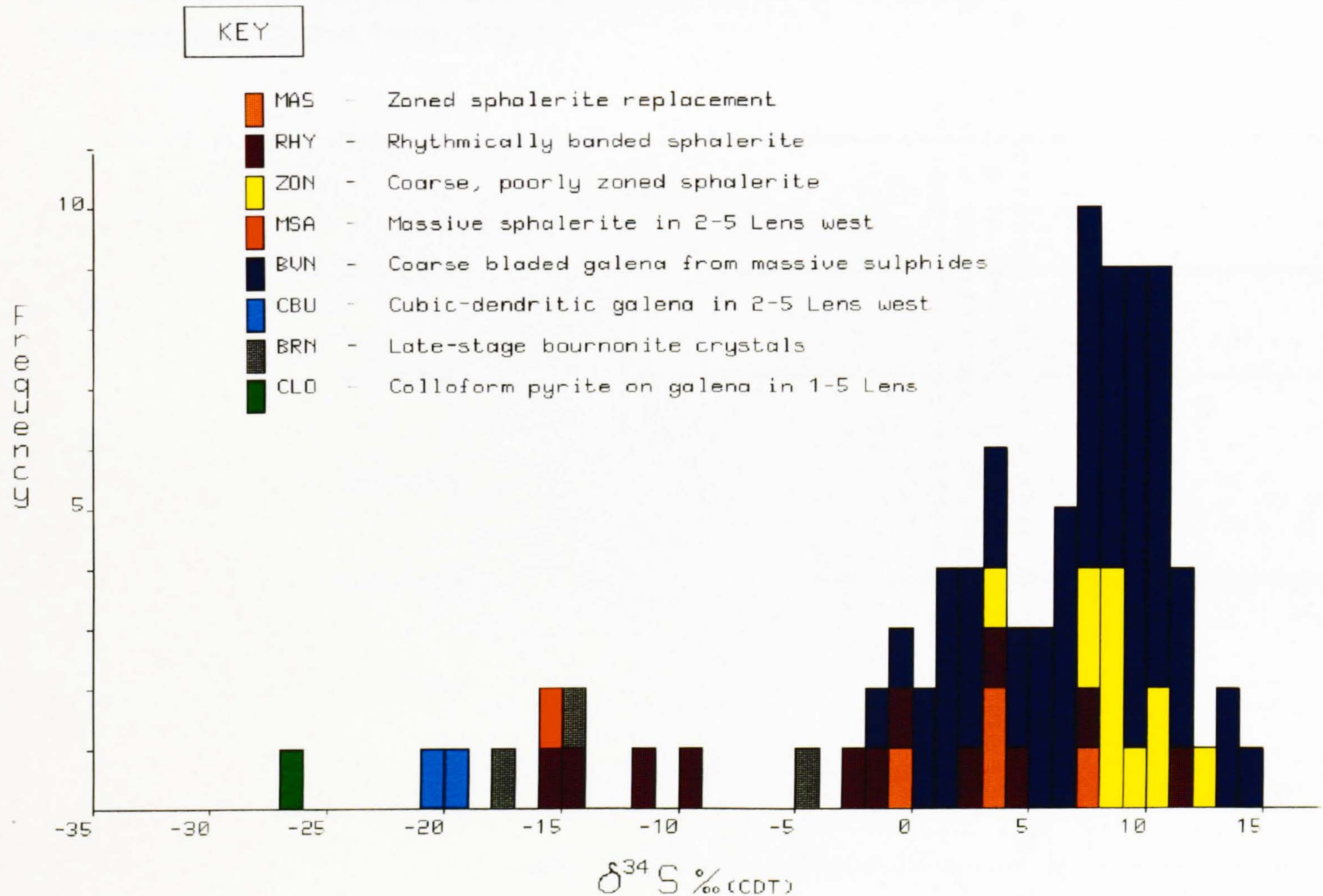
KEY
MAS - Zoned sphalerite replacement
RHY - Rhythmically banded sphalerite
ZON - Coarse, poorly zoned sphalerite
MSA - Massive sphalerite in 2-5 Lens west
BVN - Coarse bladed galena from massive sulphides
CBU - Cubic-dendritic galena in 2-5 Lens west
BRN - Late-stage bournonite crystals
CLO - Colloform pyrite on galena in 1-5 Lens
Frequency
10
5
-35
-30
-25
-20
-15
-10
-5
0
5
10
15
δ34S ‰ (CDT)

Figure 6.10 Summary of the inter-lens variation in the sulphur isotopic composition of coarse bladed galena, and a comparison with similar textures within cross-cutting veins.

Inter-Lens Variation in the Sulphur Isotopic Composition of Coarse Bladed Galena

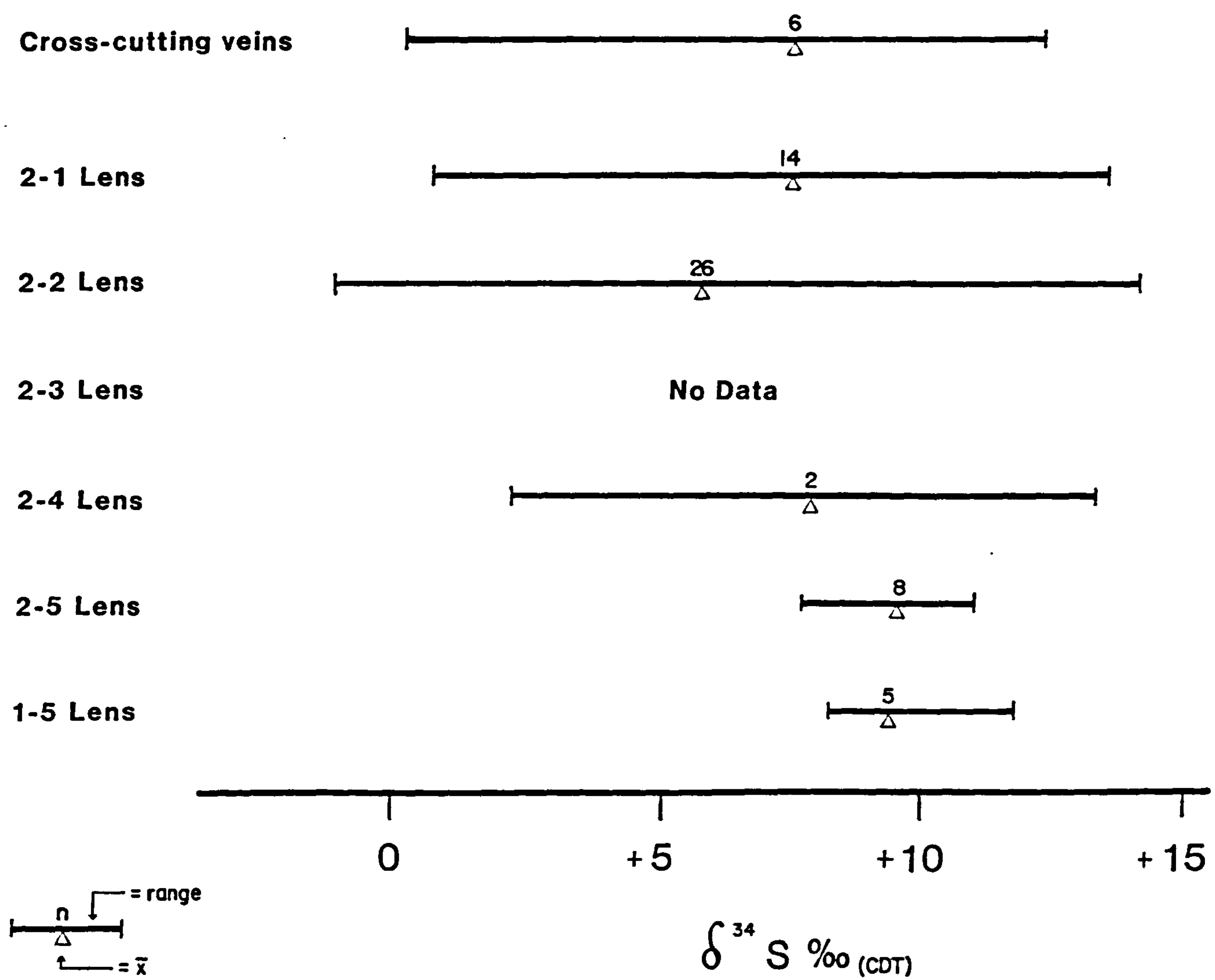

Figure 6.11 Diagrams from hand specimens and thin sections illustrating trends towards relatively lighter $\delta^{34}S$ values in paragenetically later sulphides.

(1)

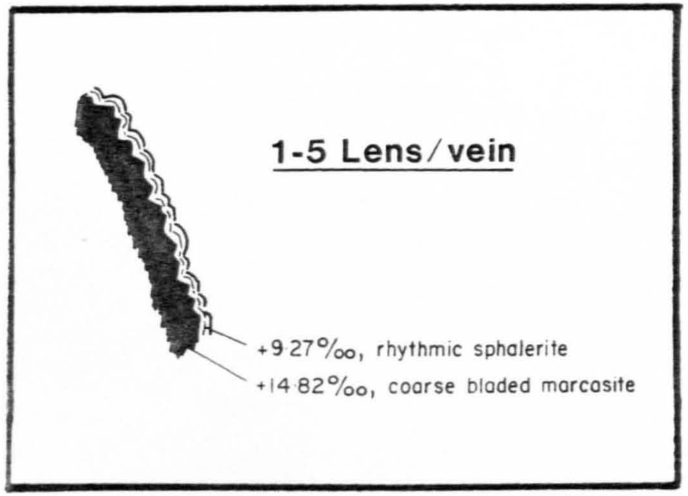

1-5 Lens/vein
+9·27‰, rhythmic sphalerite
+14·82‰, coarse bladed marcasite

(2)

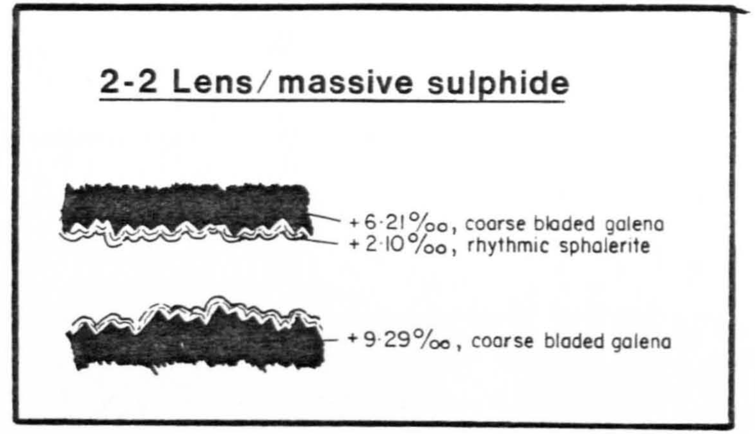

2-2 Lens/massive sulphide
+6·21‰, coarse bladed galena
+2·10‰, rhythmic sphalerite
+9·29‰, coarse bladed galena

(3)

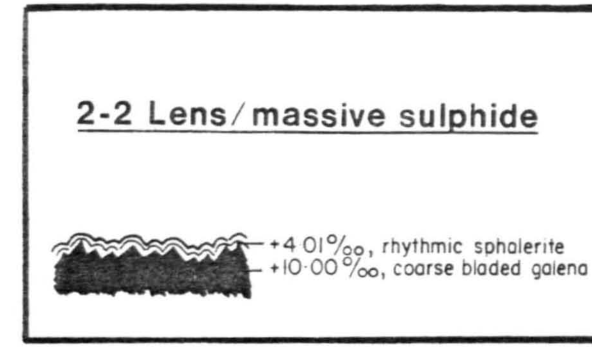

2-2 Lens/massive sulphide
+4·01‰, rhythmic sphalerite
+10·00‰, coarse bladed galena

(4)

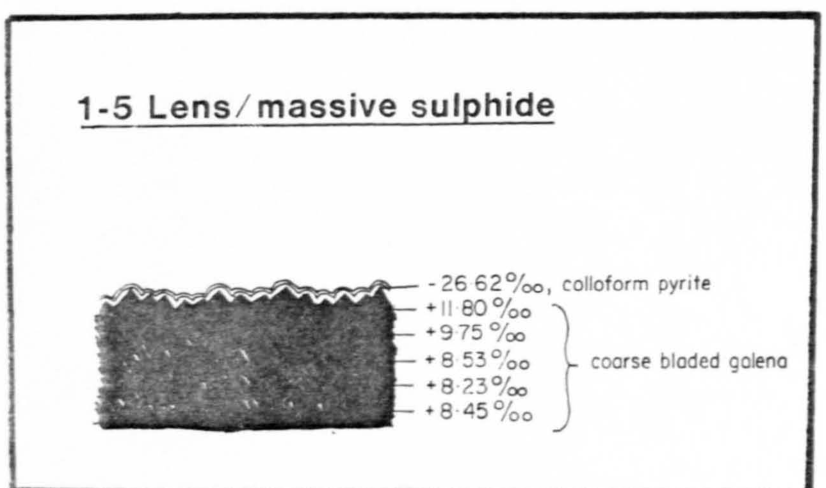

1-5 Lens/massive sulphide
-26·62‰, colloform pyrite
+11·80‰
+9·75‰
+8·53‰
+8·23‰
+8·45‰
coarse bladed galena

(5)

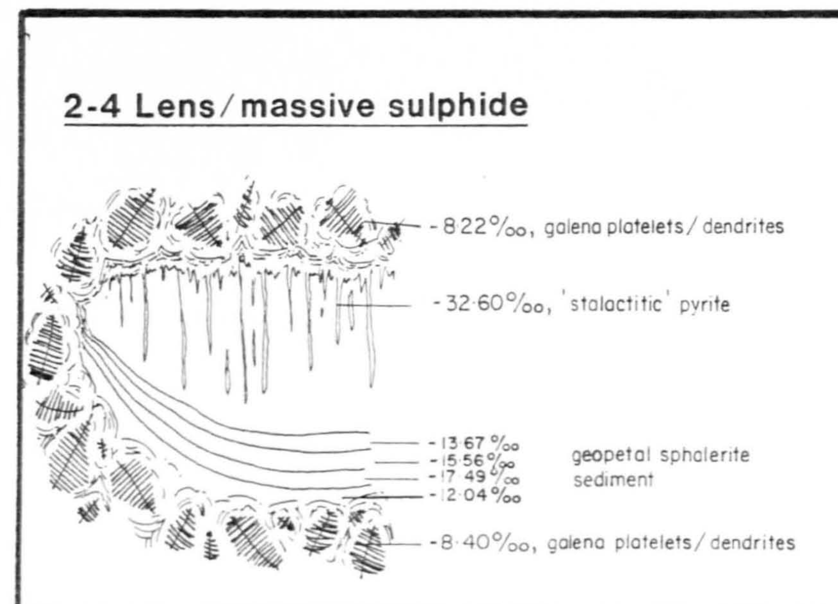

2-4 Lens/massive sulphide
-8·22‰, galena platelets/dendrites
-32·60‰, 'stalactitic' pyrite
-13·67‰
-15·56‰
-17·49‰
-12·04‰
geopetal sphalerite sediment
-8·40‰, galena platelets/dendrites

Figure 6.12 Diagram compiled from thin sections prepared from sulphides in 2-5 Lens (242S stope, 1315 and 1330 levels) illustrating the trend towards relatively lighter $\delta^{34}S$ values in later paragenetic stages.

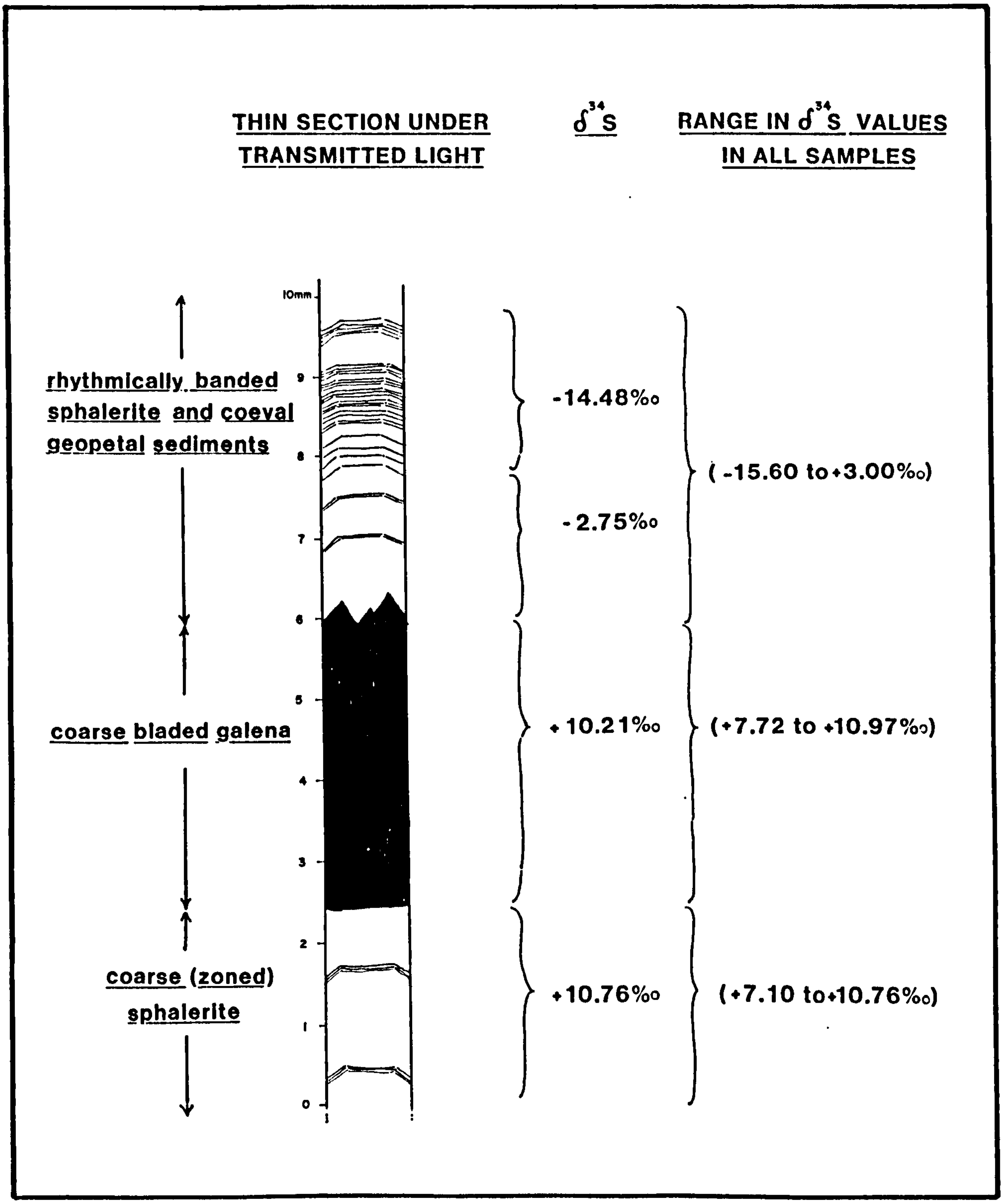
THIN SECTION UNDER TRANSMITTED LIGHT
$\delta^{34}S$
RANGE IN $\delta^{34}S$ VALUES IN ALL SAMPLES
10mm
9
8
7
6
5
4
3
2
1
0
rhythmically banded sphalerite and coeval geopetal sediments
coarse bladed galena
coarse (zoned) sphalerite
-14.48‰
-2.75‰
+10.21‰
+10.76‰
(-15.60 to +3.00‰)
(+7.72 to +10.97‰)
(+7.10 to +10.76‰)

Figure 6.13 Diagram illustrating a hand-drilled sulphur isotopic traverse across a coarse galena band from 2-1 Lens (229N, 1435 level) illustrating shifts in the isotopic composition of the galena in the direction of crystal growth.

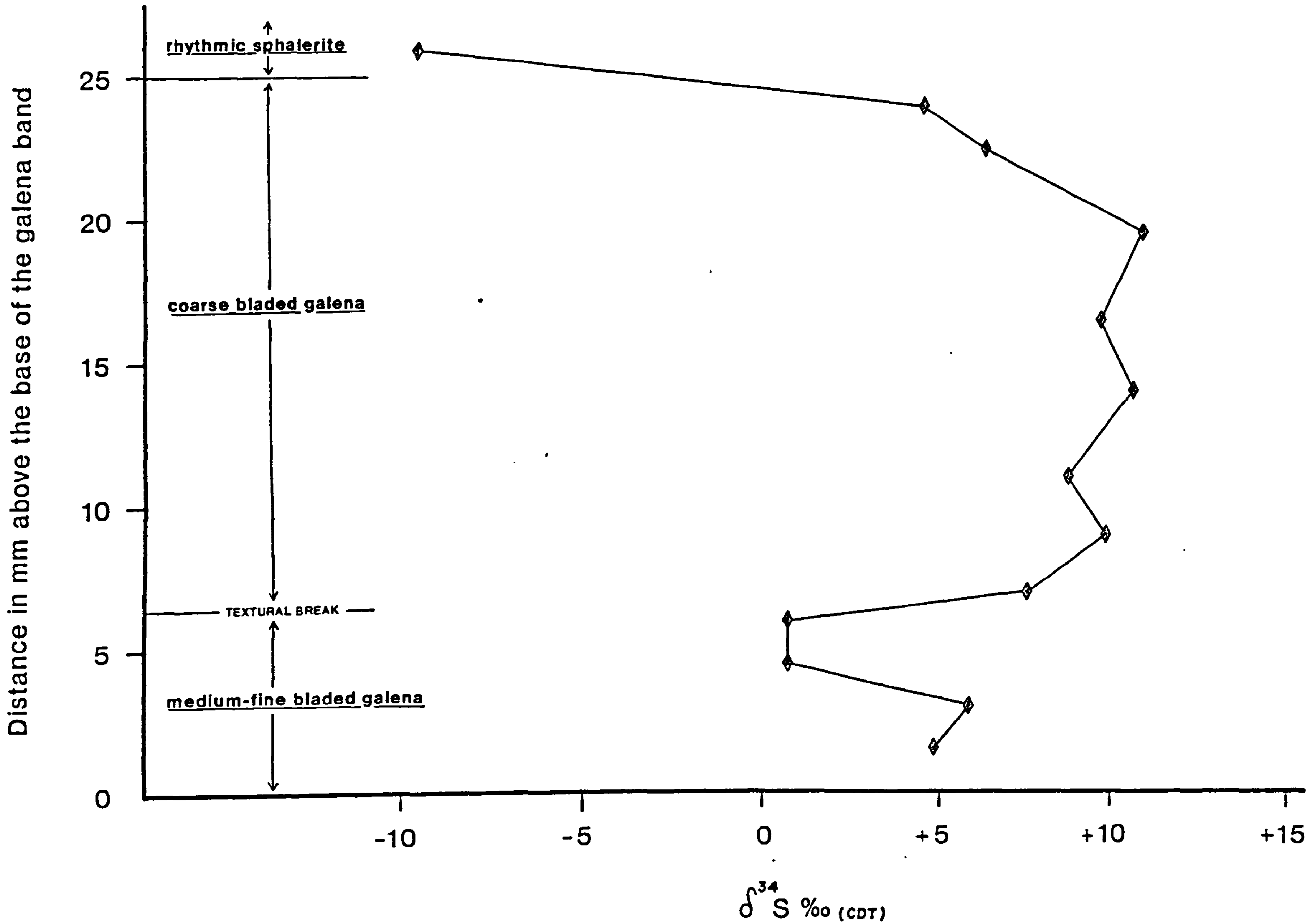
rhythmic sphalerite
coarse bladed galena
TEXTURAL BREAK
medium-fine bladed galena
Distance in mm above the base of the galena band
25
20
15
10
5
0
-10
-5
0
+5
+10
+15
$\delta^{34}S$ ‰ (CDT)

Figure 6.14 Diagram illustrating a lasered sulphur isotopic traverse across the same galena sample as that in Figure 6.13, except conducted about 1cm away from the hand-drilled traverse, illustrating the detailed nature of the shifts and fluctuations in the isotopic composition of the galena. The initial hand-drilled traverse is incorporated for comparison.

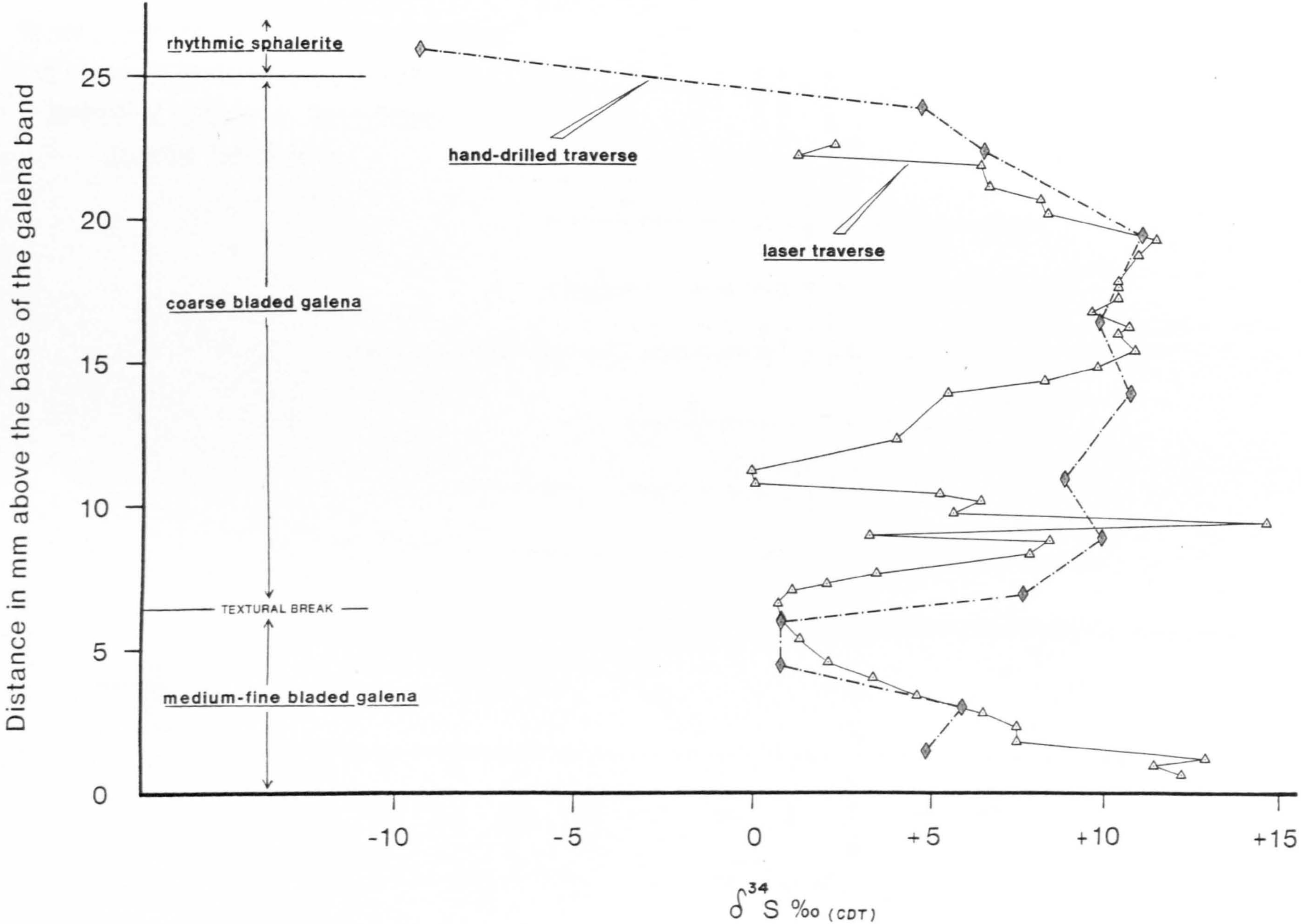
rhythmic sphalerite
coarse bladed galena
TEXTURAL BREAK
medium-fine bladed galena
hand-drilled traverse
laser traverse
Distance in mm above the base of the galena band
0
5
10
15
20
25
-10
-5
0
+5
+10
+15
$\delta^{34}S$ ‰ (CDT)

Figure 6.15 Summary of the sulphur isotopic composition of different textures in sulphide horizons deposited as open space mineralization. Similar textures within a large vein swarm in 2-5 Lens are included for comparison.

Range in the Sulphur Isotopic Composition of Different Textures Within Sulphides Deposited as Internal, Open-Space Growths, Navan Mine

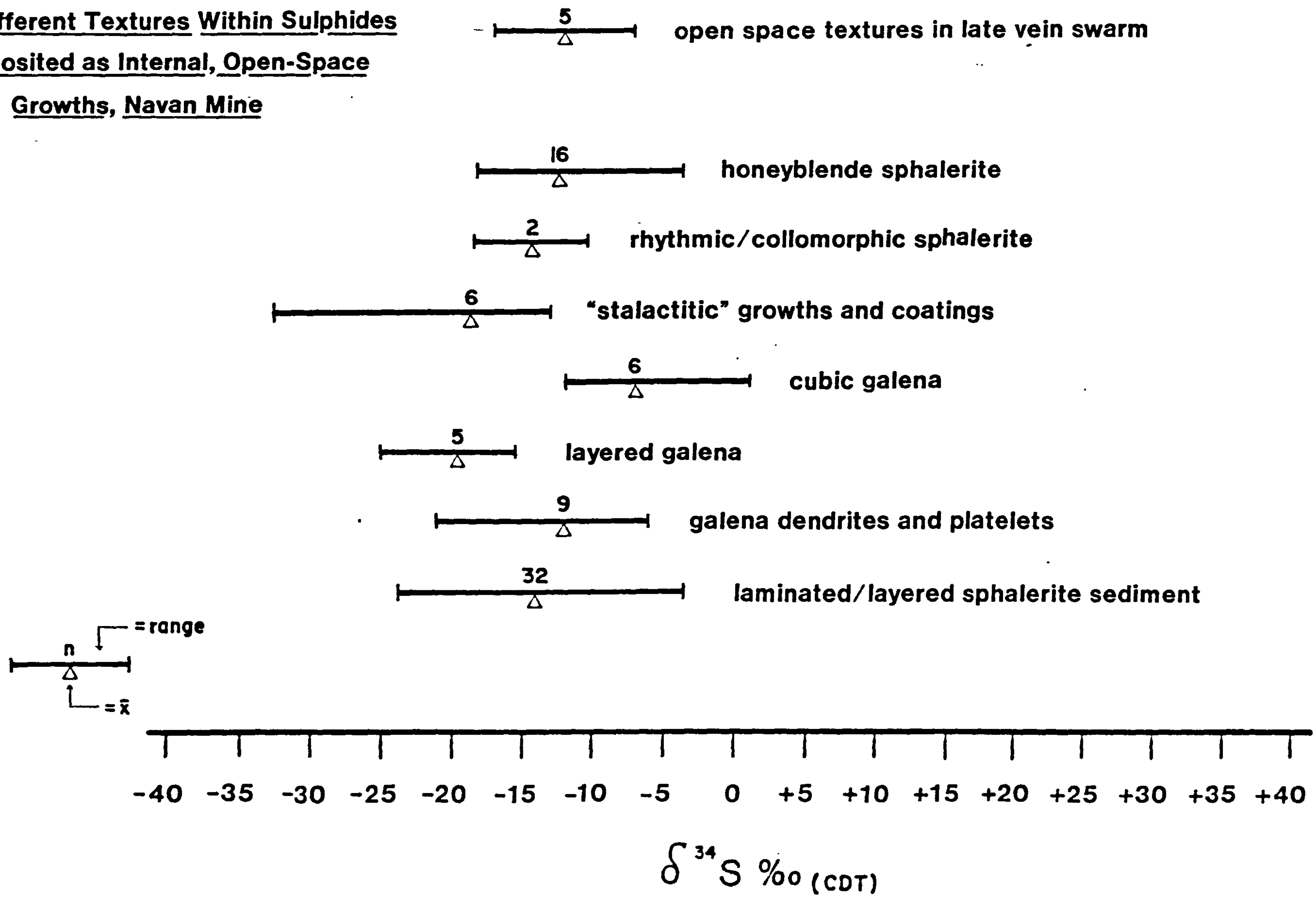

Figure 6.16 Histogram of the sulphur isotopic composition of different textures within sulphide horizons deposited as open space mineralization (Table 6.2c).

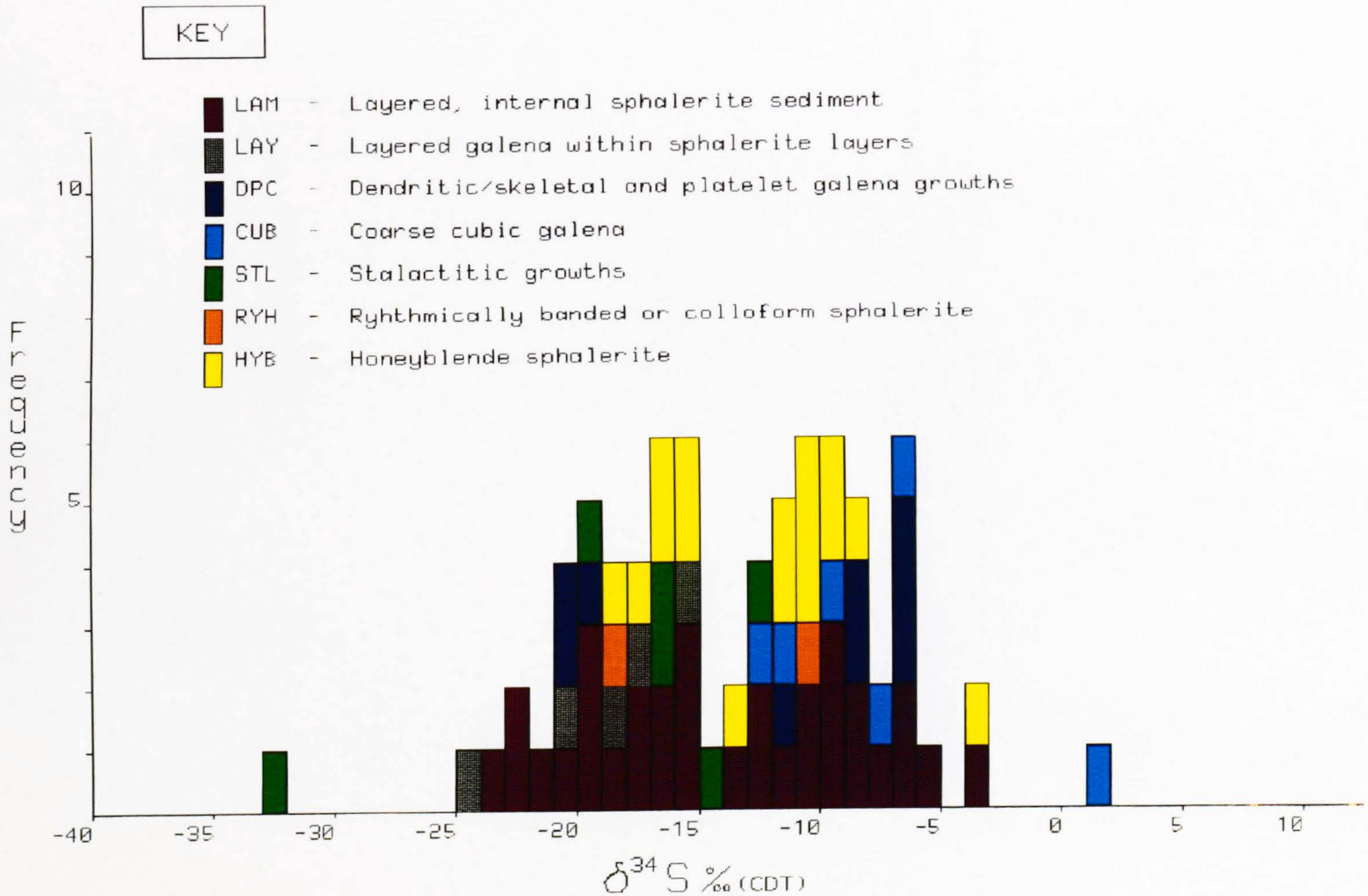
KEY
LAM - Layered, internal sphalerite sediment
LAY - Layered galena within sphalerite layers
DPC - Dendritic/skeletal and platelet galena growths
CUB - Coarse cubic galena
STL - Stalactitic growths
RYH - Ryhthmically banded or colloform sphalerite
HYB - Honeyblende sphalerite
Frequency
10
5
-40
-35
-30
-25
-20
-15
-10
-5
0
5
10
δ34S ‰ (CDT)

Figure 6.17 Histogram of the sulphur isotopic composition of different textures within cross-cutting vein sulphides (Table 6.2d).

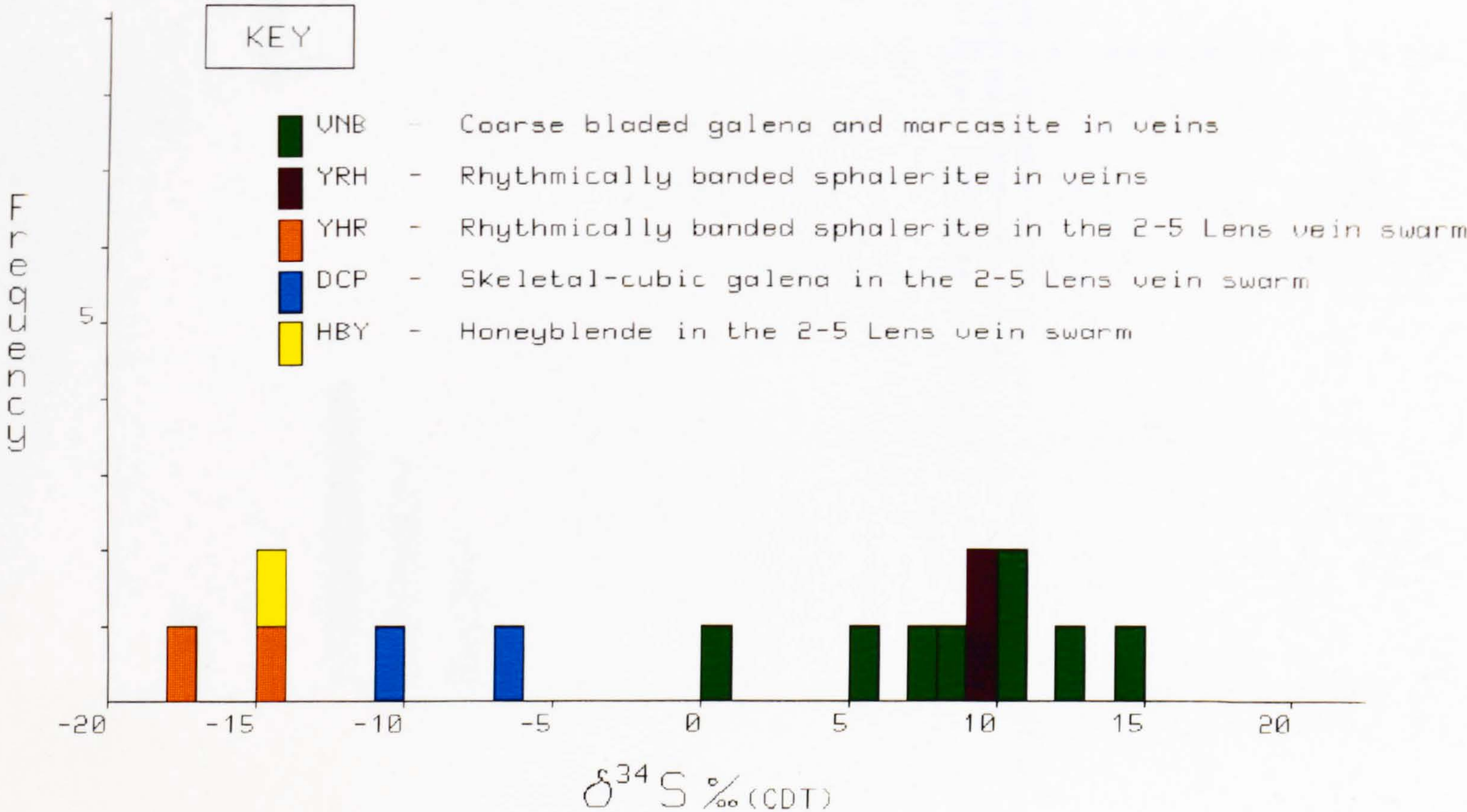
KEY
VNB - Coarse bladed galena and marcasite in veins
YRH - Rhythmically banded sphalerite in veins
YHR - Rhythmically banded sphalerite in the 2-5 Lens vein swarm
DCP - Skeletal-cubic galena in the 2-5 Lens vein swarm
HBY - Honeyblende in the 2-5 Lens vein swarm
Frequency
5
-20
-15
-10
-5
0
5
10
15
20
$\delta^{34}S$ ‰ (CDT)

Figure 6.18 Histogram of the sulphur isotopic composition of pyrite in the CGO and pyrite from small, bedding-parallel cavities in 2-1 Lens.

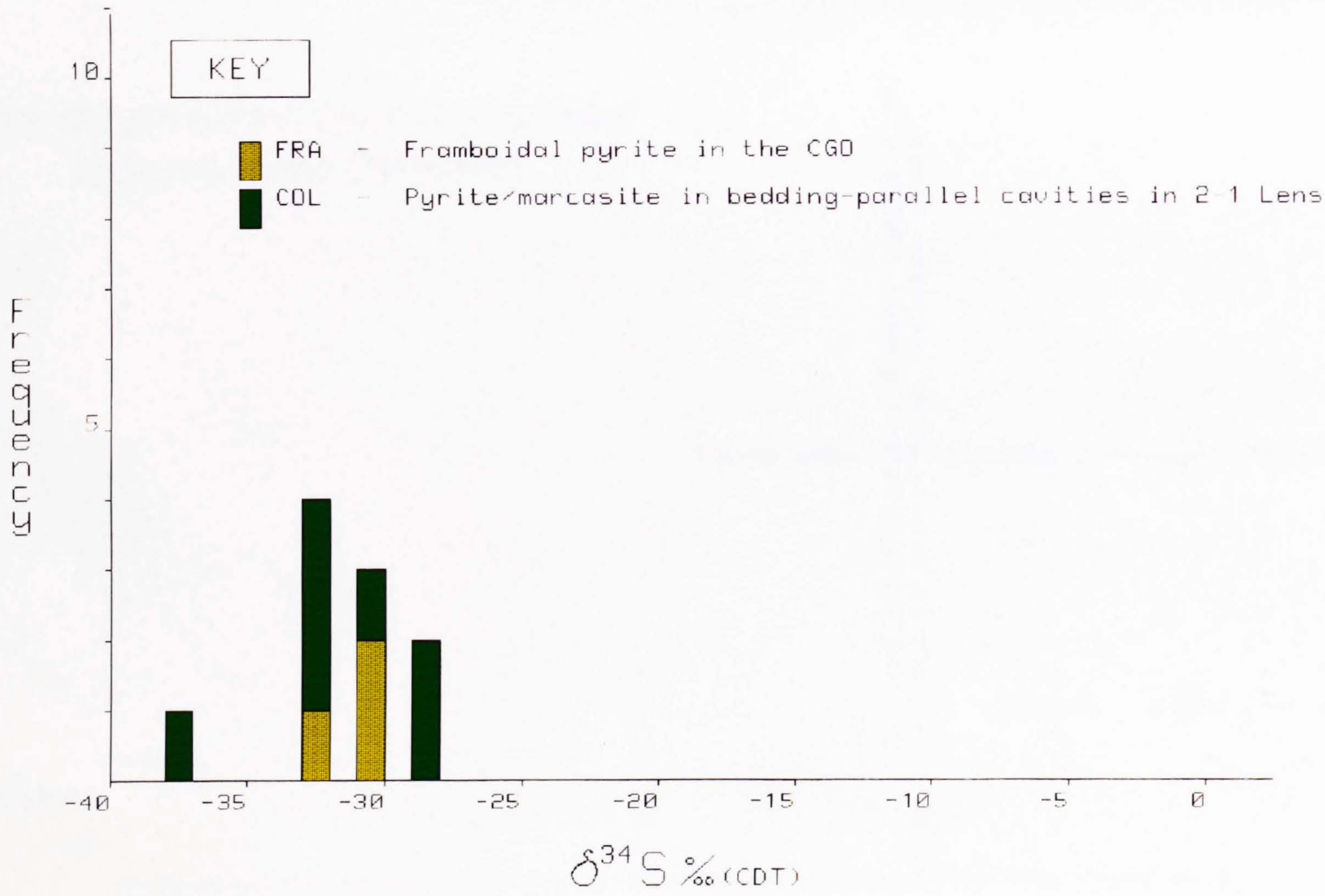
KEY
FRA - Framboidal pyrite in the CGO
COL - Pyrite/marcasite in bedding-parallel cavities in 2-1 Lens
Frequency
10
5
-40
-35
-30
-25
-20
-15
-10
-5
0
δ34 S ‰ (CDT)

Figure 6.19 Summary of the sulphur isotopic composition of barite and gypsum (Table 6.2e).

Range in the Sulphur Isotopic Composition of Barite and Gypsum, Navan Mine

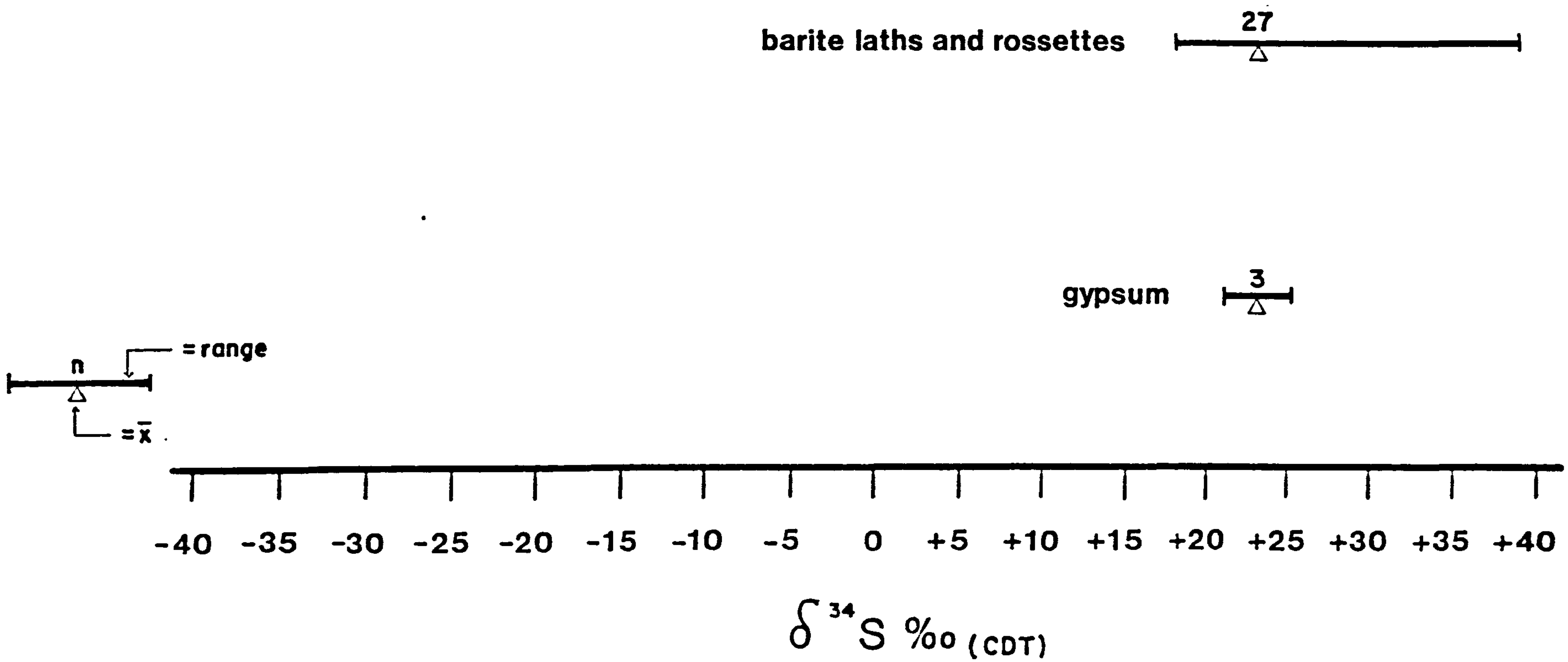

Figure 6.20 Histogram of the sulphur isotopic composition of barite and gypsum (Table 6.2e).

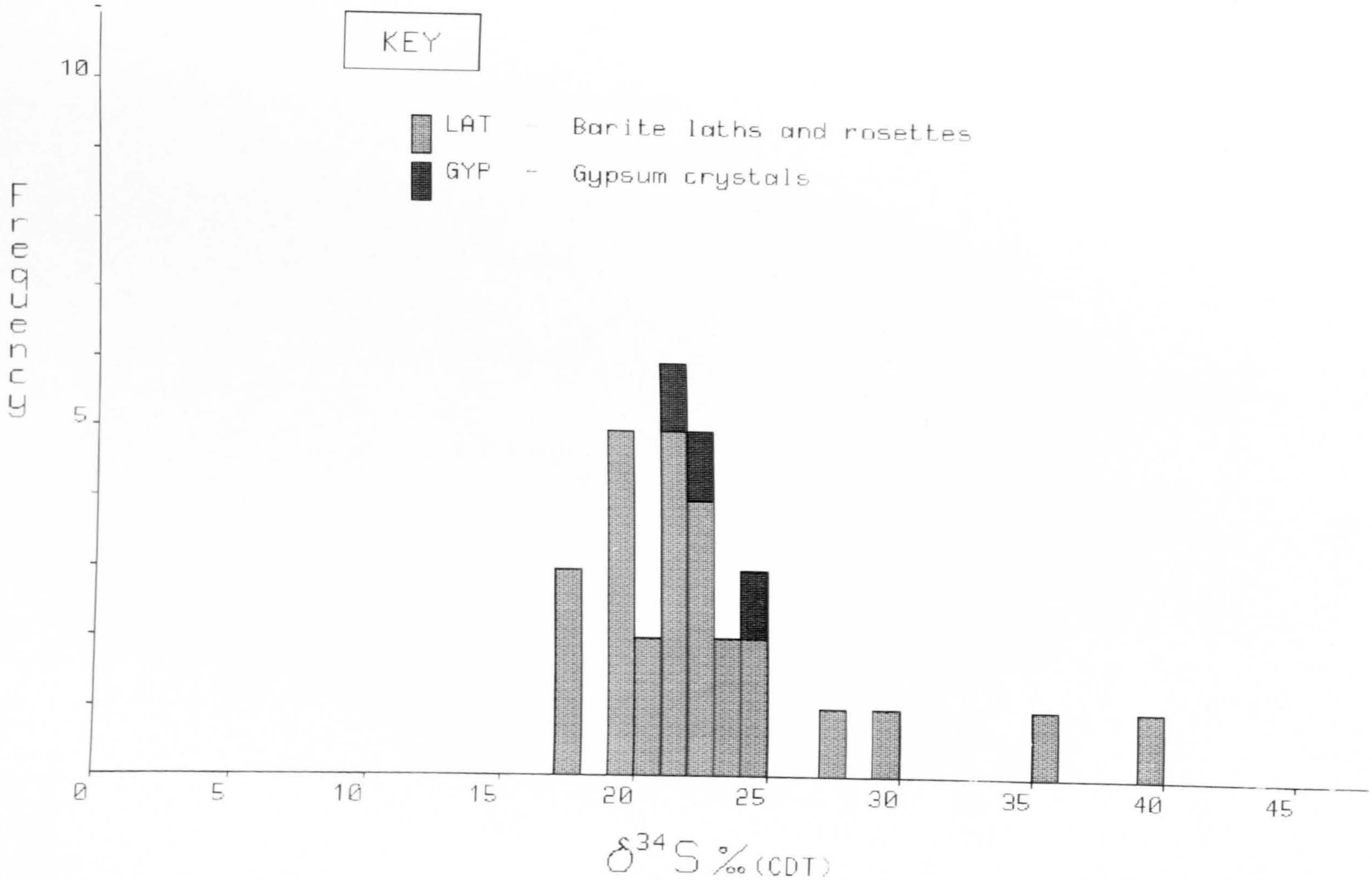
KEY
LAT - Barite laths and rosettes
GYP - Gypsum crystals
Frequency
10
5
0
5
10
15
20
25
30
35
40
45
δ34S ‰ (CDT)

Figure 6.21 Summary of the inter-lens variation in the sulphur isotopic composition of barite and a comparison with barite in late stage veins.

Inter-Lens Variation in the Sulphur Isotopic Composition of Barite

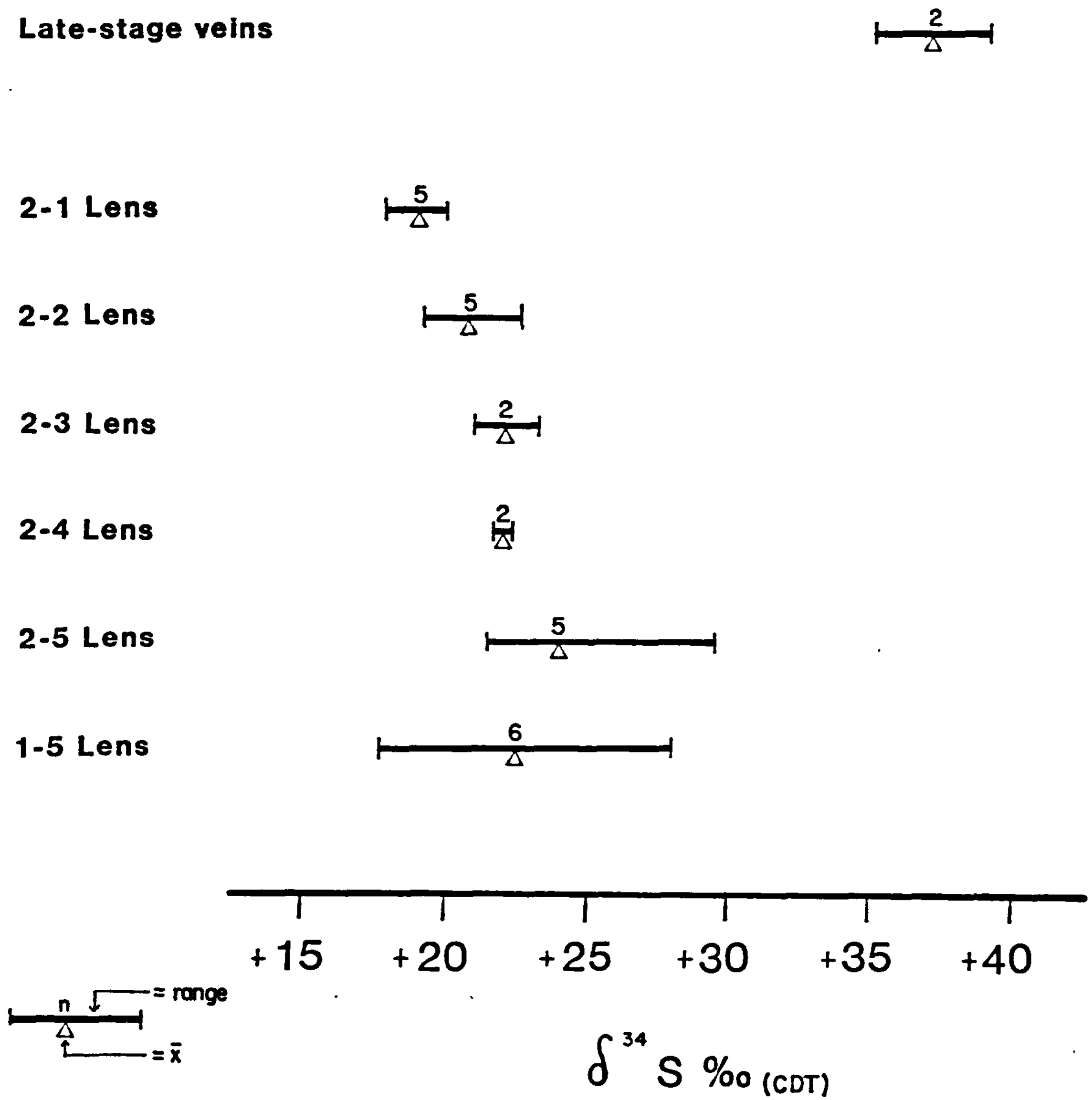

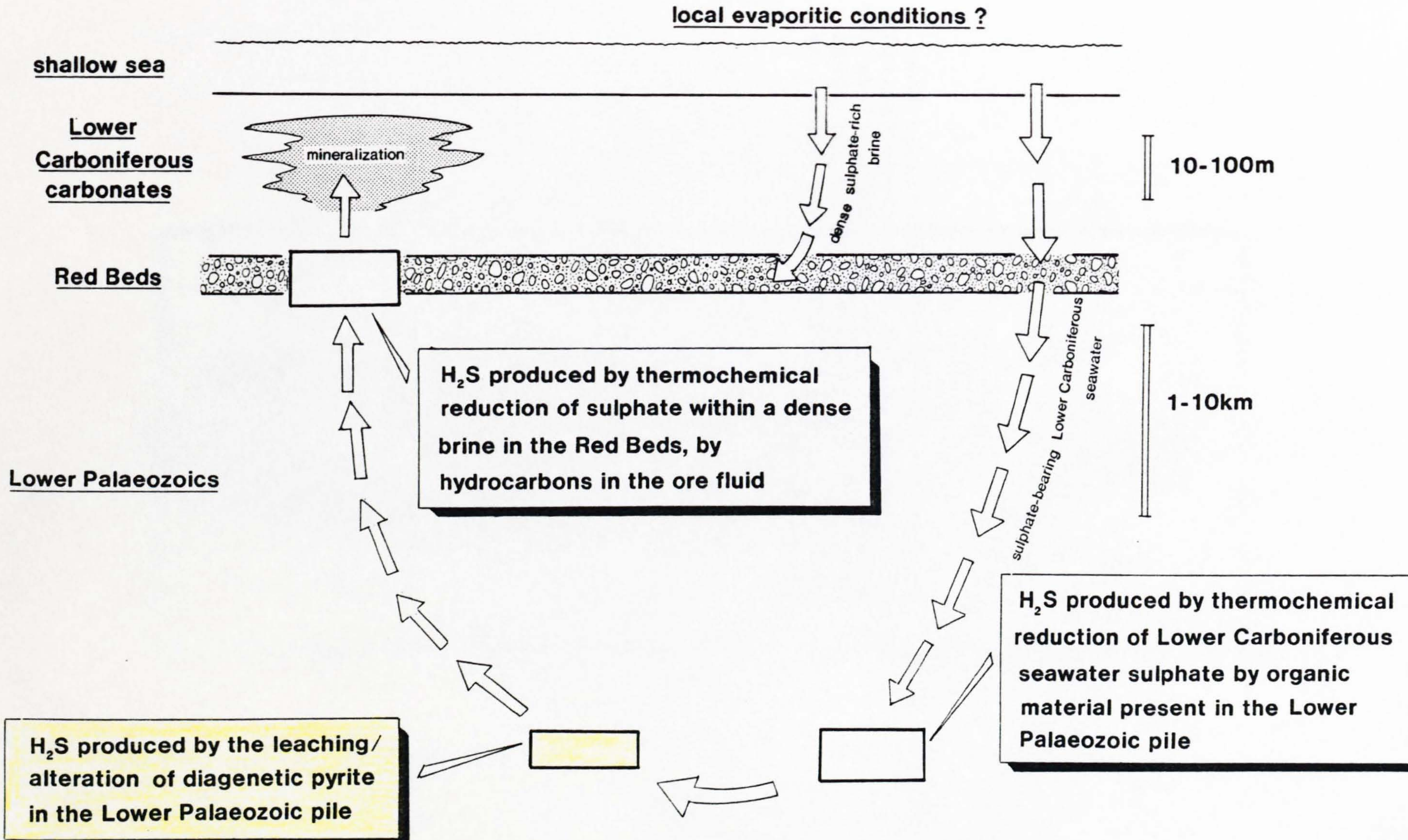
local evaporitic conditions ?
shallow sea
Lower Carboniferous carbonates
mineralization
dense sulphate-rich brine
10-100m
Red Beds
H₂S produced by thermochemical reduction of sulphate within a dense brine in the Red Beds, by hydrocarbons in the ore fluid
Lower Palaeozoics
sulphate-bearing Lower Carboniferous seawater
1-10km
H₂S produced by thermochemical reduction of Lower Carboniferous seawater sulphate by organic material present in the Lower Palaeozoic pile
H₂S produced by the leaching/alteration of diagenetic pyrite in the Lower Palaeozoic pile

FIG. 6.22

Figure 6.23 Diagram from drillcore (drillhole U80) illustrating pyrite concretions (stipple) deforming laminae in the Lower Palaeozoic host rock and implying the pyrite formed prior to lithification of the shale, ie diagenetically.

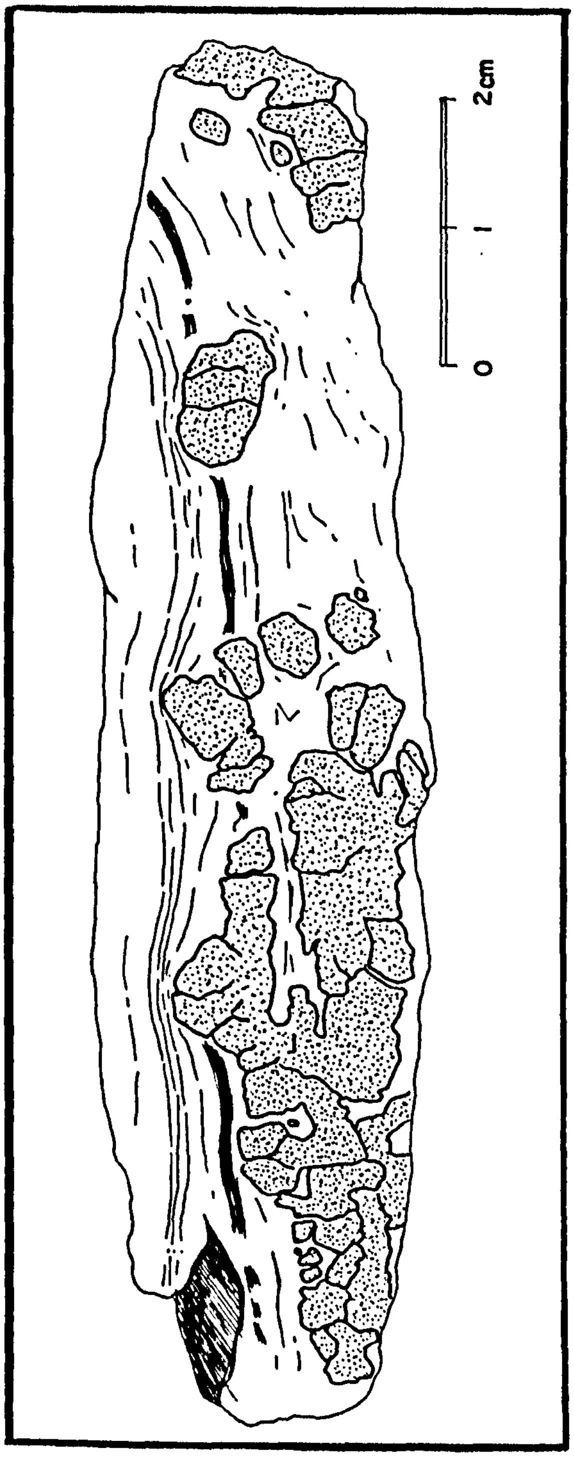
0
1
2cm

Figure 6.24 Summary of the sulphur isotopic composition of diagenetic pyrite and sulphides within veinlets in Lower Palaeozoic rocks below the Navan deposit (Table 6.2f).

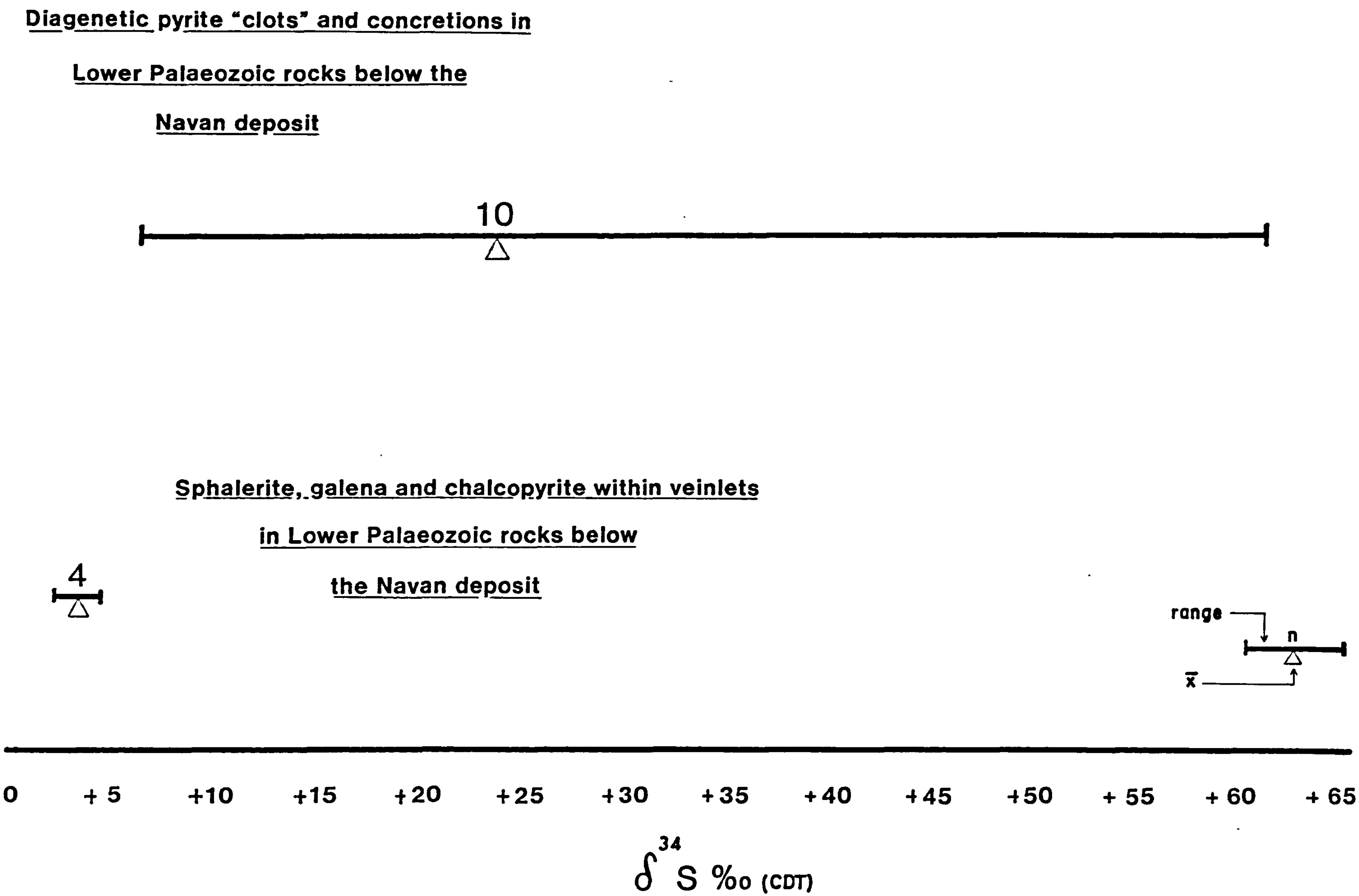
Diagenetic pyrite "clots" and concretions in
Lower Palaeozoic rocks below the
Navan deposit
10
Sphalerite, galena and chalcopyrite within veinlets
in Lower Palaeozoic rocks below
the Navan deposit
4
range
n
x̄
0
+ 5
+10
+15
+20
+25
+30
+35
+40
+45
+50
+ 55
+ 60
+ 65
δ34S ‰ (CDT)

Figure 6.25 Histogram of the sulphur isotopic composition of diagenetic pyrite and sulphides in veinlets in Lower Palaeozoic rocks below the Navan deposit (Table 6.2f).

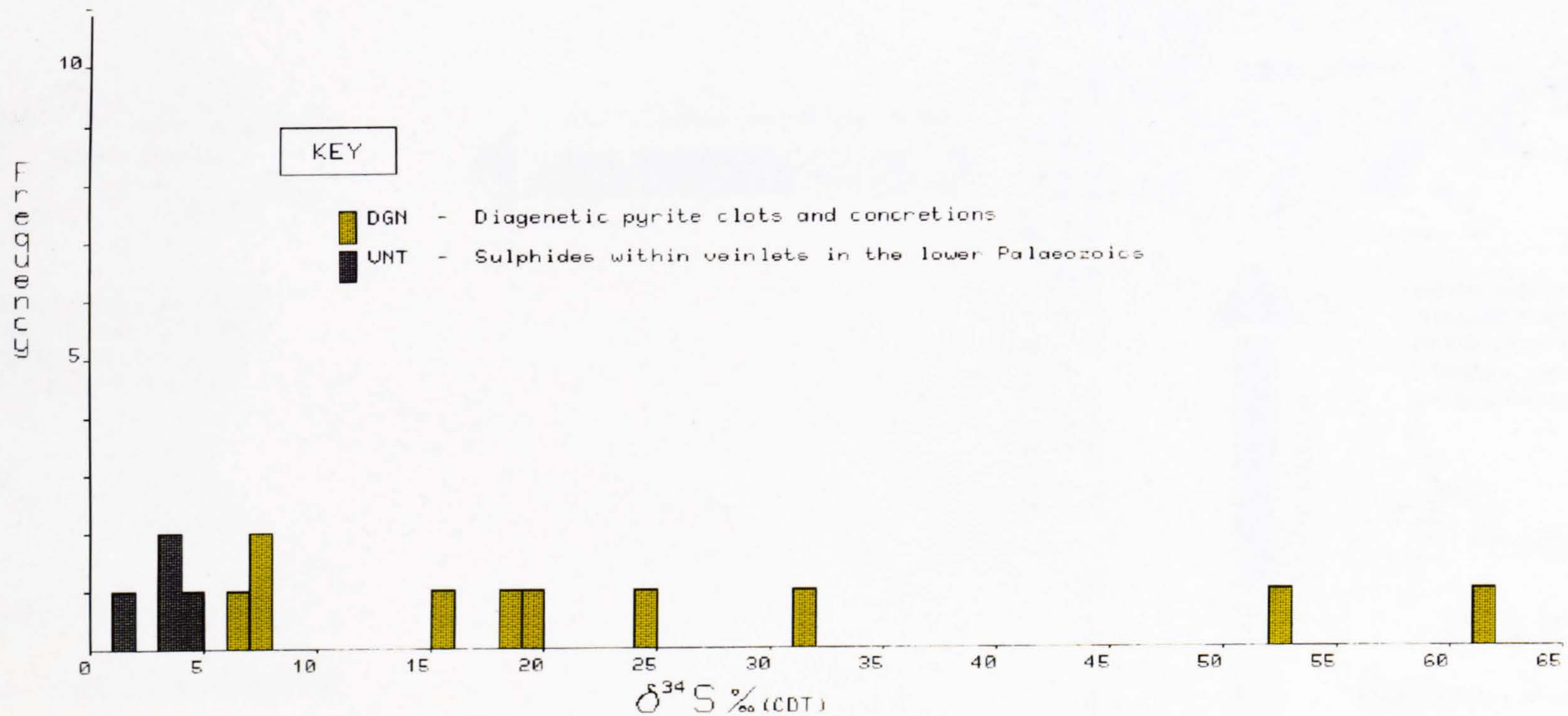
KEY
DGN - Diagenetic pyrite clots and concretions
UNT - Sulphides within veinlets in the lower Palaeozoics
Frequency
10
5
0
5
10
15
20
25
30
35
40
45
50
55
60
65
δ34 S ‰ (CDT)

Figure 6.26 Diagram illustrating the lateral variation in the sulphur isotopic composition of sulphides in the 2-5 Lens footwall.

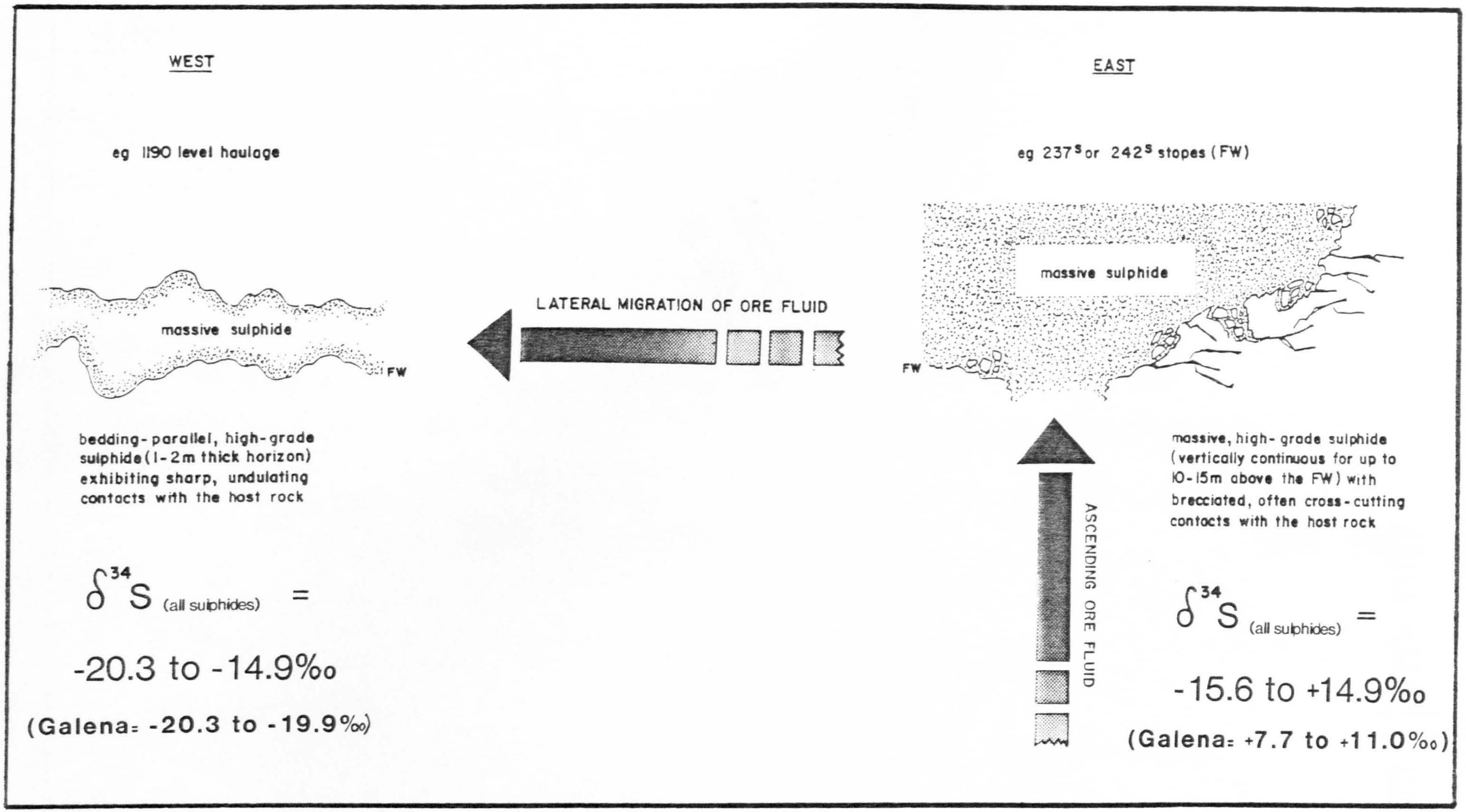
WEST
eg 1190 level haulage
massive sulphide
FW
bedding-parallel, high-grade sulphide (1-2m thick horizon) exhibiting sharp, undulating contacts with the host rock
$\delta^{34}S$ (all sulphides) =
-20.3 to -14.9‰
(Galena= -20.3 to -19.9‰)
LATERAL MIGRATION OF ORE FLUID
EAST
eg 237S or 242S stopes (FW)
massive sulphide
FW
ASCENDING ORE FLUID
massive, high-grade sulphide (vertically continuous for up to 10-15m above the FW) with brecciated, often cross-cutting contacts with the host rock
$\delta^{34}S$ (all sulphides) =
-15.6 to +14.9‰
(Galena= +7.7 to +11.0‰)

Figure 6.27 Diagram illustrating the lateral variation in the sulphur isotopic composition of sulphides in 2-2/ 1-2 Lenses.

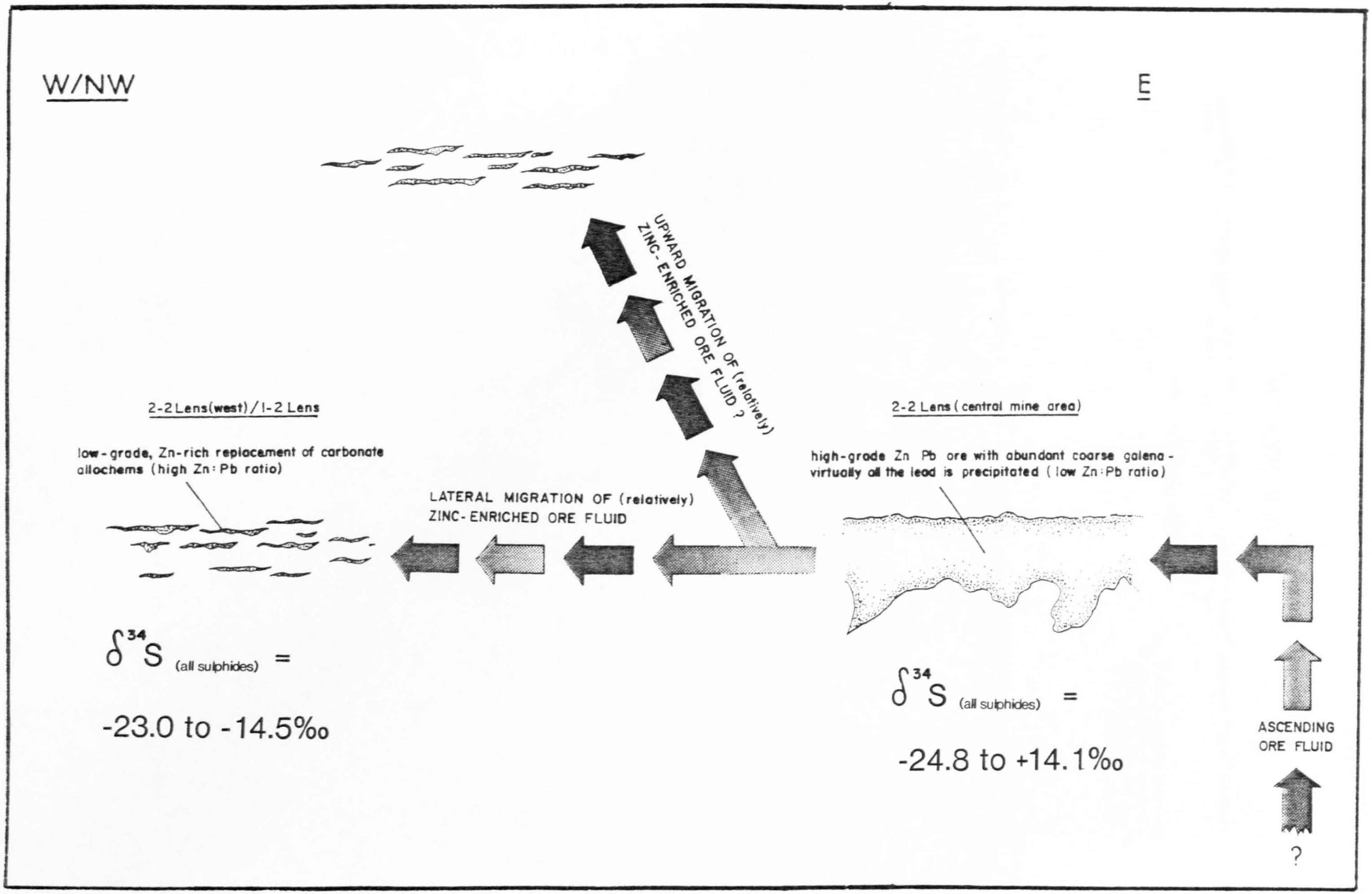
W/NW
E
UPWARD MIGRATION OF (relatively)
ZINC-ENRICHED ORE FLUID ?
2-2 Lens(west) / 1-2 Lens
low-grade, Zn-rich replacement of carbonate allochems (high Zn:Pb ratio)
LATERAL MIGRATION OF (relatively)
ZINC-ENRICHED ORE FLUID
2-2 Lens (central mine area)
high-grade Zn Pb ore with abundant coarse galena - virtually all the lead is precipitated (low Zn:Pb ratio)
$\delta^{34}S_{(all\ sulphides)}$ =
-23.0 to -14.5‰
$\delta^{34}S_{(all\ sulphides)}$ =
-24.8 to +14.1‰
ASCENDING
ORE FLUID
?

Figure 7.1 Diagram illustrating a process for the continual generation of open space beneath a dolomitic "crust" during mineralization and compaction of the stratigraphic section.

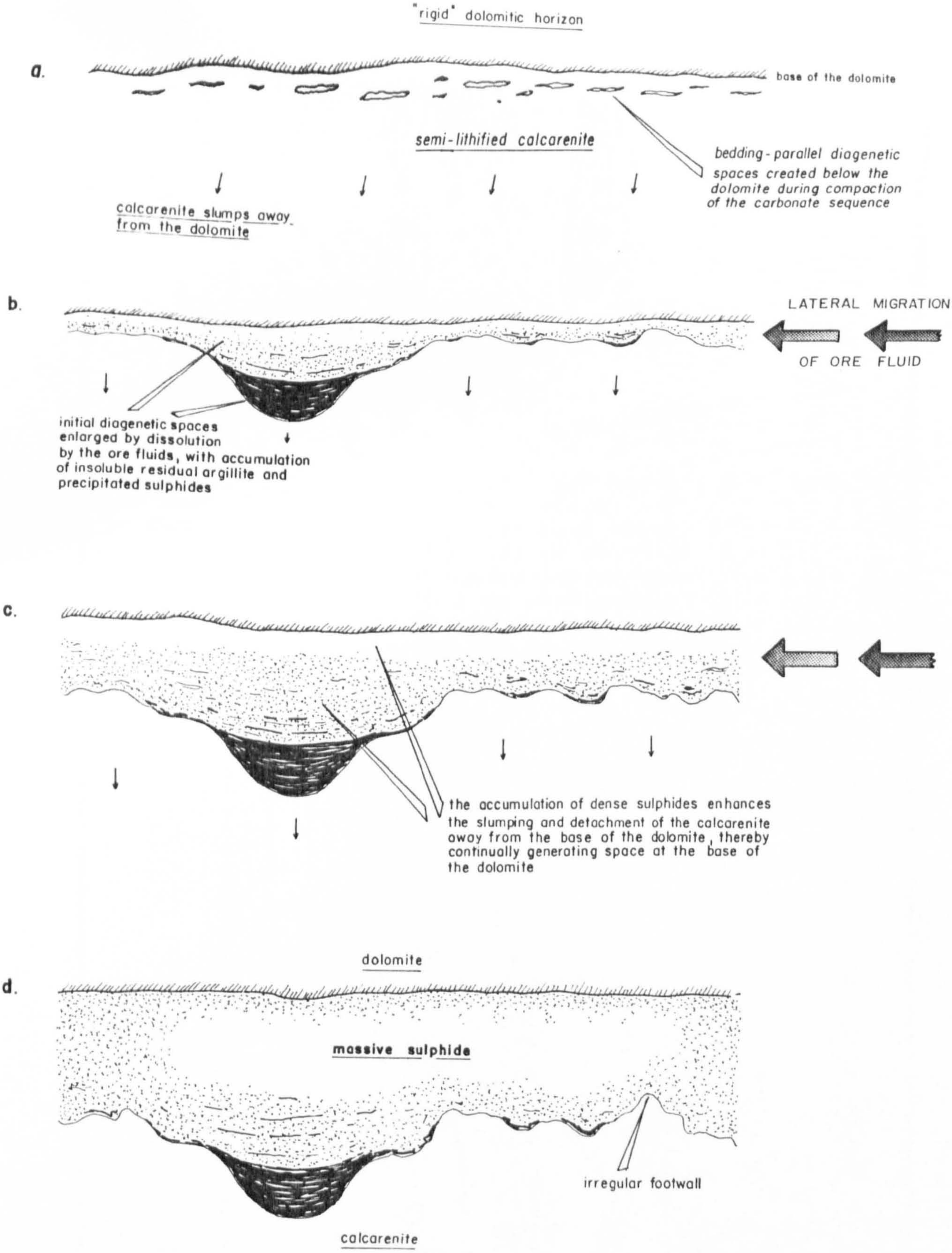
a.
"rigid" dolomitic horizon
base of the dolomite
semi-lithified calcarenite
bedding-parallel diagenetic spaces created below the dolomite during compaction of the carbonate sequence
calcarenite slumps away from the dolomite
b.
LATERAL MIGRATION OF ORE FLUID
initial diagenetic spaces enlarged by dissolution by the ore fluids, with accumulation of insoluble residual argillite and precipitated sulphides
c.
the accumulation of dense sulphides enhances the slumping and detachment of the calcarenite away from the base of the dolomite, thereby continually generating space at the base of the dolomite
d.
dolomite
massive sulphide
irregular footwall
calcarenite

Figure 7.2 Schematic diagram illustrating two possible derivations of the bacteriogenic H_2S in the Navan deposit. In both cases the H_2S is derived by the reduction of Lower Carboniferous sea water sulphate and transported in a sea water fluid. The regional gradient is exagerated for the purposes of the diagram.

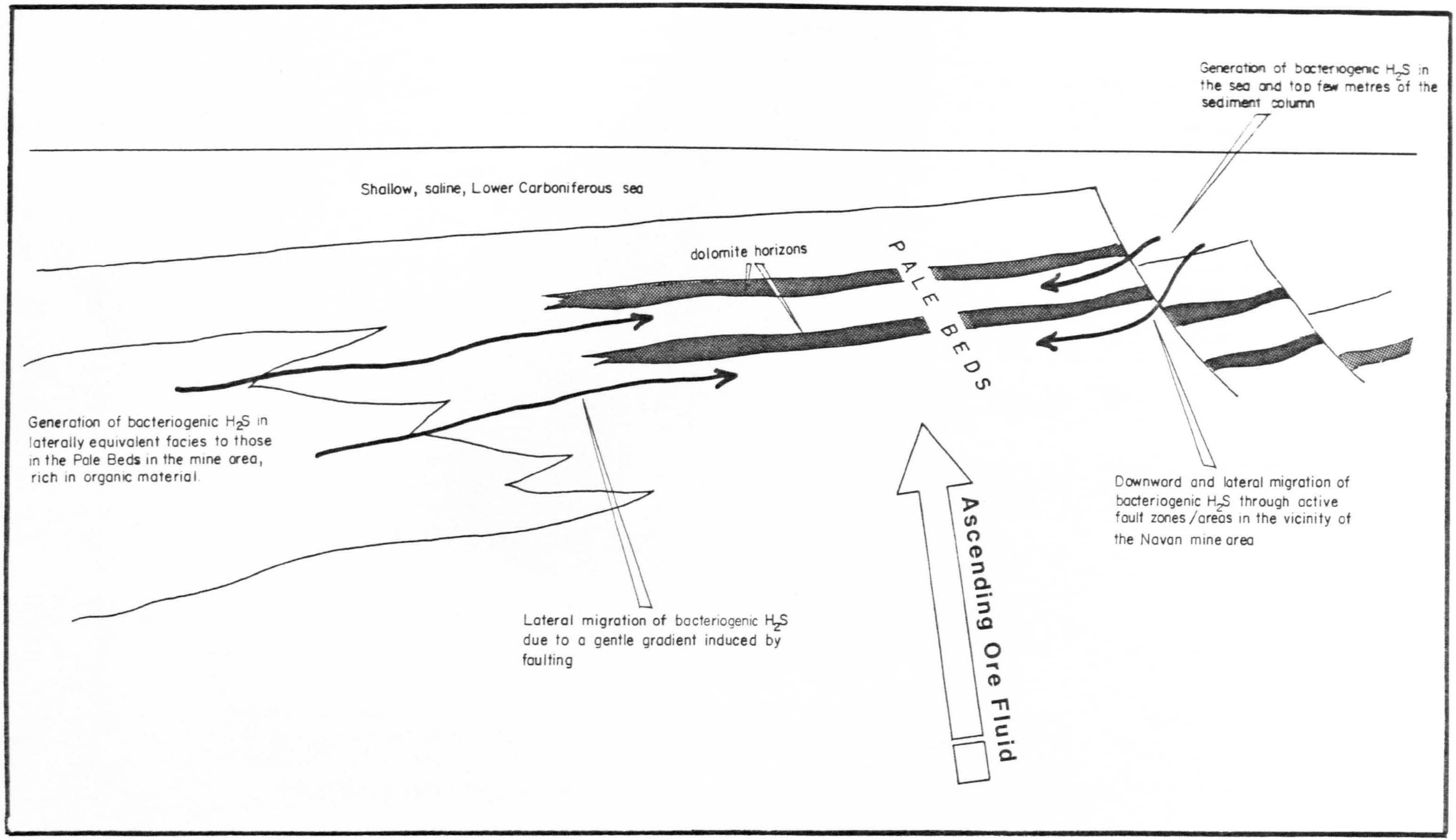
Generation of bacteriogenic H_2S in the sea and top few metres of the sediment column
Shallow, saline, Lower Carboniferous sea
dolomite horizons
PALE BEDS
Generation of bacteriogenic H_2S in laterally equivalent facies to those in the Pale Beds in the mine area, rich in organic material.
Downward and lateral migration of bacteriogenic H_2S through active fault zones/areas in the vicinity of the Navan mine area
Lateral migration of bacteriogenic H_2S due to a gentle gradient induced by faulting
Ascending Ore Fluid

Figure 7.3 Model for the mineralization at Navan during deposition of at least part of the Pale Beds sequence in late Courceyan times. The diagram illustrates a simplified picture of one pulse of ore fluid.

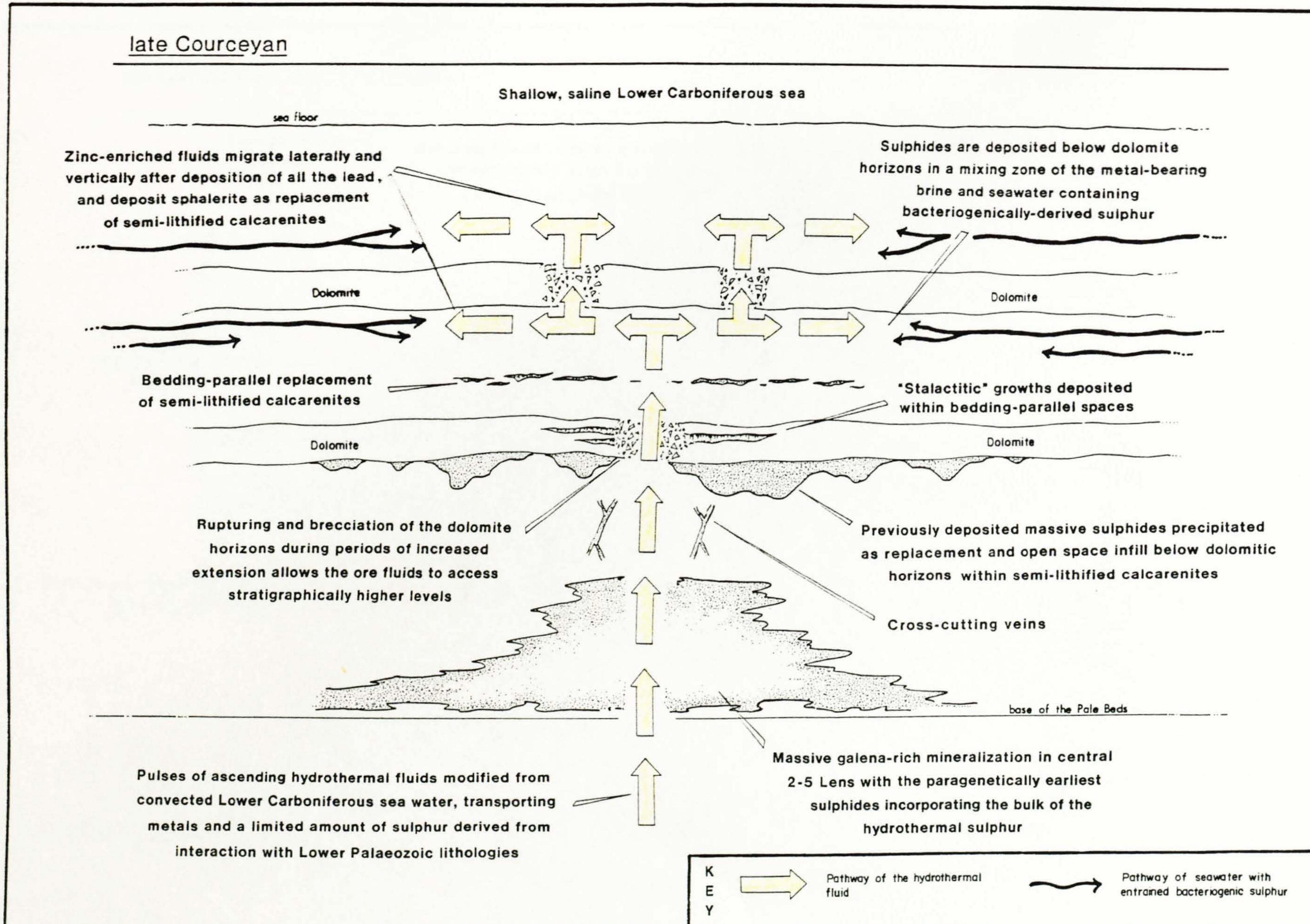
late Courceyan
Shallow, saline Lower Carboniferous sea
sea floor
Zinc-enriched fluids migrate laterally and vertically after deposition of all the lead, and deposit sphalerite as replacement of semi-lithified calcarenites
Sulphides are deposited below dolomite horizons in a mixing zone of the metal-bearing brine and seawater containing bacteriogenically-derived sulphur
Dolomite
Dolomite
Bedding-parallel replacement of semi-lithified calcarenites
"Stalactitic" growths deposited within bedding-parallel spaces
Dolomite
Dolomite
Rupturing and brecciation of the dolomite horizons during periods of increased extension allows the ore fluids to access stratigraphically higher levels
Previously deposited massive sulphides precipitated as replacement and open space infill below dolomitic horizons within semi-lithified calcarenites
Cross-cutting veins
base of the Pale Beds
Pulses of ascending hydrothermal fluids modified from convected Lower Carboniferous sea water, transporting metals and a limited amount of sulphur derived from interaction with Lower Palaeozoic lithologies
Massive galena-rich mineralization in central 2-5 Lens with the paragenetically earliest sulphides incorporating the bulk of the hydrothermal sulphur
KEY
Pathway of the hydrothermal fluid
Pathway of seawater with entrained bacteriogenic sulphur

Figure 7.4 Model for the mineralization at Navan during the deposition of the Boulder Conglomerate in late Chadian to early Arundian times. The diagram illustrates a simplified picture of one pulse of ore fluid.

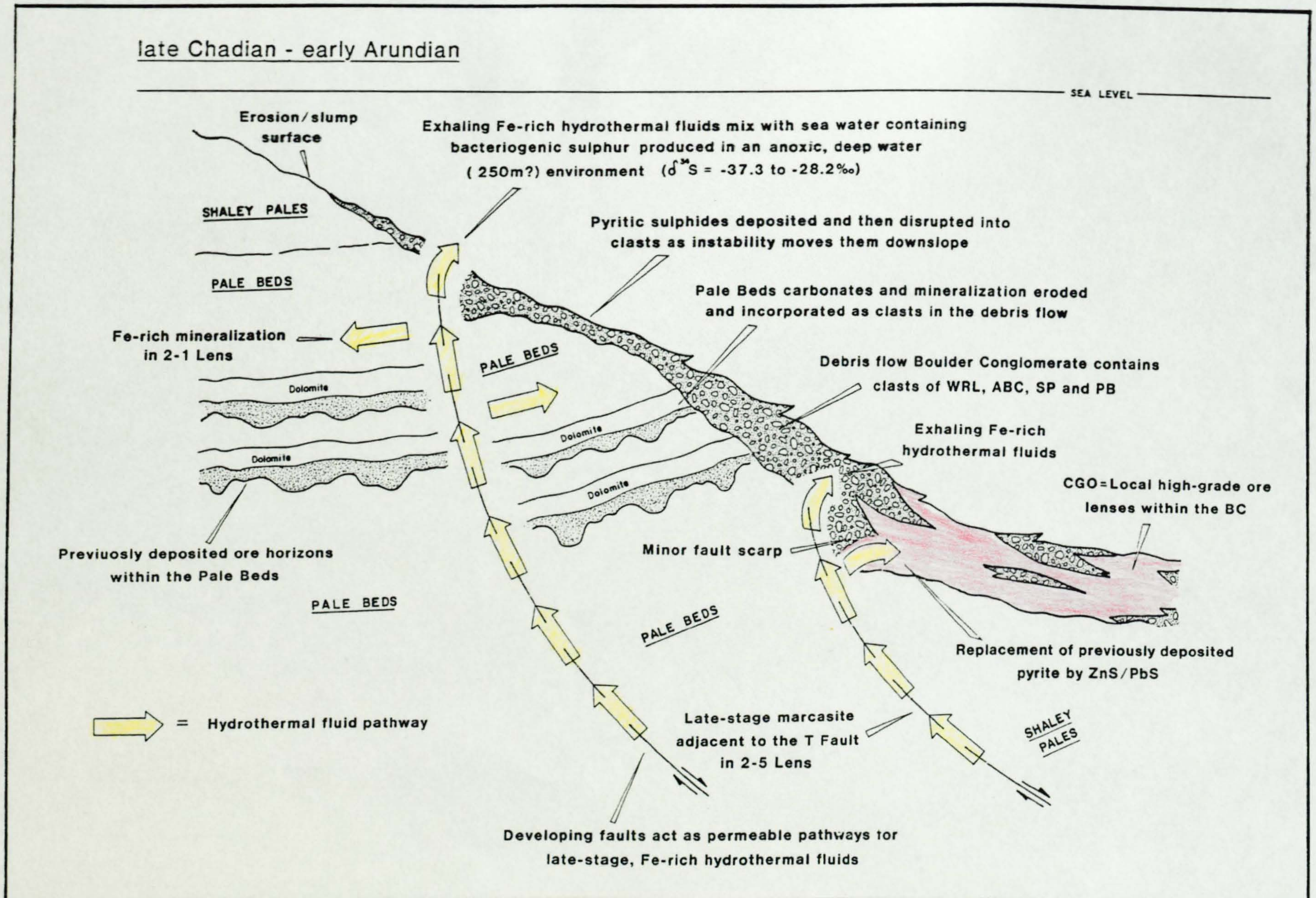
late Chadian - early Arundian
SEA LEVEL
Erosion/slump surface
Exhaling Fe-rich hydrothermal fluids mix with sea water containing bacteriogenic sulphur produced in an anoxic, deep water (250m?) environment ($\delta^{34}S$ = -37.3 to -28.2‰)
SHALEY PALES
PALE BEDS
Pyritic sulphides deposited and then disrupted into clasts as instability moves them downslope
Pale Beds carbonates and mineralization eroded and incorporated as clasts in the debris flow
Fe-rich mineralization in 2-1 Lens
PALE BEDS
Dolomite
Dolomite
Dolomite
Dolomite
Debris flow Boulder Conglomerate contains clasts of WRL, ABC, SP and PB
Exhaling Fe-rich hydrothermal fluids
CGO=Local high-grade ore lenses within the BC
Previuosly deposited ore horizons within the Pale Beds
Minor fault scarp
PALE BEDS
PALE BEDS
Replacement of previously deposited pyrite by ZnS/PbS
= Hydrothermal fluid pathway
Late-stage marcasite adjacent to the T Fault in 2-5 Lens
SHALEY PALES
Developing faults act as permeable pathways for late-stage, Fe-rich hydrothermal fluids